Precise nanomedicine for intelligent therapy of cancer

Huabing Chen[1†], Zhanjun Gu[2†], Hongwei An[2,3], Chunying Chen[3,4], Jie Chen[5,6,7], Ran Cui[8], Siqin Chen[9], Weihai Chen[10], Xuesi Chen[5,6,7], Xiaoyuan Chen[11], Zhuo Chen[12], Baoquan Ding[3], Qian Dong[12], Qin Fan[13], Ting Fu[12], Dayong Hou[3], Qiao Jiang[3], Hengte Ke[1], Xiqun Jiang[14], Gang Liu[15], Suping Li[3], Tianyu Li[16], Zhuang Liu[13], Guangjun Nie[3], Muhammad Ovais[3,4], Daiwen Pang[8], Nasha Qiu[9], Youqing Shen[9], Huayu Tian[5,6,7], Chao Wang[13], Hao Wang[3], Ziqi Wang[3], Huaping Xu[16], Jiang-Fei Xu[16], Xiangliang Yang[17], Shuang Zhu[2], Xianchuang Zheng[14], Xianzheng Zhang[10], Yanbing Zhao[17], Weihong Tan[12,18*], Xi Zhang[16*] & Yuliang Zhao[3*]

[1]*State Key Laboratory of Radiation Medicine and Protection, Jiangsu Key Laboratory of Neuropsychiatric Diseases, College of Pharmaceutical Sciences, Soochow University, Suzhou 215123, China;*
[2]*Institute of High Energy Physics, Chinese Academy of Sciences, Beijing 100049, China;*
[3]*CAS Key Laboratory for Biomedical Effects of Nanomaterials and Nanosafety, CAS Center for Excellence in Nanoscience, National Center for Nanoscience and Technology of China, Beijing 100190, China;*
[4]*University of Chinese Academy of Sciences, Beijing 100049, China;*
[5]*Key Laboratory of Polymer Ecomaterials, Changchun Institute of Applied Chemistry, Chinese Academy of Sciences, Changchun 130022, China;*
[6]*University of Science and Technology of China, Hefei 230026, China;*
[7]*Jilin Biomedical Polymers Engineering Laboratory, Changchun 130022, China;*
[8]*Key Laboratory of Analytical Chemistry for Biology and Medicine (Ministry of Education), College of Chemistry and Molecular Sciences, State Key Laboratory of Virology, and Institute for Advanced Studies, Wuhan University, Wuhan 430072, China;*
[9]*Center for Bionanoengineering and Key Laboratory of Biomass Chemical Engineering of Ministry of Education, College of Chemical and Biological Engineering, Zhejiang University, Hangzhou 310027, China;*
[10]*Key Laboratory of Biomedical Polymers of Ministry of Education, Department of Chemistry, Wuhan University, Wuhan 430072, China;*
[11]*Laboratory of Molecular Imaging and Nanomedicine, National Institute of Biomedical Imaging and Bioengineering, National Institutes of Health, Bethesda, MD 20892, USA;*
[12]*Molecular Science and Biomedicine Laboratory, State Key Laboratory of Chemo/Bio-Sensing and Chemometrics, College of Chemistry and Chemical Engineering, Aptamer Engineering Center of Hunan Province, Hunan University, Changsha 410082, China;*
[13]*Jiangsu Key Laboratory for Carbon-Based Functional Materials & Devices, Institute of Functional Nano & Soft Materials, Soochow University, Suzhou 215123, China;*
[14]*Department of Polymer Science and Engineering, College of Chemistry and Chemical Engineering, Nanjing University, Nanjing 210093, China;*
[15]*State Key Laboratory of Molecular Vaccinology and Molecular Diagnostics & Center for Molecular Imaging and Translational Medicine, School of Public Health, Xiamen University, Xiamen 361102, China;*
[16]*Department of Chemistry, Tsinghua University, Beijing 100084, China;*
[17]*National Engineering Research Center for Nanomedicine, College of Life Science and Technology, Huazhong University of Science and Technology, Wuhan 430074, China;*
[18]*Department of Chemistry and Department of Physiology and Functional Genomics, Center for Research at Bio/nano Interface, Health Cancer Center, UF Genetics Institute and McKnight Brain Institute, University of Florida, Gainesville, FL 32611-7200, USA*

†These authors contributed equally to this work.
*Corresponding authors (email: tan@chem.ufl.edu; xi@tsinghua.edu.cn; zhaoyl@nanoctr.cn)

Precise nanomedicine has been extensively explored for efficient cancer imaging and targeted cancer therapy, as evidenced by a few breakthroughs in their preclinical and clinical explorations. Here, we demonstrate the recent advances of intelligent cancer nanomedicine, and discuss the comprehensive understanding of their structure-function relationship for smart and efficient cancer nanomedicine including various imaging and therapeutic applications, as well as nanotoxicity. In particular, a few emerging strategies that have advanced cancer nanomedicine are also highlighted as the emerging focus such as tumor imprisonment, supramolecular chemotherapy, and DNA nanorobot. The challenge and outlook of some scientific and engineering issues are also discussed in future development. We wish to highlight these new progress of precise nanomedicine with the ultimate goal to inspire more successful explorations of intelligent nanoparticles for future clinical translations.

**nanomedicine, nanoparticles, cancer therapy, cancer imaging, intelligent therapy**

1   Introduction

Cancer is a leading cause of mortality worldwide, and it is estimated that more than 21.0 million people may suffer from cancer by the year of 2030 [1]. Many efforts have been made to develop efficient approaches to diagnose and treat cancer. To date, a variety of therapeutic approaches including chemotherapy, molecularly targeted therapy, gene therapy, radiotherapy, immunotherapy, phototherapy, and embolotherapy have been extensively applied to treat cancers in clinic. To improve the clinical performances with reduced adverse side effects, the nanomedicine as an emerging strategy has been recently explored to provide innovative diagnostic or therapeutic regime towards precise cancer therapy, as evidenced by successful developments of commerical products such as Abraxane and considerable formulations in clinical trials. These nanoparticles have been rationally fabricated using different biocompatible materials such as organic compounds, proteins, lipids, polymers, and inorganic nanomaterials [2], leading to flexible designs of multifunctional high-performance nanoparticles for satisfying cancer-specific imaging and drug delivery.

We here attempt to give an introduction of the recent development and future trends in field of cancer nanomedicine (Scheme 1), particularly focusing on intelligent cancer treatments using several types of nanoparticles towards personalized cancer therapy (Scheme 2). To date, the extensive efforts have been continuously made to fabricate intelligent nanomedicine in response to biomarkers, receptors, and tumor microenvironments for precise therapy of cancers. To achieve accurate cancer therapy, the nanoparticles are demanded to achieve reasonable spatiotemporal distribution of imaging or therapeutic agent at targeted site. In addition to prolonged blood circulation with reduced interactions with blood components and reticuloendothelial

system (RES) as a prerequesite for favorable pharmacokinetics, the capacities to achieve reasonable extravasation and penetration in tumor, preferable cellular uptake, and considerable intracellular release of payloads, are needed to be rationally constituted to overcome multiple transport barriers in cancer-specific drug delivery. Thus, the characteristics such as size, charge, morphology, surface chemistry, and intelligence of intrinsic nanoarchitectures should be comprehensively considered to facilitate the efficient delivery of imaging agent or drug to the subcellular target in tumors, which frequently suffers from the sophisticated nano-bio interactions with various tissues (e.g. liver, kidney, spleen, brain, and tumor), and nonspecific interactions with endothelial cells, blood vessels, extracellular matrices, and healthy cells in their transport processes [3,4]. The targeting efficiency and clearance of nanoparticles usually depend on these nano-bio interactions, which can determine subsequent imaging or therapeutic performance, as well as safety issue. Hence, the rational design of nanoparticles with controllable characteristics might offer preferable nano-bio interactions to overcome the sophisticated barriers in transport processes, reasonably ensuring the development of high-performance imaging or therapeutic nanoparticles for cancer nanomedicine.

The intelligent nanoparticles have been extensively explored for cancer therapies such as chemotherapy, gene therapy, immunotherapy, phototherapy, and radiotherapy. The designs of such intelligent nanoparticles often rely on their ability to respond to the external or intrinsic stimuli in tumor site, thereby producing precise tumor localization and activatable imaging signals/intracellular release of payloads for enhanced imaging contrast or therapeutic efficacy. Generally, exogenous stimuli including light, temperature, ultrasound, and magnetic field are locally utilized to trigger the intelligent changes of nanoparticles at tumor site, while in-
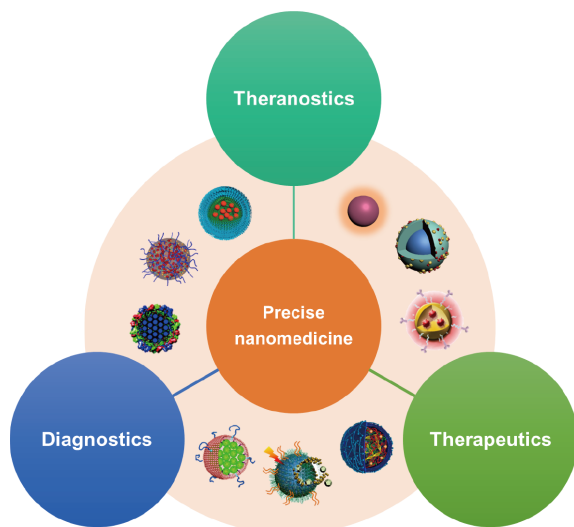
Scheme 1 Schematic illustration of precise nanomedicine for intelligent therapy of cancer (color online).

Scheme 2 Various nanoparticles for intelligent therapy of cancer discussed in this review (color online).

trinsic stimuli are able to ensure the nanoparticles to automatically display smart delivery in response to tumor microenvironment and hallmark such as tumor vasculature, hypoxia, extracellular matrice, acidic pH, highly over-expressed receptor/enzyme/protein, intracellular species (e.g. esterase, adenosine triphosphate (ATP), reactive oxgen species (ROS), glutathione). Hence, once the nanoparticles overcome the transport barriers, their smart or stimuli-responsive characteristics might be rapidly activated for producing imaging signals or drug release at tumor site. Inspired by these intelligent characteristics, a variety of unique strategies have been recently explored as emerging trends including tumor imprisonment of metallofullerenol nanoparticles, supramolecular chemotherapy, and DNA nanorobot, showing significantly improved anticancer efficacy with reduced adverse side effects through both efficient delivery and smart release [5]. For instance, DNA nanorobot that could function as a cancer therapeutic in response to a molecular trigger *in vivo* was reported to specifically deliver

thrombin to tumor-related blood vessels and induce intravascular thrombosis for successful tumor necrosis and tumor growth inhibition [6]; The principle of host-guest complexation was also utilized to incorporate chemotherapeutic guest using supramolecular host, resulting in their improved anticancer efficacy with reduced adverse side effect [7]. Gadolinium metallofullerenol nanoparticles were able to suppress tumor metastasis by imprisoning tumor instead of damaging tumor cells [8], providing a tumor imprisonment strategy for efficient cancer therapy. Although these strategies are distinctly different from conventional design principles of nanoparticles, their translational developments are being explored from conceptual explorations. In consideration of the clinical translations of nanoparticles, their characteristics and nano-bio interactions might cause potential safety issue, reasonably resulting from size, charge, morphology, chemical composition and intermolecular interactions of nanoparticles. Then, the nanotoxicity is highly important for facilitating the clinical translation of the nanoparticles. The comprehensive investigation of nanotoxicity can act as an effective tool for addressing their safety concern, thus facilitating clinical translation of nanoparticles.

In this review, we demonstrate the recent advances of several types of nanoparticles in the investigation of cancer nanomedicine for intelligent cancer diagnosis and therapy (Scheme 2). The comprehensive understanding of their structure-function relationship is discussed for intelligent cancer nanomedicine including various cancer imaging and therapeutic applications, as well as nanotoxicity. In particular, a few emerging strategies are highlighted such as metallofullerenol nanoparticles, supramolecular chemotherapy, and DNA nanorobot. The challenge and outlook of some scientific and engineering issues are also discussed for future development.

2 New strategies for cancer nanomedicine

Recently, some unique imaging or therapeutic nanoparticles have been explored as the emerging platform for their applications in cancer nanomedicine. We summarize a few intriguing approaches that are found to be able to signifiantly improve the tumor accumulation and retention, smart and efficient delivery, as well as imaging-guided therapy including metallofullerenol nanoparticles for imprisoning tumor, supramolecular chemotherapy, DNA nanorobot, *in vivo* self-assembled nanostructure, ROS-responsive nanoparticles, and protein nanoreactor. In these approaches, some new designs such as endohedral metallofullerene, host-guest chemistry, DNA scaffold, self-assembly chemistry, ultrasensitive diselenide and tellurium bonds, and controllable protein nanocage, play key roles for their applications in cancer nanomedicine.

2.1 Gadolinium metallofullerenol nanoparticles as emerging tumor caging agent for imprisoning tumor

The nanoparticles have been exploited as effective vehicles for chemotherapeutic drugs, oligonucleotides, or other bioactive molecules where reducing systemic toxicity and improving pharmacokinetics are considered as the main purpose. In contrast to the conventional nanoparticles that directly kill cancer cells and have associated toxicity, a novel and highly efficient strategy has been proposed and developed in recent years [9]. Instead of killing cancer cells directly, scientists have restricted their communication with the tumor microenvironment using nano-construct that personified all the essential biologic properties. For instance, the pioneering study performed in 2005 by Chen and Zhao *et al.* [10] have demonstrated the anti-tumor activity of $Gd@C_{82}(OH)_{22}$ nanoparticles in the H22 hepatoma-implanted mice. Interestingly, the $Gd@C_{82}(OH)_{22}$ nanoparticles have no influence on tumor cells directly but indeed improve immunity and regulate the oxidative defense system *in vivo* for producing potent anti-tumor effect. Throughout the years, Chen and Zhao *et al.* have already elucidated the anti-tumor mechanisms of metallofullerenols using cutting-edge and high-rapid screening techniques such as gene-array and molecular simulation, further leading to the widespread applications in regulating tumor metastasis, drug resistance, impediment of angiogenesis, immune stimulation, cancer stem cells, and oxidative stress through tumor imprisonment (Figure 1).

In a study by Meng *et al.* [8], gadolinium metallofullerenol nanoparticles were found to restrict the tumor metastasis via imprisoning cancer cells. The production of metalloproteinases (MMPs) was inhibited by these nanoparticles along with restriction in cancer cells' invasiveness. In a tissue invasion animal model, the thick fibrous cage was found to serve as a "prison" and restrict the communication between cancer and tumor associated macrophages, ultimately inhibiting MMPs production. More recently, Liu *et al.* [11] elucidated the prisoning behavior of $Gd@C_{82}(OH)_{22}$ nanoparticles by disclosing the underlying mechanism of fibroblast cell regulation. $Gd@C_{82}(OH)_{22}$ nanoparticles were found to activate TNFR2/p38 MAPK signaling pathway via promoting TNF-α binding to tumor necrosis factor receptors 2 (TNFR2), ultimately leading to the increase of cellular collagen expression. The molecular dynamics simulations were also employed to study the mechanism of $Gd@C_{82}(OH)_{22}$-induced TNF-α and TNFR interaction at molecular level, revealing a "bridge-like" mode of interaction. This study provides the core considerations into the principle and design of $Gd@C_{82}(OH)_{22}$ nanoparticles as a potential tumor imprisoning agent. Kang *et al.* [12] found that $Gd@C_{82}(OH)_{22}$ nanoparticles were able to inhibit pancreatic tumor metastasis. The activity and expression of MMPs were also demonstrated to be restricted by $Gd@C_{82}(OH)_{22}$. The spe-
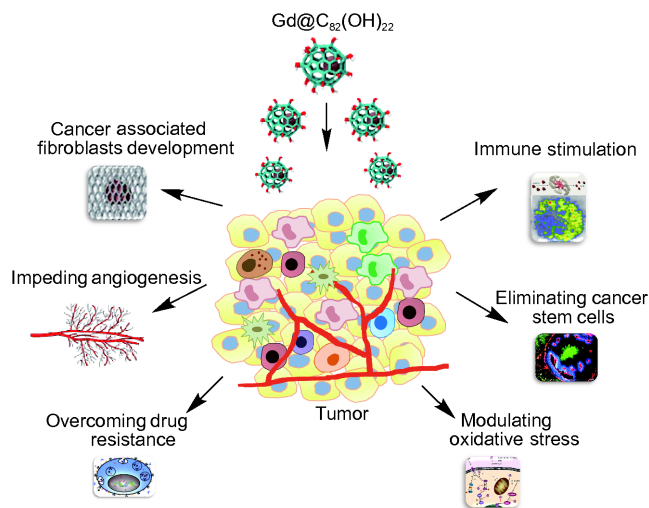

Figure 1 Illustration of novel approach to confine tumor using $Gd@C_{82}(OH)_{22}$ nanoparticles as emerging tumor caging agent for tumor imprisonment (color online).

cificity of $Gd@C_{82}(OH)_{22}$ nanoparticles in binding and MMP suppression allows themselves to act as a potential platform for treating pancreatic cancer. Pan *et al.* [13] further explored the epigenetic mechanism of $Gd@C_{82}(OH)_{22}$ in human pancreatic cancer metastasis. $Gd@C_{82}(OH)_{22}$ nanoparticles upregulated reversion-inducing cysteine-rich protein with Kazal motifs (RECK), while at the meantime downregulated metastasis-associated protein 1 (MTA1), HDAC1, HIF-1a, and MMP-2/9, ultimately leading to suppression of tumor metastasis. $Gd@C_{82}(OH)_{22}$ nanoparticles also served as a HDAC1 inhibitor to activate RECK expression by inhibiting the interaction between HDAC1 and MTA1 for suppressing pancreatic cancer cell invasion and metastasis.

Currently, available molecular angiogenesis inhibitors suffer from some challenges due to their small targeting range among many angiogenic factors, eventually leading to a fragile effect. Meng *et al.* [14] developed the $Gd@C_{82}(OH)_{22}$ nanoparticles, which were functionalized with multiple hydroxyl groups. At the mRNA level, these nanoparticles were able to simultaneously down-regulate more than 10 angiogenic factors that were further validated at protein levels. These nanoparticles displayed a preferable *in vivo* anti-tumor activity, which is comparable to that of paclitaxel. Liang *et al.* [15] further found that the growth of cisplatin-resistant human prostate cancer (CP-r) tumors in athymic nude mice was inhibited by cisplatin in the presence of $Gd@C_{82}(OH)_{22}$ nanoparticles. The defective endocytosis of CP-r cancer cells was restored upon its pretreatment with $Gd@C_{82}(OH)_{22}$ nanoparticles, subsequently resulting in enhanced intracellular accumulation of cisplatin and formation of cisplatin-DNA adducts. This intracellular accumulation of cisplatin in CP-r cancer cells was able to be further improved by $Gd@C_{82}(OH)_{22}$ through the reduced fluidity of plasma membrane or altered cytoskeleton.

In the prognosis and development of cancer, down-regulation of the immune response has a very vital role, while its upregulation has potential clinical significance. In a study by Liu *et al*. [16], Gd@C$_{82}$(OH)$_{22}$ nanoparticles possessed obvious anti-tumor effect because of their immunomodulatory effect on T cells and macrophages. Due to the treatment of Gd@C$_{82}$(OH)$_{22}$ nanoparticles, cytokine balance was polarized as evidenced by the increased production of Th1 cytokines (IL-2, IFN-g and TNF-α) and decreased production of Th2 cytokines (IL-4, IL-5 and IL-6) in serum. Moreover, at high doses the nanoparticles further stimulated the immune cells for the release of more cytokines, thereby inhibiting the tumor growth. In another study by Yin *et al*. [17], Gd@C$_{82}$-(OH)$_{22}$ nanoparticles were found to be able to protect the cells from oxidative damage induced by H$_2$O$_2$, reduce ROS production intracellularly, and stabilize the mitochondrial membrane potential. Tang *et al*. [18] further elucidated the anti-tumor mechanism of Gd@C$_{82}$(OH)$_{22}$-activated macrophages. Gd@C$_{82}$(OH)$_{22}$ nanoparticles were able to activate the macrophages via NF-κB signaling pathway and enhanced mitochondrial metabolism, phagocytosis and cytokine secretion, thus resulting in the tumor growth inhibition. The lung metastasis was also suppressed upon treatment with Gd@C$_{82}$(OH)$_{22}$-activated autologous macrophages.

More recently, Liu *et al*. [19] demonstrated the specific inhibitory effect of Gd@C$_{82}$(OH)$_{22}$ nanoparticles on breast cancer stem cells (CSCs). The Gd@C$_{82}$(OH)$_{22}$ nanoparticles that were nontoxic to the normal mammary epithelial cells blocked the epithelial-to-mesenchymal transition, resulting in the eradication of breast cancer stem cells. In normoxic conditions, Gd@C$_{82}$(OH)$_{22}$ nanoparticles mediated these effects by blocking TGF-β signalling. Under hypoxic conditions, their cellular uptake was facilitated where these nanoparticles functioned as a bi-potent inhibitor of HIF-1α and TGF-β activities, thus enhancing CSCs elimination. Hence, gadolinium metallofullerenol nanoparticles as a nontoxic CSC specific inhibitor possess a promising therapeutic potential. To date, many scientists have highlighted the importance of metallofullerenol nanoparticles as a new strategy to cage tumors for potential cancer theranostics, as indicated in a research highlight by Fadeel *et al*. [20]. In another perspective, Balogh [9] further made a comment that "these findings are of great interest, because they not only portray a new anticancer strategy, but a deeper understanding of this nanomedicine may lead to a new class of efficient anticancer pharmaceutics that are safe to use". Owing to its diverse nature and non-toxic behavior, metallofullerenol nanomaterials as the clinically potential agent have a great promise for cancer therapy.

2.2   Supramolecular chemotherapy

Chemotherapy is currently among the most effective anti-cancer therapeutic modalities in clinical treatments. However, many chemotherapeutic agents suffer from substantial drawbacks including poor water-solubility, and low therapeutic specificity among normal cells and cancer cells, which often result in severe adverse side effects and greatly impede the therapeutic efficacy of anticancer drugs.

Supramolecular chemotherapy, generated from the marriage between chemotherapy and supramolecular chemistry, refers to a supramolecular strategy for decreasing the undesired cell damage of clinical anticancer drugs on normal cells, and improving their anticancer bioactivity against cancer cells. There are three necessary points in the strategy of supramolecular chemotherapy. The first point is that the anticancer core of clinical anticancer drugs must be disguised by supramolecular hosts on the basis of noncovalent interactions to avoid their serious damages against normal cells during drug delivery process. The second point is that one of the cancer biomarkers, which is overexpressed in some cancer microenvironments, can be incorporated into the supramolecular host, thus releasing the disguised anticancer drug and recovering its anticancer efficacy. And the third point is that the cooperative enhancement of anticancer performance needs to be achieved by simultaneously regaining the anticancer bioactivity of anticancer drug and consuming the over-expressed cancer biomarker, which is essential to cell proliferation for cancer cells. Following these three points, we can design various supramolecular anticancer drugs for supramolecular chemotherapy, thus providing more opportunities for effective anticancer treatments (Figure 2).

As a proof of concept, an advantage of host-guest chemistry using cucurbit[7]uril was utilized to encapsulate oxaliplatin [7], which is a first-line chemotherapeutic drug for colorectal cancer. Through their host-guest complexation, the cytotoxicity of oxaliplatin against colorectal normal cells was significantly decreased. More importantly, an over-expressed cancer biomarker, spermine, was utilized to competitively replace oxaliplatin from the host cavity in cancer cells, thus realizing its controlled release and recovering its anticancer bioactivity. Since spermine is essential for cancer cell growth and proliferation, the consumption of spermine and controlled release of oxaliplatin were found to further increase its anticancer bioactivity. Moreover, inspired by the concept of polymer therapeutics raised by Ringsdorf [21], the advantages of supramolecular chemotherapy and polymer therapeutics were combined through marrying supramolecular recognition units with polymeric structures, and therefore a strategy of supramolecular polymeric chemotherapy was developed as a new nanomedicine [22], in which the main-chain cucurbit[7]uril-PEG copolymer was employed to carry oxaliplatin, thus successfully prolonging its circulation time and leading to better anticancer performance in the tumor-bearing mice. It is expected
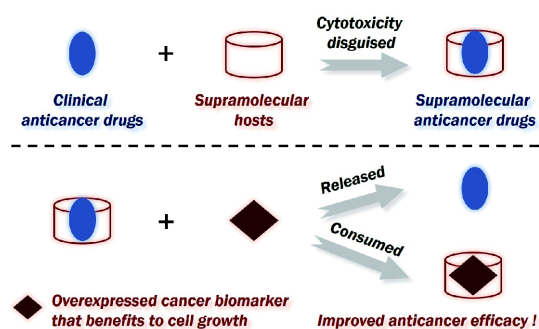
Figure 2 Schematic representation of the characteristics of supramolecular chemotherapy (color online).

that more functions such as targeting ability and responsiveness to tumor microenvironment may be also introduced into the polymeric systems through polymerization, which may help in increasing the accumulation of therapeutic agents in tumor. It is also highly anticipated that the supramolecular chemotherapy can be extended to many other clinical chemotherapeutic drugs for decreasing their severe side effects and improving their anticancer bioactivity, thus bringing a new horizon of chemotherapy.

2.3   Nanorobots for targeted therapy of cancer

Natural mechanical devices carry out critical tasks for cell function, including genetic information storage, DNA replication, intracellular transport, ion pumping, and cell motility. Inspired by nature, the artificial devices and machines on the molecular scale have been designed, constructed, and operated. The unique chemical and physical properties that enable biological macromolecules such as DNA and protein to serve as parts of natural devices, can also be utilized to construct artificial, robotic molecular structures, efficiently performing mechanical or computational tasks.

The field of structural DNA nanotechnology has been developed during the past decade, and DNA molecules can serve as building blocks for self-assembly of a wide range of nanostructures [23]. In particular, DNA origami is a unique approach that enables the rational design and production of DNA nanostructures with well-formed homogenous geometries, precise spatial addressability as well as marked biocompatibility [24]. The advances in structural design trigger the biological application of DNA nanostructures, especially utilizing them as drug delivery nanocarriers for cancer treatment. In contrast to traditional polymer-based or inorganic particle-based nanocarriers, DNA nanostructures with unique structural properties and excellent biocompatibility act as a considerable alternative for drug delivery to avoid undesirable side effects and maximize efficacy. The current progress in DNA origami-based drug delivery, such as DNA triangle or tube origami for doxorubicin delivery to

tumor cells [25] or xenografted mice [26], gold nanorod-DNA origami nanocomplex for therapeutic and diagnostic functions [27,28], DNA origami-based gene and chemotherapeutics combination therapy *in vivo* [29], have been reported.

Among all the available biomaterials, protein-based nanoparticles have been a brilliant target of investigation due to their magnificent structures and properties [30]. The naturally biocompatible protein nanocarriers have shown good biodegradability characteristics [30,31], thus showing low side effect and high safety. Those properties make them suitable targets for medical applications [32]. In addition, because of their container-like shapes and different amount of amphiphilicity which allow them to interact with both drug and solvent, protein-based nanoparticles are excellent vectors to deliver antitumor drugs [30,33]. There are various types of protein-based nanoparticles including animal proteins, plant proteins, and viral proteins [32,34]. Albumin and gelatin from animal proteins as well as phycocyanin from microalgae have been intensively investigated [35]. Recently, the researches on plant proteins and milk proteins have been commenced [33]. Protein-based nanoparticles consist of three particular interfaces, i.e. internal, external, and inter-subunit, which provide different targets of modification to design nanorobots [30]. By having the drug entrapped in the proteins, the drug's solubility and stability can be improved. These smart robotic systems have a great potential for drug delivery yet to be discovered [35].

As excellent building blocks for the design and construction of nanorobotics systems, DNA and protein molecules have been shown to sense, actuate and exert critical functions. In recent years, several DNA and protein-based robotic nanostructures have been utilized as imaging probes and cargo delivery vehicles in cultured cells [36], multicellular organisms [37], and insects [38]. Yet, effectively using nanorobots that can work as intelligent drug vehicles in mammals are still challenging. To pursue the goal of building nanorobots that can execute therapeutic functions efficiently and safely, the research groups in National Center for Nanoscience and Technology recently have described two distinct strategies for developing autonomous, programmable nanorobots for cancer therapy. In these work, self-assembly DNA [6] and protein nanorobots [39] have been constructed and injected into the diseased animals to find and destroy the life-threatening tumors.

For promoting tumor progression and metastasis, cancer cells create a microenvironment that is enriched in signals that are associated with angiogenesis. Depriving tumors of nutrients and oxygen by selective occlusion of tumor blood vessels and leaving tumor to "starve to death", have emerged as an attractive therapeutic goal in the treatment of cancer. Thrombin, a coagulation protease, is short-lived in the circulation and rapidly induces coagulation events. It has never

been used as an injectable vessel occluding agent in cancer therapy. With the objective of expanding the available tools for tumor vessel occlusion, Li *et al*. [6] developed the intelligent thrombin-loaded nanorobots based on DNA origami technique. The entire addressable origami nanostructure could organize the multiple therapeutic cargoes and tumor targeting ligands with rationally designed numbers and patterns. The tubular-shaped DNA origami nanorobot was constructed with thrombin positioned into its inner cavity, thus protecting the assembled molecular cargoes from being interfered with the external environment (Figure 3). The nanorobot was functionalized with nucleolin-specific DNA aptamers (AS1411) on the external surface due to the high expression of nucleolin on the surface of tumor endothelial cells. The attached DNA aptamers served not only for tumor targeting delivery but also for stimuli-responsive reconfiguration of this DNA nanorobot to reveal thrombin and activate coagulation at the tumor site. The intravenously injected DNA nanorobot was able to deliver thrombin specifically to the tumor-associated vessels, thereby initiating intravascular thrombosis and vessel occlusion. Importantly, the results in the mice bearing breast cancer, ovarian cancer, melanoma and lung cancer, confirmed that the thrombin delivery to the tumors via DNA nanorobot triggered tumor necrosis and tumor growth inhibition. In addition, the nanorobot has been proved to be safe and immunologically inert in normal mice and Bama miniature pigs, reasonably eliciting no detectable changes in blood coagulation parameters and histological morphology.

Chemotherapeutic agents affect the growing tumor cells by interfering with DNA synthesis, leading to the cell apoptosis. However, these drugs are not targeted, thus making them have severe adverse side effects on normal tissues [40]. One of the problems in cancer treatment is the hydrophobicity of most drugs and their insufficient delivery to the tumor sites. Generally, the liposomes and polymeric nanoparticles are used to load the drugs, but this method has its drawbacks such as difficulty in controlling their stability, rapid clearance by RES, as well as low safety and efficiency in clinical trials. As an emerging strategy, the natural proteins such as albumin are shown to improve the efficacy and safety of paclitaxel delivery [41]. In another study, another natural protein, GroEL, was also considered as an intelligent nanoparticle for delivering doxorubicin (DOX) into tumor cells [39]. There are two mechanisms of action that are proposed for DOX including the prevention of topoisomerase-II repair action and damage to cell membrane, DNA, and proteins by generating free radicals [42]. GroEL is an ATPase from chaperonin family with a double layer cage structure (Figure 4), which can enable GroEL to capture the antitumor drug. Once in the tumor site, GroEL was able to bind with plectin, a highly expressed cell structural protein in some cancer cells. In the presence of adequate ATP, GroEL was able to undergo a conformational change, thus causing an alteration in hydrophilicity of the inside section and subsequent release of DOX. It is thought that this nanorobot only binds to the surface of the cells and does not enter them, letting it escape the lysosomes, therefore avoiding the deletion of the nanoparticles. The *in vitro* and *in vivo* examinations further confirmed an efficient and specific delivery of the drug to the tumor site without immunogenicity [39].

Together, DNA origami and natural protein complex GroEL demonstrated how to take advantage of the intelligent properties of macromolecules to develop nanorobots that facilitated the delivery of the cargos for promoting anticancer activity. The design strategies of DNA origami nanoparticles and protein nanorobots enable the facile optimization for efficient therapy of various tumors. These aforementioned
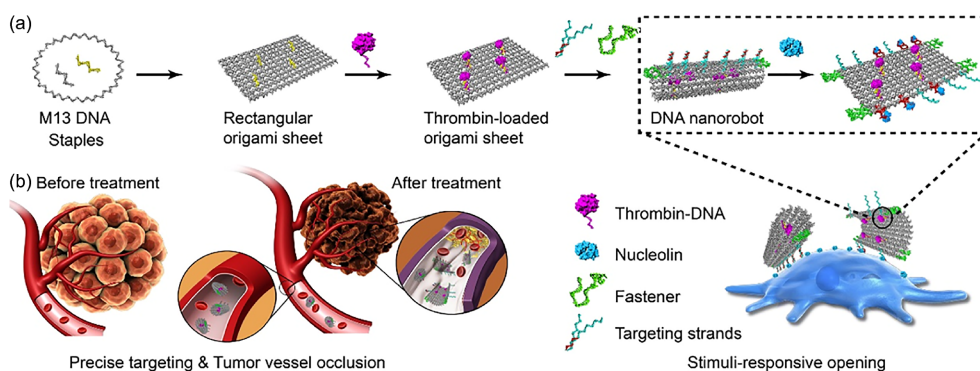

Figure 3 Schematic representation of the therapeutic mechanism of nanorobot-Th within tumor vessels. (a) DNA origami sheet is prepared by annealing the mixture of M13 DNA scaffold and staples strands. Thrombin molecules are arranged at four designated locations on the origami sheet. Addition of the fasteners and targeting strands results in the formation of thrombin-loaded, tubular DNA nanorobots with additional targeting aptamers at both ends. Closed nanorobot binds to tumor endothelial cells by recognizing the cell surface targeting protein, nucleolin, and the tube subsequently opens to expose the encapsulated thrombin. Thrombin induces a localized thrombosis by activating platelets and inducing fibrin generation. (b) DNA nanorobot-Thrombin was administrated to tumor xenografted mice by tail vein injection and targeted tumor-associated vessels to deliver thrombin. The nanorobot-Th binds to the vascular endothelium by recognizing nucleolin and opens to expose the encapsulated thrombin, which induces localized thromboses, tumor infarction and cell necrosis [6] (color online).
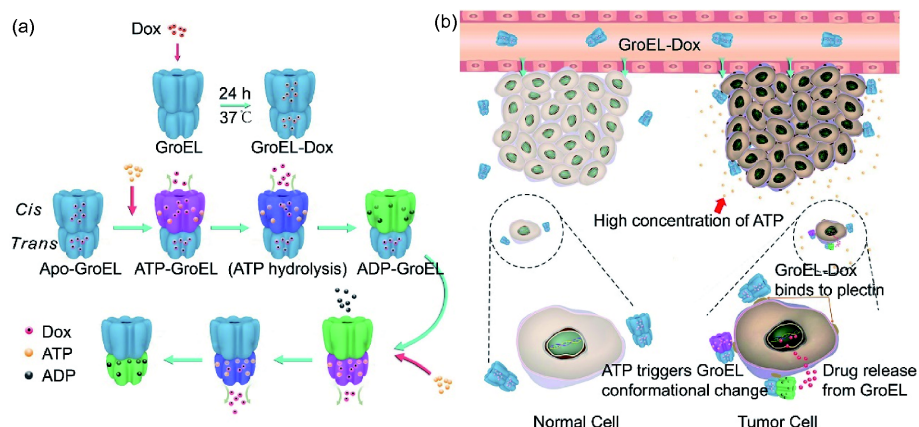
Figure 4 Schematic illustration of assembly and release of GroEL-DOX and their mechanism of action in tumor cells. (a) DOX is loaded into GroEL and ATP triggers its release from *cis* and *trans*-ring of GroEL by causing a conformational change. (b) When GroEL-DOX gets to the tumor vasculature, it enters tumor microenvironment. It can attach to plectin, which is highly expressed on the tumor cells and since there is an augmented level of ATP, a conformational change occurs to GroEL and as a final step DOX is released. It can pass through the lipophilic cell membrane and penetrate into the cell nucleus and commence apoptosis [39] (color online).

results demonstrate the advantages of nanorobotic systems for intelligent drug delivery, confirming that the nanomedicine might lead to successful exploration of more efficient cancer therapy. Although the drug-loaded nanorobots have not yet been translated into clinical application, they are currently under rapid development. Moreover, the multiple cargoes-loaded nanorobots could accomplish the ultimate goal of cancer therapy. We believe that therapeutic nanorobots that are multifunctional, highly tunable and biologically amenable, represent a powerful means to efficiently treat tumors.

2.4 ROS-responsive nanoparticles for the combination of chemotherapy and radiotherapy

Chemotherapy and radiotherapy are two mainstream treatment modalities in cancer management. Chemotherapy represents a popular cancer treatment method using chemotherapeutic agents, while the radiotherapy uses the ionizing radiation to control or kill malignant cells. Although these conventional cancer therapies show reasonable efficacy in various kinds of cancers, their low efficiency and severe side effects still limit their development, thus calling for new strategies in cancer treatment [43–45]. The combination of chemotherapy and radiotherapy exhibits improved therapeutic outcomes, thus receiving much attention in both basic research and clinical translation [46,47]. In radiotherapy, the ionizing radiation is introduced to kill cancer cells directly by damaging DNA and indirectly by generating free radicals. Among the ionizing radiations, γ-radiation is one of the most widely used due to its strong power and deep penetration [48,49]. Exposure to γ-radiation can induce the ROS production and cause cell apoptosis [50]. Xu and Zhang *et al.* [51] proposed the concept that ROS produced by γ-radiation might trigger the response of ROS-responsive drug

delivery vehicles. If anticancer drugs are loaded in such smart delivery vehicles, they are able to be released at the site of irradiation. Thus, the combination of chemotherapy and radiotherapy can consequently be achieved. Since the severe side effects of γ-radiation limit the dosage of irradiation in clinical applications, the delivery vehicles need to be ultrasensitive to ROS.

Xu and Zhang *et al.* [52] have demonstrated that diselenide bonds are ultra-sensitive to both oxidation and reduction stimuli. Taking advantage of this unique property, a positively charged diselenide-containing block copolymer was designed to fabricate a γ-radiation-responsive hydrogel by the complexation with a peptide amphiphile [53]. The hydrogel was constructed by long crosslinked nanofiber networks. Under 0.5 kGy γ-radiation, ROS produced by radiation cleaved the diselenide bonds on the backbone of this block copolymer. Then, the long fibers in the networks were broken into short fragments, and then the hydrogel was disrupted, resulting in a γ-radiation-induced gel-sol transition. In contrast, a disulfide-containing block copolymer hydrogel with similar structure was still intact under 5 kGy γ-radiation, demonstrating the ultra-sensitivity of diselenide bonds. However, 0.5 kGy is still a relatively high dosage for human bodies. Therefore, the systems that are more sensitive to γ-radiation are urgently desired.

In the hydrogel, ROS diffusion is restricted by the densely crosslinked nanofiber networks. Hence, it is hard for ROS to break diselenide bonds buried inside the hydrogel, resulting in a less sensitivity to γ-radiation. If diselenide bonds can be exposed in an aqueous solution, they might become more sensitive to γ-radiation. Based on this hypothesis, the diselenide-containing polymeric micelles were prepared as the γ-radiation-responsive nanoparticles. The polymeric micelles were able to release DOX under γ-radiation as low as 5 Gy (Figure 5) [54]. This γ-radiation-responsive property
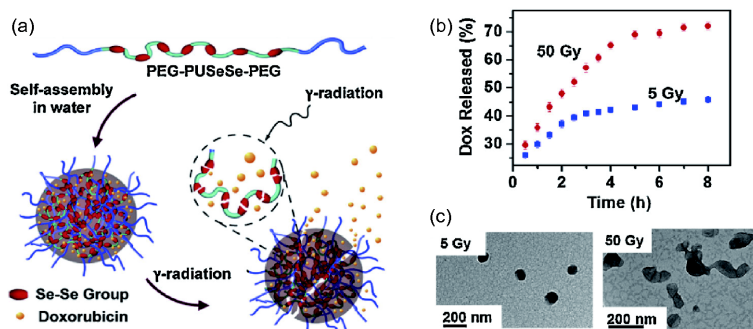
Figure 5 Diselenide-containing polymeric micelles loaded with Dox responded to γ-radiation as low as 5 Gy. (a) Schematic illustration of γ-radiation responsive release of Dox; (b) release profile of polymeric micelles under different doses of γ-radiation; (c) TEM figures showed morphology of polymeric micelles after different doses of γ-radiation [54] (color online).

could be observed using transmission electron microscope (TEM) imaging and DOX release experiment. Under 5 Gy radiation, the micelles swelled slightly and released about 45% DOX in 6 h. When the dose was increased to 50 Gy, the micelles were partly collapsed into irregular aggregates, followed by the release of more than 70% DOX in 6 h. When the dose reached 500 Gy, the micelles were completely collapsed and released most of the loaded DOX.

5 Gy is a low dosage closed to the clinical dosage. However, it would be preferable if the dosage can be further decreased to 2 Gy, which is the dosage received by a patient for one day in real clinical radiotherapy. Hence, more sensitive materials to ROS are highly demanded. A tellurium-containing polymeric micelle system was reported, and this system was found to respond to a low concentration of ROS or low dose of γ-radiation (Figure 6) [55]. The tellurium-containing molecules showed a lower oxidative potential than that of selenium-containing molecules with similar structures, revealing a preferable sensitivity to oxidation stimuli. The tellurium-containing micelles swelled from 40 to 250 nm after γ-radiation as low as 2 Gy, thereby showing a great potential for clinical applications.

Nanoparticles that combine chemotherapy with radiotherapy to achieve preferable therapeutic efficacy has been explored for many years. However, ROS-responsive materials are seldom introduced into this area. Sensitivity of drug delivery vehicles to ROS is one of the main obstacles, because the ROS level generated by radiation is in a low level. In recent years, diselenide bonds and tellurium were found to be ultra-sensitive to ROS. The development of diselenide- and tellurium-containing polymers not only proposes an idea to make use of ROS generated in radiotherapy, but also pushes forward the applications of ROS-responsive nanoparticles in combination of chemotherapy and radiotherapy.

2.5 *In vivo* self-assembled nanostructures for nanomedicine

Nanomedicine utilizes the remarkable properties of self-as-

sembled nanomaterials for the diagnosis, treatment, and prevention of diseases [56–58]. Although self-assembled nanomaterials show significant therapeutic advantages for various of biomedical applications, their clinical translation has not progressed as rapid as the plethora of positive preclinical results [59–61]. Low bioavailability [62,63], and potential toxicity [64,65] have been considered as a main barrier that restricts their clinical translation. Firstly, the delivery efficiency *in vitro* is not equal to the delivery efficiency *in vivo*, which usually depends on the overall efficiency of four processes including circulation, penetration, influx and release. Secondly, the *in vitro* experiments are difficult to truly reflect the process *in vivo*. In spite of the self-assembled nanoparticles in the thermodynamic equilibrium [66], their structures [62], morphologies [67] and functionalities [63], might be changed upon exposure to biological fluids such as plasma and biointerface. In addition, the potential toxicity of nanoparticles is always the focus of attention [65,68,69]. Although efforts in some aspects have met with various of success [70], it is still difficult to balance all aspects at the same time [63]. Interestingly, the recent findings in biology have provided the exciting insights for constructing nanostructures by *in vivo* self-assembly for applications in nanomedicine. Recently, the concept of "*in vivo* self-assembly" that means a well-ordered self-assembly of nanoparticles from exogenous molecules in bio-environments (e.g., cells, tissues and living animals) with nature-mimicking biological functions has been demonstrated (Figure 7) [71–79]. This new strategy displays enhanced effectiveness of diagnosis and treatment with the significant improvement of the pathological specificity and bioavailability [71–79]. Owing to these advantages, the development of *in vivo* self-assembled nanostructures in cancer nanomedicine has been attracted widespread attention. The design and assembly methods of *in vivo* self-assembled nanostructures are thus described for their biological applications.

The *in vivo* self-assembled nanoparticles combine the advantages of nanomaterials and small molecules to improve the bioavailability of bioactive molecules while reducing
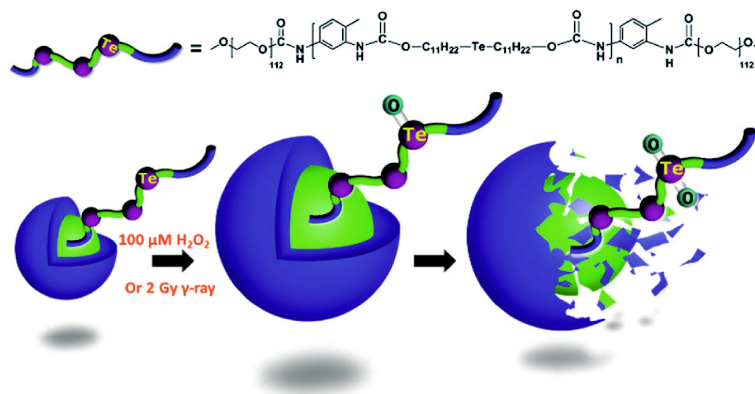
Figure 6   Tellurium-containing polymeric micelles respond to low concentration of ROS or low dose of γ-radiation [55] (color online).
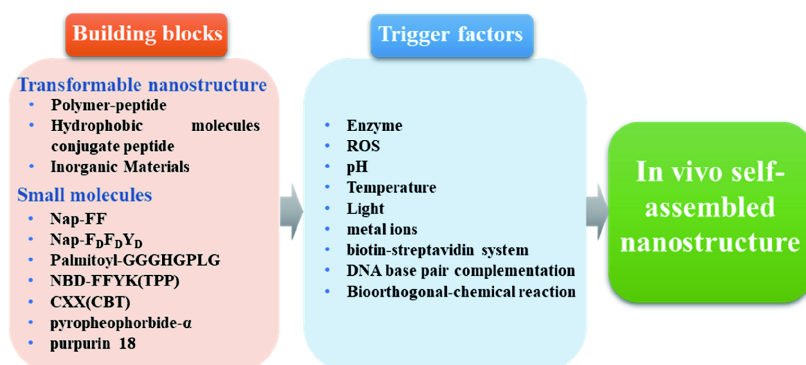

Figure 7   Schematic illustration of the design of *in vivo* self-assembled nanostructures in physiological environment, in which the building blocks and triggering factors are two important components (color online).

systemic toxicity. These nanoparticles are adapt to the complex physiological environment, thereby resulting in a preferable design for simulating the function of biological macromolecules.

In vivo self-assembly of transformable nanostructures have significant value for *in vivo* delivery and detection strategies where surface chemistry and morphology play the critical roles in determining the targeting and pharmacokinetics of nanostructures [80]. This strategy could evidently improve the bioavailability of drugs and contrast agents [75]. As we know, the self-assembled nanostructures are constructed through the noncovalent or intermolecular forces (e.g. π-π stacking, electrostatic interactions, hydrogen bonding, and van der Waals forces) [81]. The morphology of nanoparticles could be transformed by changing these forces as well.

At present, there are several factors that are used to trigger the morphology transformation *in situ*. Among those, pH, ROS [82], enzymes [72, 74, 80], metal ions [67], light [83] and temperature [78], have been applied to change the hydrophilic-hydrophobic balance of the nanoparticles in response to tumor microenvironment. Some nanoparticles are able to achieve the controlled morphology changes, such as changing from nanoparticles to nanofibers [75] or from mi-

crosphere to nanosphere [84,85]. For instance, the self-assembled polymer-peptide nanoparticles were designed to transform into the nanofibers, which exhibited high efficient antibacterial activity for multivalent cooperative interactions with bacterial membranes by enzyme-triggering in infectious site [74]. In addition, the bis-pyrene-peptide was found to achieve the *in situ* morphological transformation by regulating π-π interaction and intermolecular hydrogen bonding [72], thereby displaying obvious advantages in inhibiting tumor metastasis [72] and treatment [75]. Another main factor that can trigger the morphology transformation is the intermolecular recognition such as biotin-streptavidin system [86], DNA base pair complementation [87], and chemical reaction-mediated covalent cross-linking in tumor environmental [88]. Many units are aggregated together without a specific self-assembled structure. The cross-linked aggregates "chemically lock" were found to reduce the IC_{50} value of paclitaxel by 124 times in comparison to that of paclitaxel itself, and also help in reducing multidrug resistance [88]. As a result, the transformable nanoparticles in the lesions could be significantly enriched, together with prolonged resident time, thus improving the diagnosis and treatment of diseases.

In vivo self-assembly of small molecules exhibits unique properties in the diagnosis and treatment of diseases due to combining the advantages of small molecules and nanoparticles. This strategy not only shows the deep penetration of small molecules, but also shows the high accumulation and long-term retention of nanoparticles, while also reducing the potential long-term toxicity of metabolic organs. *In vivo* self-assembly of exogenous small molecules has more challenge than *in vivo* self-assembly of transformable nanoparticles. The major challenge remains in controlling the small molecules from monomer to self-assembly in complex and dynamic physiological environment.

Currently, there were two types of building blocks used for the *in vivo* self-assembly. The most used building blocks include peptides [89–91], which are biocompatible and easy to be regulated by triggering of tumor microenvironment [92]. For example, an intracellular enzyme-catalyzed polymerization approach was demonstrated for efficient synthesis of polypeptide monomer and *in situ* self-assembly of topology-controlled nanostructures [78]. Another type of building blocks includes π conjugated aromatic dye molecules with assembly behaviour, such as pyropheophorbide-α [73], and purpurin 18 [76]. A responsive small-molecule that was self-assembled into the nanofibers in tumor site, exhibited the assembly-induced retention (AIR) effect, thus causing enhanced photoacoustic imaging and tumor therapeutic efficacy (Figure 8) [76]. Moreover, the recent researches in biology also provide some new insights on the assemblies of small molecules for modulating essential cellular processes [93]. All above evidences show a potential value of the *in vivo* self-assembly of small molecules for the diagnosis and treatment of diseases.

The *in vivo* self-assembled nanostructures have been a subject of utmost fundamental interest in recent years, in which its construction rules are established towards functional nanoparticles *in vivo* with novel properties. The fundamental understanding of self-assembly in complex and dynamically physiological environments is still encountered with many challenges. Firstly, it is well known that most macromolecules in living organisms are self-assembled by a variety of intermolecular forces. Therefore, a high-level self-assembly with good biological functions through the synergy of multiple intermolecular forces also need to be constructed. Secondly, the structure of self-assembly is critical for achieving their functions. As a result, a deep understanding of the assembly mechanism is urgently desired to build a precise assembly structure *in vivo*. Thirdly, it is still difficult to *in-situ* characterize the refined structure of the assembly, which can contribute to the understanding of the relationship between structure and their function. Briefly, the *in vivo* self-assembly acts as a very promising approach for cancer therapy, which deserves to work together for in-depth exploration in future.

2.6   Protein nanoreactors for cancer theranostics

Proteins, with superior nature of biocompatible, biodegradable and low-immunogenic properties, have been extensively utilized for the construction of functional nanoparticles for cancer theranostics [33]. To date, several methods are applied to fabricate protein-based nanomedicine, including non-covalent encapsulation, covalent protein-drug conjugates, as well as *in situ* biomineralization using proteins as nanocage templates. Several types of proteins including bovine serum albumin, human serum albumin and ferritin have been reported to bind a variety of metal ions such as Cu^{2+} and Fe^{2+} for specific physiological or pathological process, reasonably due to their various metal binding sites such as cysteine residues, N-terminal amine, and multi-metal binding sites [94]. In particular, some of
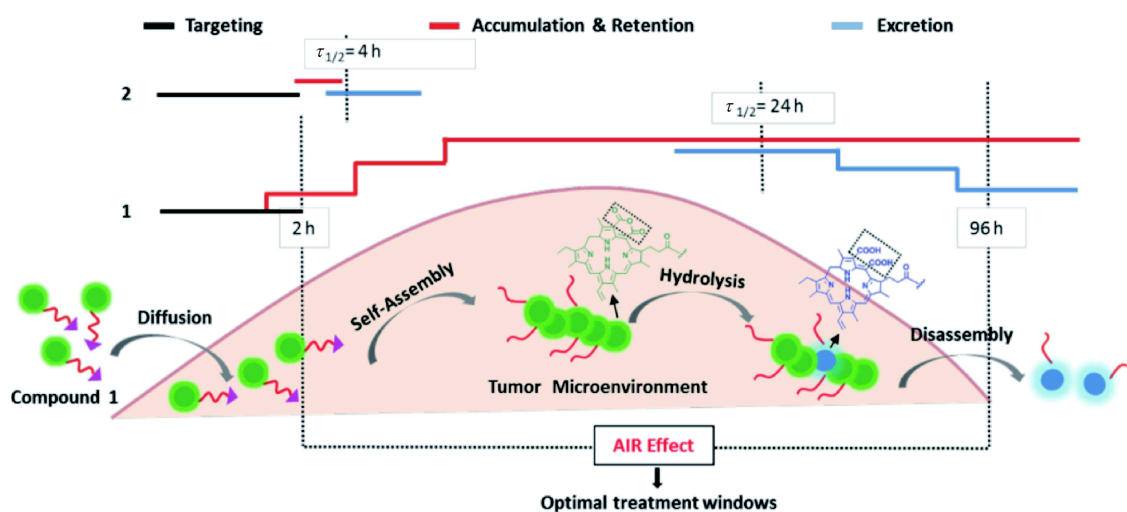

Figure 8   The schematic illustration of the AIR effect of compound **1** in tumor site compared with compound **2**, which was quickly excreted from the tumor [76] (color online).

these protein molecules might show an expanded conformation of hollow nanocages in acidic or basic solution, due to their excessive charged groups and molecular chain flexibility at unfolded status [95–97]. Thus, these expanded protein molecules with hollow cavities have been exploited as protein-templated nanoreactors, thereby facilitating the construction of metal or metal chalcogenide nanocrystals inside protein nanocages. Reasonably, the protein nanocages as the nanoreactor template have been recently explored to achieve cancer-targeted drug delivery in cancer nanomedicine. The protein-templated synthesis process includes the binding of metal ions within protein hollow cavities, controlled growth of imaging or therapeutic inorganic nanocrystals through reduction or precipitation reaction, as well as susbseqeunt purification [98–101]. The protein-templated nanoreactor shows versatile advantages including precisely controlled synthesis in mild condition, monodispersed size distribution, prolonged circulation time, preferable tumor accumulation, and significantly increased cellular uptake for improving imaging or therapeutic performance.

Albumin is one of the most abundant plasma proteins, which plays a key role for endogenous compound transportation. Human serum albumin (HSA) is widely applied as efficient drug nanocarrier for encapsulations of chemotherapeutic drugs [102–106], anti-inflammatory drugs [107–111], and others [112,113], which could significantly improve their pharmacokinetics and efficacy as well as reduce adverse side effects. The first clinically approved nanoscale HSA-based formulation, Abraxane, has been approved by the Food and Drug Administration (FDA) in 2005, and this formulation was fabricated by loading anticancer drug paclitaxel (PTX) within HSA to generate the protein nanoparticles (ca. 130 nm) for enhanced therapeutic efficacy and decreased incidence of serious toxicities [114]. Furthermore, several Abraxane-like nanoparticles have been developed through encapsulation of docetaxel, rapamycin and cisplatin using HSA, thus indicating the crucial role of albumin for highly efficient drug delivery [115,116]. More importantly, albumin is capable to act as single molecule nanoreactor to facilitate the protein-templated synthesis of various functional nanoclusters or nanocrystals for efficient cancer imaging and therapy. For instance, Au nanoclusters have been developed via a biomineralization process using bovine serum albumin as bioinspired template and reduction agent, in which Au(III) ions were bound within albumin molecules, followed by adjusting pH to ~12 to activate the reduction potential of albumin molecules and induce progressive reduction to generate Au nanoclusters *in situ* for cell imaging [98,117]. Similar reduction process using albumin-templated nanoreactor was also used to construct ultrasmall chelator-free radioactive [^{64}Cu]Cu nanoclusters with high radiolabeling stability, leading to highly sensitive positron emission tomography (PET) imaging [118]. Nevertheless,

these nanoclusters synthesized from albumin nanoreactor could achieve prolonged blood pool circulation, but still suffer from poor tumor targeting capacity due to their extremely small size. Thus, a major challenge still remains in exploring a controlled synthesis method using protein nanoreactor for cancer-targeted nanomedicine.

As magnetic resonance imaging (MRI) contrast agent, gadolinium oxide nanoparticles have been reported to have the better proton relaxivity than clinically used gadolinium chelates, which might be attributed to the overall relaxation effect of both surface and interior gadolinium on water proton through their high cooperativity [99,119–123]. Therefore, using protein nanoreactor, size-tunable Gd_2O_3 nanocrystals were synthesized through precisely controlled nanoprecipitation reaction by tuning several factors such as Gd^{3+} ions concentration, reaction temperature, pH and time [124]. The resulted Gd_2O_3 nanocrystals with an average diameter of up to ~13.5 nm had the longitudinal relaxivity as high as ~12.0 $mM^{-1} s^{-1}$, showing a 4-fold increase when compared with Gd-DTPA (3.2 $mM^{-1} s^{-1}$), and then leading to the preferrable tumor accumulation and distinctly enhanced contrast [124]. Moreover, the controlled synthesis via albumin nanoreactor can be also applied to construct various semiconductor nanocrystals, through nanoprecipitation reaction within albumin after binding of transition metal ions (e.g. Cu^{2+}, Co^{2+}, Ni^{2+}, Bi^{2+}) and noble metal ion (e.g. Ag^+) (Figure 9) [125–129]. For instance, the protein-ion complexes were formed by introducing metal ions within albumin solution at basic environment, followed by adding S^{2-} ions to induce the nucleation and growth of metal sulfide nanocrystals through nanoprecipitation reaction inside the cavity of albumin [125–127]. These metal sulfide nanocrystals showed the size-dependent physicochemical properties such as enhanced photothermal conversions for potent tumor hyperthermia, optimal NIR-II fluorescence for tumor illuminating, as well as improved X-ray attenuation for CT contrast imaging. Besides, some functional molecules such as near-infrared (NIR) fluorescence dye (Cy7.5), photothermal Cypate, or radionuclide (^{99m}Tc) can be further conjugated on the surface of protein nanoreactors for additional cancer imaging or therapy [125,128–130], allowing albumin nanoreactor to act as a general and versatile nanoplatform for multifunctional nanotheranostics.

Moreover, the morphology of nanomaterials could also be controlled using albumin nanoreactor. Zero-dimensional Te nanodots, instead of thermodynamically preferable one-dimensional Te nanostructures, were constructed in the restricted space in the cavity of albumin nanoreactor through reduction process of entrapped TeO_3^{2-} by $NaBH_4$. The resulted Te nanodots within albumin generated both photothermal effect through non-radiative relaxation and abundant ROS under NIR light exposure, showing a preferable photoinduced synergistic cancer therapeutic efficacy [131]. In
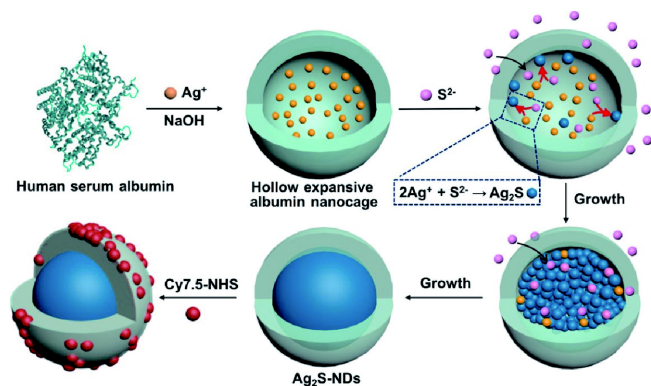
Figure 9 Schematic illustration of theranostic Ag_2S nanodots generated via albumin-templated nanoreactor method [126] (color online).

addition, two simultaneous precipitation reactions were able to be induced within the single albumin nanocages to generate hybrid nanoparticles such as Gd_2O_3/CuS nanocrystals [125,132] and Gd_2O_3/Au hybrid nanoprobe [133] through a facile one-pot synthetic process, reasonably indicating the rational role of albumin nanoreactor for multifunctional nanoparticles in a controllable and facile way.

Multi-subunit proteins such as ferritins (24 subunits) can provide "natural" nanoscale hollow spherical cavity with 8–9 nm internal diameter as a nanoreactor to synthesize various functional nanoparticles [134–139]. Ferritin nanoreactor has been utilized to generate manganese oxide nanoparticles [140,141], cadmium sulphide quantum dots [142], uranyl oxide nanoparticles [134], cobalt platinum nanoparticles [143], and magnetic mineral magnetite, in addition to the storage of several multi-nuclear metal nanoclusters [144]. In the aspect of nanomedicine application, aqueous PbS quantum dots were constructed through nanoprecipitation of Pb^{2+} by S^{2-} in the hollow cavity of horse spleen apoferritin for NIR fluorescent imaging [145]. Similar approach was used to synthesize biocompatible Au-Ft nanocomplex, showing tremendously improved fluorescence with red-shifted and tunable emissions for targeted cancer imaging [101,146]. Additionally, MRI contrast agents based on Mn(III) oxyhydroxide and iron oxide nanoparticles were also developed via ferritin-templated nanoreactor method for enhancing MR imaging *in vivo* and visualizing tumor tissues via peroxidase activity of iron oxide [140,141,147,148]. The CuS semiconductor nanodots were synthesized inside ferritin nanoreactor with radioactive incorporation of ^{64}Cu for PET/ photoacoustic (PA) dual-modal imaging, as well as effective photothermal tumor ablation (Figure 10) [149]. The cobalt-doped ferritin magnetic nanoparticles were also fabricated for cancer hyperthermia under alternating magnetic field, thus generating preferable hyperthermal efficiency to achieve distinct anticancer efficacy upon exposure to the alternating magnetic field [150]. Thus, the ferritin nanoreactor shows a great potential for multifunctional cancer
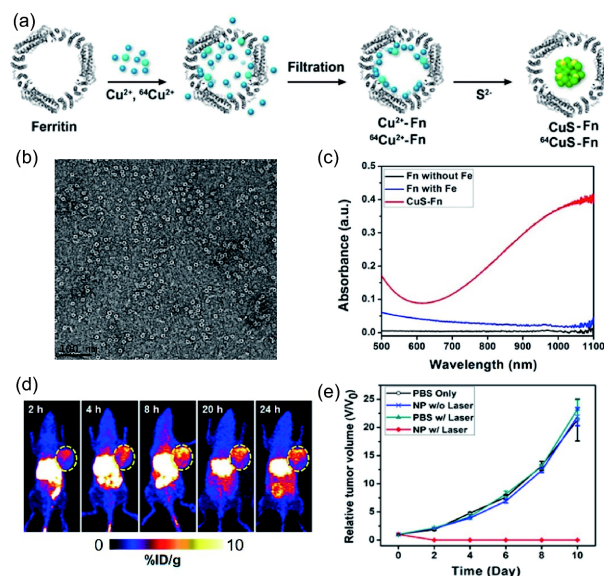

Figure 10 Ferritin caging CuS nanoparticles for efficient cancer theranostics. (a) Synthetic process of Ferritin caging CuS nanoparticles (CuS-Fn NCs) via nanoreactor method; (b) TEM images of CuS-Fn NCs with negative staining; (c) UV-Vis absorbance spectra of Fn without iron, Fn and CuS-Fn NCs; (d) PET images of tumor bearing mice at 2, 4, 8, 20, and 24 h post-injection of CuS-Fn NCs; (e) tumor growth profiles of the mice suffering from different treatments [149] (color online).

nanomedicine.

Another natural nanocage is provided by viral capsids, the assembly of protein subunits, which offers robust and monodispersed cavities for potential construction of nanoparticles [151–153]. The inorganic nanocrystals were achieved through a biomineralization reaction in the hollow inner space of cowpea chlorotic mottle virus (CCMV) capsids, which consists of 180 coat protein subunits of 20 kDa each, with an outer diameter of 28 nm and an inner diameter of 18 nm [151]. The nanocrystalization of tungstate (WO_2^{4-}) and vanadate ($V_{10}O_{28}^{6-}$) inside the capsid was successfully induced to generate monodisperse nanoparticles with an average diameter of 15 nm [154]. Similar fabrication processes were also applied to synthesize monodisperse iron oxide nanoparticles of 24 nm for potential MRI [155], and TiO_2 nanoparticles with photocatalytic activity [156]. In particular, the photo-initiated reaction within the cavity of CCMV could be used for generation of Prussian blue nanoparticles with an average diameter of ~18 nm [157]. In the preparation process, negatively charged $[Fe(C_2O_4)_3]^{3-}$ ions were firstly entrapped in the interior space of CCMV capsid and then reduced to Fe(II) ions after photoreduction, followed by further reaction with encapsulated $[FeCN6]^{3-}$ to construct the Prussian blue nanoclusters (Figure 11) for possible photothermal therapeutics. Several other viral capsids including bacteriophage T7 [158], bacteriophage MS2 [159], and rod-shaped tobacco mosaic virus (TMV) [160–163] can also be utilized as the nanoreactors for controlled synthesis of various functional nanoparticles and nanowires,
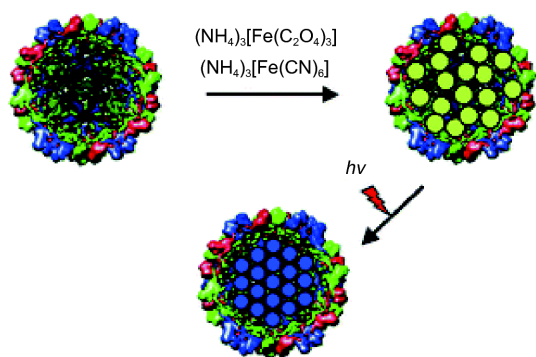
Figure 11 Schematic illustration of Prussian blue nanoparticles inside CCMV capsid [157] (color online).

demonstrating a great potential in virus capsid-templated nanoparticles for cancer nanomedicine.

To date, the protein nanoreactors have been developed to generate various well-defined functional nanoparticles with small size in a facile, mild, and controlled manner, showing a great potential in cellular uptake and tumor accumulation for cancer imaging, therapy, or theranostics. However, more efforts should be also devoted into the development of protein nanoreactors with some new biomineralization mechanisms, which allow organic anticancer compounds to form nanoparticles within protein nanocages for their cancer-targeted delivery. It is concluded that the protein nanoreactor strategy provides a valuable paradigm to improve the applicability and performance of protein nanoparticles for efficient cancer nanomedicine.

3 Nanoparticles for cancer diagnosis/imaging

Highly efficient diagnostic or imaging agents can accurately detect biomolecules in tumor site or provide precise tumor localization, thereby offering effective early diagnosis and therapeutic monitoring for precise cancer therapy and management. In this review, we summarize a few types of nanoparticles for intelligent cancer diagnosis including nucleic acid nanostructures, fluorescence nanoprobes, radionuclide nanoparticles, and quantum dots, which are able to effectively to provide considerable guidance for intelligent cancer therapy.

3.1 Nucleic acid-based nanostructures for cancer management

Cancer is a leading cause of mortality worldwide [164,165], and the researchers have already advanced the use of nanoparticles as a promising platform for cancer nanomedicine [166,167]. Specifically, nucleic acid (NA), with its positive biocompatibility, biodegradability and unparalleled programmability, has been exploited for its application in per-

sonalized cancer treatment. With an understanding of the nature of NA molecules, many techniques have been developed to build NA-based materials such as hybridization chain reaction (HCR), rolling circle amplification (RCA), origami, strand displacement reaction (SDR), and enzymatic replication [168]. These techniques show that NA molecules can provide various structures with multifunctional applications. Among these structures, programmable DNA-based nanostructures, including nucleic acid nanoflowers and nanospheres, nucleic acid nanohydrogels, spherical nucleic acids, nucleic acid micelles and nucleic acid-based metal-organic framework, have recently drawn broad attention for cancer nanomedicine (Figure 12).

Many programmable DNA-based nanostructures have been built to accurately detect biomolecules *in vivo*, providing a rich resource for investigating physiological processes at the cellular level. In 2017, for example, Tan group [169] developed an intracellular DNA nanoprobe to accurately image tumor-related mRNA. This probe could alter its structure in the presence of the target mRNA, virtually eliminating false-positive signals. A three-dimensional (3D) DNA amplifier (Figure 13) [170] and 3D DNA logic gate triangular prism (Figure 14) [171], have also been constructed to target tumor cell biomarkers.

To resolve some drawbacks in Watson-Crick base-pairing among small DNA building blocks, the noncanonical self-assembled nanoflower with densely packed DNA was engineered using RCR. DNA matrix, a constituent of the nanoflower, has been further modified with different dyes, thereby providing a platform that is able to perform multi-fluorescence emission at a single-wavelength excitation for multiplex fluorescent cellular imaging [172,173]. Lee *et al.* [174] combined several functional biomolecules with DNA nanospheres (DNANSs), which were produced by rolling circle amplification (RCA) with several functionalized dNTPs. After being stained by DNA-specific dyes, the self-assembled DNANSs were used as a barcode to detect tumor cells circulating in the bloodstream. However, DNANSs had a size range of 600–700 nm, thus limiting their advanced biological applications *in vivo*. Recently, inspired by Watson-Crick base-pairing between DNA strands and liquid crystal phases from duplex DNA, Bi group [175] synthesized the uniform NA nanospheres with about 200 nm in diameter. Different from previous work, only four strands were necessary in these assemblies, and the remaining overhangs were used as a tool to combine functional groups with the nanospheres, such as fluorophores and aptamers.

The hydrogels with high payload capacity have been explored for biotechnological and biomedical applications such as biosensors. However, these hydrogels have some intrinsic drawbacks including lack of controllability and bulky size. To address this issue, Tan group [176] presented a stimuli-responsive DNA nanogel with controllable release for tar-
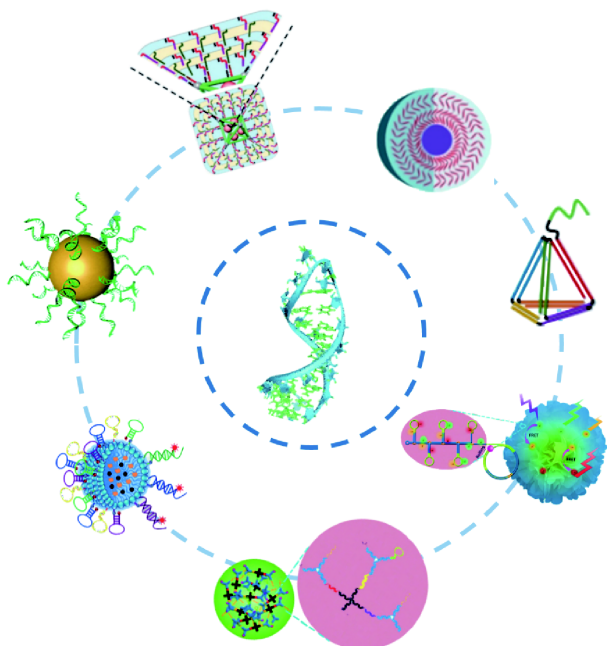
Figure 12   Schematic illustration of various nucleic acid-based nanostructures (color online).
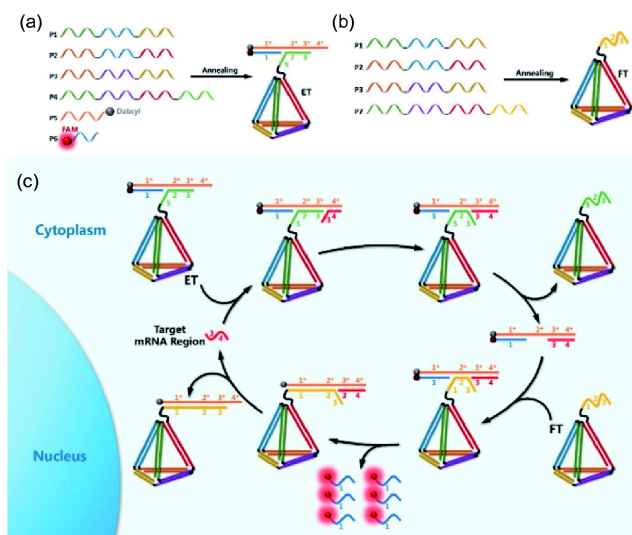

Figure 13   Assembly of the ET module (a) and the FT module (b); (c) mechanism of EDTD for catalytic signal enhancement of specific mRNA expression in living cells [170] (color online).

geted gene therapy. These DNA nanohydrogels were able to be degraded by glutathione (GSH) in the intracellular environment, thus leading to the disulfide cleavage in the nanohydrogels and subsequent controllable release of therapeutic genes, cell-specific DNA aptamers, as the targeting recognition molecules. Zhang *et al*. [177] synthesized water-soluble DNA-grafted polycaprolactone (DNA-g-PCL) brushes. Differed from spherical NAs (SNAs) and DNA tetrahedrons reported in previous studies, two novel structural units, consisting of DNA-g-PCL framework and a
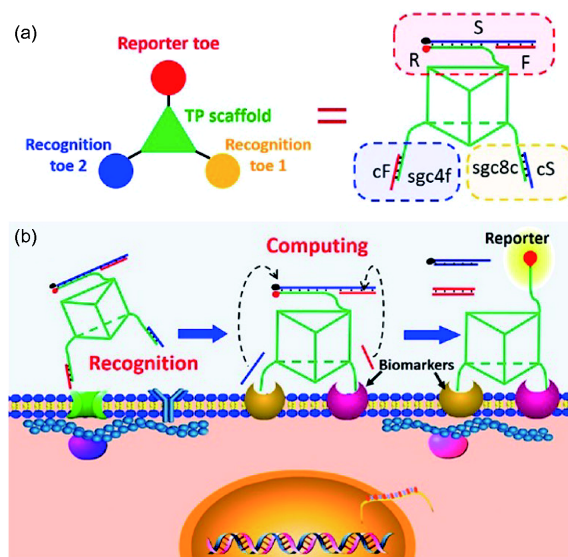

Figure 14   Working principle of DNA engineered nanomachine. (a) Structural diagram of DNA-logic gate TP nanomachine, which contains reporter toe, recognition toe 1, recognition toe 2 and DNA TP scaffold. Strand cS is completely complementary to strand S and a piece of sgc8c, whereas strand cF is completely complementary to strand F and a piece of sgc4f. (b) Scheme of aptamer-based 3D DNA nanomachine for targeted cell surface computing. Two aptamers recognize and bind to their membrane biomarkers, thus releasing cS and cF from respective recognition toes. Driven by DNA strand displacement reaction, the fluorescence signal in reporter toe switches to "ON" from its original quenched (OFF) state [171] (color online).

single chain linker with siRNA, were designed. By changing the ratio of siRNA-L and DNA, the nanogel was assembled with tunable size. Thus, with an SNA-like structure, the stability and efficiency of cellular uptake was enhanced, providing an advanced platform for effective siRNA delivery to tumor microenvironment.

Willner *et al*. engineered a structure consisting of a metal-organic framework (MOF) with NA strands. To address the basic limitations of inorganic materials, including low loading capacity and background leakage, MOF nanoparticles were modified with NA-based stimuli-responsive hydrogels. Then, when the nanoparticles entered the tumor and encountered the overexpression of ATP, the coated hydrogels were degraded through the formation of an aptamer-ATP complex. This construct showed effective drug loading and controllable release of payload [178,179].

Since 1996, Mirkin *et al*. [180] have extensively explored SNAs, especially in biological applications. They designed the core structure of SNAs with AuNPs, AgNPs, iron oxide, quantum dots, silica and Buckminsterfullerene C_{60}. These inorganic cores have been further modified with highly functional oligonucleotides for monitoring, spacing and linking chemical groups for avoiding nuclease degradation [181]. SNAs exhibited different levels of cellular uptake by changing the surface density of DNA, demonstrating a potent and nontoxic platform for gene regulation without the ne-

cessity of a transfection agent, both *in vivo* and *in vitro* [182,183]. In order to evaluate the therapeutic efficiency of siRNA-SNA, Mirkin *et al.* also generated a gold-based nanomaterial functionalized with siRNA oligonucleotides, which were targeted to the iRFP670-O^6-methylguanine DNA methyltransferase (MGMT) fusion protein expressed in orthotopic glioblastoma multiforme tumors. The NIR protein (iRFP670) was used to visualize and quantify the expression of oncoproteins in tumor tissue in real time, thus conferring SNAs with therapeutic capability. Zhang and Gao *et al.* [184] have combined SNAs with precisely engineered molecular beacons for imaging *in vivo*.

Micellar structures have been introduced as a potential drug carrier owing to their hydrophobic core. The amphiphilic DNA block copolymer, which forms the micelles in aqueous solution like other amphiphilic copolymers, has drawn a close attention [185,186]. Tan group [187] designed a self-assembled aptamer-micelle nanostructure to target various tumor cells for precisely delivering drug payloads, providing an integrative therapeutic treatment. Moreover, the amphiphilic micelles have been designed as a potential co-delivery carrier for two drugs with different solubility, thereby showing enhanced antitumor efficacy as compared to individual drugs. An anti-MDR1 molecular beacon (MB)-based micelle has also been developed with further functionalization of NA. This all-in-one system is an excellent platform for monitoring and silencing MDR1 mRNA, as well as programmed release of doxorubicin [188]. Tan group [189] have recently developed the lipid-conjugated floxuridine (a pyrimidine analog that inhibits the S-phase) homomeric oligonucleotide (LFU20) micelles, which could be inserted into albumin to form a LFU20/albumin complex after intravenous injection, thereby offering advanced therapeutic efficacy.

Over the past few decades, an increased interest in the development of NA constructs has been received for cancer nanomedicine, resulting in effective cancer detection, advanced anticancer efficacy, and imaging-guided treatment. NA-based nanomedicine with stable and controllable nanostructures is considered as the emerging candidate for monitoring, targeting, and delivering drug payloads through responding to exogenous or intrinsic stimuli, and provide an insightful tool for intelligent cancer nanomedicine.

3.2   High-contrast nanoprobes for fluorescence imaging of cancer

Early diagnosis of cancer is crucial for the treatment outcome of patients. Molecular imaging has provided a non-invasive method for cancer diagnosis [190,191]. The widely used molecular imaging methods include MRI, positron emission tomography (PET), single-photon emission computed tomography (SPECT), and ultrasound imaging. These methods

are limited by their intrinsic disadvantages, such as insufficient spatial resolution and detection sensitivity, involvement of radiation, and high cost [192,193]. In comparison, optical imaging is a low cost and non-radiative imaging modality [194]. Fluorescent probes have shown a great potential in the *in vitro* detection of analytes. Recently, the development of NIR fluorescent probes has demonstrated their advantages of optical imaging for *in vivo* applications [195,196]. For cancer diagnosis, smart fluorescent probes have been developed according to a variety of specific recognition mechanisms, including targeting cancer biomarkers, recognizing whole cancer cells, and sensing tumor-specific microenvironment.

Cancer cells differ from normal cells in the over-expression of a series of biomarkers. By developing fluorescent probes that can specifically bind to the biomarkers or change their fluorescence signals upon response to the biomarkers, the detection of cancer cells by optical imaging can be enabled. Cyclooxygenase-2 (COX-2) is absent or low expressed in most normal cells, but highly expressed in tumors, such as stomach tumor, pancreas tumor, and colon tumor [197,198]. Fan and Peng *et al.* [198] developed a red-emitting fluorescent probe (NANQ-IMC6) for detecting COX-2. The probe is based on linking a chemically modified indomethacin, a substrate of COX-2, to nitroacenaphthene-quinone (NANQ) fluorophore (Figure 15(a)). Interestingly, this probe exhibited the different response to COX-2 at different concentration ranges. At the low levels of COX-2 (<0.085 μg/mL), corresponding to inflammation, the probe showed a turn-on response to COX-2. While at high levels of COX-2 (>0.085 μg/mL), corresponding to some tumor tissues, the probe showed a blue shift of emission wavelength. In this way, the probe can not only detect tumor from normal tissues, but also differentiate tumor from inflammation. Similarly, Fan and Peng *et al.* [199] also developed a turn-on fluorescent probe for neutral cholesteryl ester hydrolase 1 (KIAA1363), which is over-expressed in various aggressive breast cancer, melanoma, as well as ovarian human cancers, and achieved a high-contrast tumor detection in the mice models. β-galactosidase (β-gal) is an important biomarker for cell senescence and primary ovarian cancers. A red to NIR emitting fluorescent probe was developed by grafting a β-gal activatable unit onto a chromophore [200] (Figure 15(b)). This probe exhibited a turn-on and ratiometric response to β-gal, and high specificity in differentiating tumor from normal tissues. The over-expressed levels of γ-Glutamyltranspeptidase (GGT) are associated with tumorigenesis in several human cancer cells, such as cervical and ovarian cancers. A red-emitting probe was thus explored by conjugating GGT-specific substrate unit with boron-dipyrromethene (BODIPY) chromophore [201], which showed a rapid turn-on response to GGT. In addition, the self-quenching of chromophores can be a significant issue for
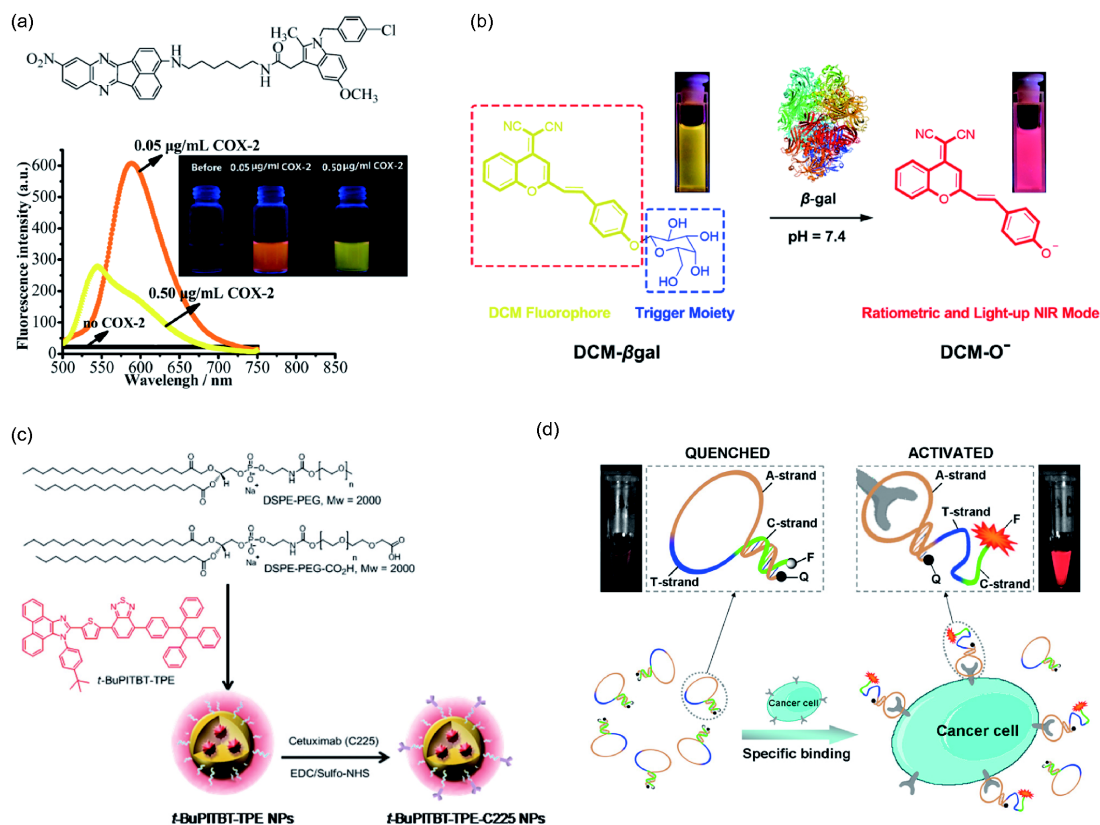
Figure 15   (a) Chemical structure of COX-2 probe and the different probe response at low or high COX-2 concentrations [198]. (b) Chemical structure of β-gal activatable probe and its turn-on mechanism [200]. (c) Structure of cetuximab-conjugated AIE nanoprobe [203]. (d) Structure of the activatable aptamer probe. Its fluorescence will be turned on upon binding to target cancer cells via a conformational alteration [207] (color online).

fluorescence imaging and detection. Tang *et al.* [202] has introduced a series of chromophores whose fluorescence emission can be enhanced upon aggregation, named as aggregation-induced emission (AIE). For instance, an AIE-based tumor-targeting nanoprobe was constructed by making red-emitting AIE fluorogens (*t*-BuPITBT-TPE) into the nanoparticles and conjugating with cetuximab (Figure 15(c)) [203]. The obtained nanoprobe enabled the targeted imaging of EGFR-overexpressed cancer cells.

In addition to the probe design of targeting a specific tumor biomarker, Tan *et al.* [204,205] used the whole cancer cells as targets to screen aptamers for specific targeting to cancer cells. The cell-SELEX (Systematic Evolution of Ligands by EXponential enrichment) method was used for aptamer screening and identified aptamers that could specifically target various kinds of cancer cells, such as liver cancer cells and B-cell lymphoma. By conjugating the aptamer with NIR dye such as Cy5, the detection of tumor tissues was achieved by NIR fluorescence imaging [204]. Based on this strategy, the simultaneous and sensitive detection of multiple cancer cells has been also realized by using multiple aptamers that are specific for different cancer cell lines [206]. While labeling the aptamer with a NIR dye has enabled the targeted imaging of tumors, the nonspecific binding and accumula-

tion of the probe can still cause high background signals for *in vivo* imaging. To address this issue, Wang and Tan *et al.* [207] further developed an activatable aptamer probe, which displayed a quenched fluorescence in its free state, and an activated fluorescence upon binding to the cancer cells via a conformational alteration (Figure 15(d)). This fluorescence enhancement led to a high contrast for tumor detection in the mice models.

Besides cancer cells, tumor microenvironment is another important target for the development of tumor imaging probes. Acidic extracellular pH (e.g. 6.5–6.8) is a characteristic feature of tumor microenvironment. Gao *et al.* [208] developed a extracellular pH-activatable nanoprobe by conjugating poly(ethylene glycol)-*b*-poly(2-(hexamethyleneimino) ethyl methacrylate) copolymer with a NIR dye Cy5.5 (Figure 16(a)). These dyes were quenched inside the nanoprobes, but the fluorescence was recovered when the nanoprobes were disassembled under a lower pH condition. The nanoprobe was thus found to exhibit an extremely sharp response to a subtle change of pH, together with a 102-fold fluorescence activation ratio between pH 6.7 and 7.4 (Figure 16(b)). Using this probe, a broad range of tumors were detected at high imaging contrasts, including breast cancer, prostate cancer, head and neck cancer, lung cancer, brain
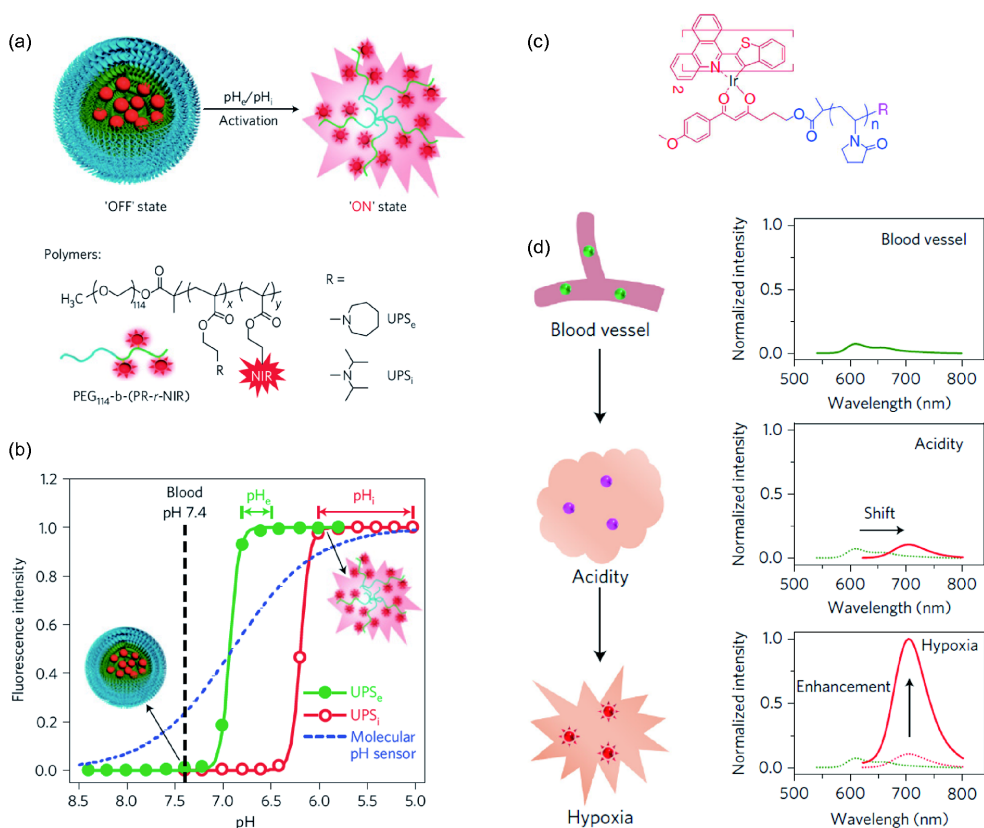
Figure 16 (a) Structure of the extracellular pH-activatable nanoprobe and (b) its response to the change of pH condition [208]; (c) chemical structure of the hypoxia-responsive probe [209]; (d) two-step response of the successively activatable probe to the acidic and hypoxic tumor microenvironment [211] (color online).

cancer, and pancreatic cancer. Hypoxia is another characteristic feature of most solid tumors. Jiang *et al.* [209,210] developed the phosphorescent probes based on iridium complex and poly(*N*-vinylpyrrolidone) (PVP) (Figure 16(c)). The probes were quenched in normal tissues, but exhibited a strong NIR phosphorescence in hypoxic tumor tissue. The probes allow the highly sensitive detection of primary tumor and tumor metastasis in lungs and lymph nodes, and even detect thousands of cancer cells in the early stage of tumor formation. Moreover, they further developed a successively activatable probe, which showed a two-step response in tumor microenvironment [211,212]. This response included the first emission wavelength shift upon response to acidity and subsequent emission intensity enhancement upon response to hypoxia (Figure 16(d)), thus amplifying tumor microenvironment signals and improving the tumor detection sensitivity. Using this probe, the metastatic tumor nodules of as small as 1 mm in the liver were detected with high imaging contrast.

These smart nanoprobes have demonstrated the high specificity and sensitivity of the optical imaging method for tumor imaging. A major challenge for the application of optical probes for cancer diagnosis is the lack of imaging depth. However, the development of NIR-II imaging probes and photoacoustic probes has brought significant improve-

ment on the imaging depth [213–216]. Besides, more systemic evaluation of long-term toxicity of the probes is needed for further clinical translation. In general, with further evaluation and optimization, the smart optical probes can provide powerful and valuable tools for intelligent diagnosis of cancer.

3.3 Radioactive nanoparticles for radionuclide imaging of cancer

Nanomedicine has distinctly and progressively revolutionized the way of dealing with cancer diagnosis and therapy. There are a range of imaging techniques such as computed tomography (CT), MRI, optical imaging (OI), sonography, positron emission tomography (PET), single photon emission computed tomography (SPECT), cerenkov luminescence imaging (CLI), and radioluminescence imaging (RLI), which have been developed for not only disease diagnosis but also guiding nanomedicine development [217–220]. Among these imaging modalities, the radionuclide-based imaging techniques including PET, SPECT, CLI and RLI with intrinsic high sensitivity that can provide visualized and quantitative molecular characteristics of intra-/inter-heterogeneity of various malignancies, offer preferable capacity in early diagnosis and patient monitoring as compared

to anatomic imaging. On the other hand, the radioactive nanoparticles integrated with multimodality and multi-function, rather than single-component radiotracers, have been rapidly recognized as an important tool, in which the structural, physical and chemical tunability are combined to refine therapeutic delivery/efficacy at the molecular scale [221,222].

The development of cancer nanomedicine, is expected to boost the progress of precision and personalized medicine due to its multiple advantages, including its customizability to design desirable physicochemical and biological properties for satisfying specific requirements such as targeting, pharmacokinetics, intracellular delivery, multimodal imaging and therapy. The favorable features of the nanoparticles in molecular imaging include the following [223–225]: (1) their size/structure-dependent properties, which is an essential regulator to achieve signal augmentation effect; (2) their large ratio of surface area to volume, resulting in much higher quantity of surface motifs; (3) their broad diversity of elemental composition (e.g., noble/transition metals, lanthanides, radioisotopes and nonmetals), which is an intrinsic benefit for achieving multimodal imaging and therapy.

Both PET and SPECT are based on detection and measurement of gamma photons that result from radioactive decay of radiotracer at the distributed region in the living subject (Figure 17(a)). While the CLI relies on the detection of light emission, which is produced from charged particles (such as β^- and β^+ emitted by radionuclide) traveling with a speed exceed the phase velocity of light in a dielectric medium [226,227]. The Cerenkov (or Cherenkov) radiation was discovered almost a century ago. However, the short wavelength of Cerenkov radiation is highly absorbed in living organisms. To address this disadvantage, Cerenkov radiation energy transfer imaging (CRETI) has been proposed by producing highly red-shifted emission using quantum dots. CLI and CRETI have been recently applied for biomedical imaging as well. For instance, molecular imaging using CLI was extended by Tian and co-workers [228–235]. In a similar fashion to CRETI, RLI relies on the detection of light emission from the energy conversion of ionizing radiation from radionuclide via scintillator nano-phosphors, which is independent of Cerenkov radiation [236]. Both CLI and RLI for *in vivo* optical imaging are of great attention as they allow the luminescence imaging with common optical imaging system without the use of optical filters. The wide option of radioisotopes and use of clinically approved probes, provide a great potential for not only the preclinical research but also for the clinical application, such
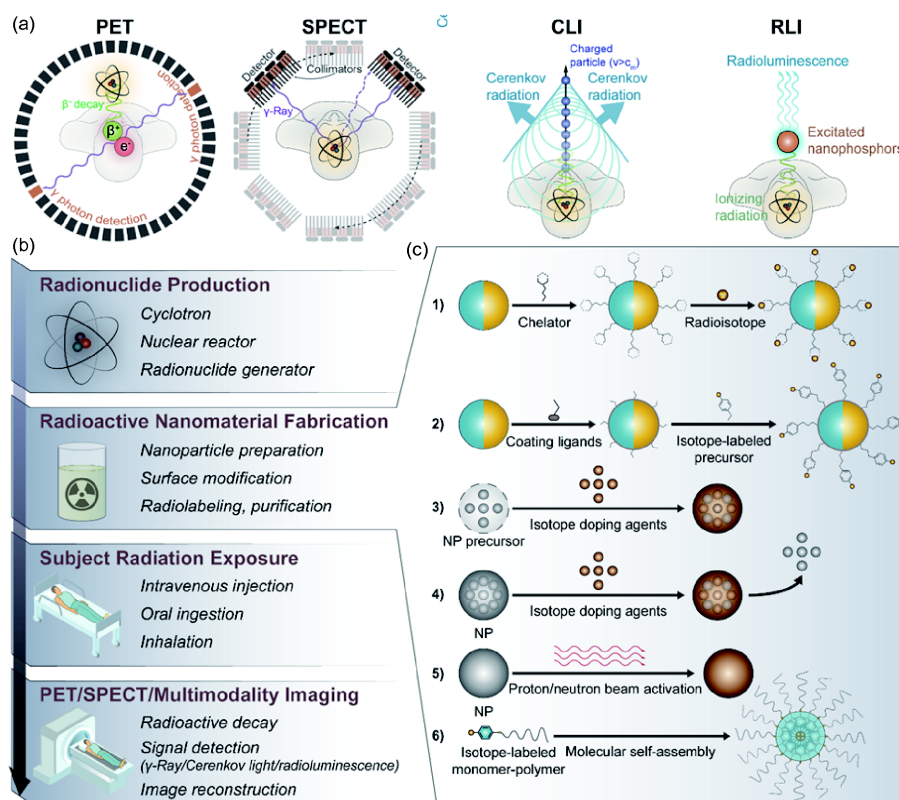
Figure 17 Schematic overview of (a) the principles of PET, SPECT, CLI and RLI. (b) Proposed flowchart of general procedures for nanomaterial-assisted PET, SPECT and multivalent approach. (c) Common strategies for radioactive nanomaterial fabrication: (1) chelator-assisted surface radiolabeling; (2) rapid covalent attachment; (3) nanomaterial surface/core-doping via chelator-free methods; (4) isotope/cation exchange; (5) proton/neutron beam activation; (6) molecular self-assembly of radiolabeled precursors (Note: blue/yellow semispheres denote applicability of both organic and inorganic nanomaterials) (color online).

as image-guided surgery [237–239].

In general, the overall procedure of radionuclide-based imaging is highly conserved due to the limited operation time and radiation exposure (Figure 17(b)). Radionuclides are often produced by cyclotron, nuclear reactors or radionuclide generators [240]. Depending on the half-life of certain radioisotopes, the transport distance should be considered for accessing the imaging facility. For both PET and SPECT, the prepared radioactive nanoparticles are immediately administered to the subject, followed by their distribution in the target site and subsequent imaging examination. The rational design of radioactive nanomaterials involves the consideration of nanoplatform design, imaging characteristics, radioisotope selection, radiolabeling and targeting strategy. Importantly, the selection of radioisotope relies on the monitoring duration, availability, multi-isotope imaging and biological relevance. The isotopes with positron emission (β$^+$ decay) for PET scan usually have relatively short half-lives and are closely aligned with the biological half-life of the tracer, while the isotopes emit gamma radiation used in SPECT generally have longer half-life and are more readily available with reduced expense as compared to those used in PET [241]. Although PET has the preferable sensitivity and spatial-temporal resolution over SPECT, SPECT is able to quantitatively visualize multiple isotopes via simultaneous refinement of emission energies, which allows the increased throughput with multiple functional characteristics [242].

The existing radioactive nanoparticles are mainly divided into two categories (Figure 18) [243] including inorganic nanoplatform (e.g., silica, gold, iron oxide, cupper, semi-conducting materials, and metal-organic complexes) [244], and organic nanoplatform (e.g., liposomes [235,245], vesicles [246,247], micelles [248], polymerics [249], peptides, and proteins [149]). The radionuclide can be either furnished on the surface of nanomaterials or doped in the nanoparticles via various chemical and physical approaches [221,250,251]. In consideration of practical use of radioactive nanoparticles, the radio-labeling procedure should be rapid and reproducible. Since only low concentration of the radionuclide is used, the purification step has to be simple and effective. Besides, the radiolabeling is required to have a minimized alteration on physicochemical properties and pharmacoki-
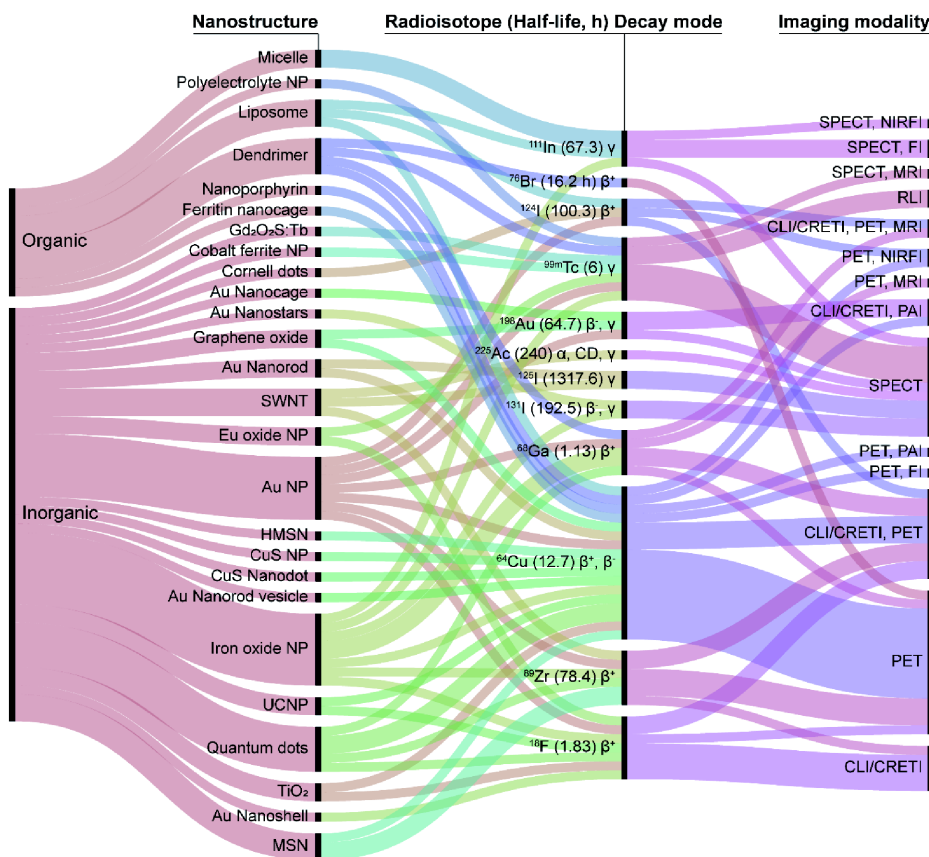
Figure 18   Alluvial diagram quantitatively maps the extent of relations between nanostructure, radioisotope and imaging characteristics among organic and inorganic radioactive nanomaterials. The inorganic class is the most popular one for radionuclide-based imaging, in which iron oxide, gold, quantum dots and silica NPs are frequently used nanoplatforms. ^{64}Cu, ^{89}Zr, ^{18}F and ^{68}Ga are mostly reported in PET and CLI/CRETI, while ^{99m}Tc, ^{111}In, ^{125}I, ^{131}I are commonly used in SPECT. ^{99m}Tc is also a major radionuclide for RLI application. SWN: single-walled carbon nanotube; MSN: mesoporous silica nanoparticles; HMSN: hollow mesoporous silica nanoparticle; EC: electron capture; UCNP: upconverting nanoparticles; CD: cluster decay; FI: fluorescence imaging; NIRFI: near-infrared fluorescence imaging; MRI: magnetic resonance imaging; PAI: photoacoustic imaging. Note: Alluvial diagram was obtained using RAWGraphs [243] (color online).

netics of nanoparticles.

Conventional strategies to prepare radioactive nanoparticles often involve surface functionalization by using radiometal ion chelation (Figure 17(c-1)) and effective binding with radiolabeled prosthetic groups (Figure 17(c-2)). In this regard, the inorganic nanoparticles are commonly coated with reactive groups through several strategies including thiol-capped radiolabeled molecules bound to gold nanoparticles [252], silylation of hydroxyl groups on surface of silica or metal oxide nanoparticles [253], and bisphosphonate attachment on metal oxide nanoparticles [254], as well as attachment on coating surface through click conjugation or other covalent bond [255,256]. However, these core-shell coating methods via chelators and reactive molecules might affect the overall size and surface charge of nanoparticles, possibly resulting in undesired *in vivo* behavior and toxicity issue. Then, several alternative methods have been developed to address these issues [250,257]. For example, the radionuclide doping as a well-established approach can allow a trace amount of the radionuclide to be added into nanoparticles during the formation (Figure 17(c-3)). In this case, a variety of radionuclide-doped nanostructures such as nanorods, nanocages, nanodiscs and nanospheres can be produced through radioactive co-precipitation in a strict control of experimental conditions such as radioactivity, solubility, concentration, precursor ratio, counter ion identity and ionic strength [258]. Alternatively, the radionuclide can be encapsulated in specific metal-storage proteins such as ferritin nanocages, which have high binding affinity to some metal ions such as Cu^{2+}, Ni^{2+}, and Co^{2+}. It has been reported that such approach is applicable to ^{64}Cu and generate the stable ^{64}CuS-ferritin nanocages for PET imaging and optical theranostics [149].

The direct chemical bond formation on the surface of nanoparticles as another promising method has been widely applied for metal-based nanoparticles, silica nanoparticles, and graphene [259–266]. The adsorption process usually involves intrinsic interactions between the surface and radionuclide [250]. Aside from direct radiolabeling approaches, the radionuclide can be doped into the nanoparticles through isotopic exchange or by cation exchange (Figure 17(c-4)). The $^{19}F/^{18}F$-substitution is a typical isotopic exchange for radiolabeled nanoparticles [250]. In contrast, the heteronuclide exchange (cation exchange), inspired by postsynthetic transformations of nanocrystals, has also been applied for radiolabeling of pre-fabricated nanoparticles [267–269]. Another post-radiolabeling approach is to activate non-radioactive nanoparticles through neutron/proton beam in a nuclear reactor (Figure 17(c-5)) [270–273]. This simple and rapid *in situ* activation can be employed to all metal-based nanoparticles for convenient use with post-activation modification. In addition, to satisfy the pharmacokinetic and biodegradation criteria for cancer theranostics,

the organic-based radioactive nanoparticles through the self-assembly of radiolabeled-supramolecular system also offer a great potential for multimodal cancer diagnosis and therapy (Figure 17(c-6)). An engineered radiolabeled monomer-polymer bearing specific physicochemical properties can be self-assembled into the micelles or polymersomes via the intermolecular interactions such as amphiphilic, electrostatic and ionic interactions [274,275].

The use of radioactive nanoparticles as diagnosis, monitoring and theranostic systems intends to improve the therapeutic efficacy by providing the insights of *in vivo* behaviors with highly sensitive radionuclide-based imaging. Although many radiolabeling advances have been explored, there is still much improvement to be done, such as the preclinical validations of both nanoplatforms and radiolabeling methods in animal models. More importantly, the clinical translation of various radioactive nanoparticles may be obstructed by the safety issues in human subjects (e.g., potential toxicology, pharmacokinetics and pharmacology). Based on previous understanding of nanomedicine [218,276–279], the development of radioactive nanoparticles may more likely center on the facile strategies to find the shortcut for the translation from bench to bedside.

3.4 Quantum dots for medical diagnostics of cancer

As the desire of precise personalized therapy of cancers is increasing, it is urgently needed to find a powerful tool to realize the molecular detection and confirmation of multiple tumor antigens (biomarkers) with both high affinity and specificity [280,281]. Semiconductor quantum dots (QDs) with unique optical properties are emerging as a new class of fluorescent labels for cancer biomolecular imaging and detection [282–284]. For example, compared to organic fluorescent dyes, QDs have unique features such as size- and composition-tunable light emission, high fluorescence quantum yield, long-term photostability. In addition, multicolor QDs can be simultaneously excited by a single light source with minimal emission overlapping because of the broadband absorption and narrow emission peaks. These properties allow QDs to act as a valid tool for diagnosis of tumors based on multiple biomarker detection [285–289].

The quantity and statistical differences of tumor biomarkers are important for cancer screening and diagnosis. However, cancer biomarkers often have very low concentrations. So the first challenge of cancer diagnosis is the low detection limit. Secondly, the molecular information on both patterns and quantities could be helpful to understanding of the tumor heterogeneity [290]. However, the conventional tumor diagnosis is mainly based on the results of pathological sections, which often fail to provide enough essential molecular information for treatment decision. QDs can be suitably used for the quantification of the tumor

biomarkers [291–293]. Researchers used QDs to detect multiplex tumor biomarkers for molecular subtyping [285,290,294] (Figure 19). Even five molecular subtypes of breast cancer based on the quantitative molecules information could be quantitatively analyzed in routine practice [290], which might help formulate personalized comprehensive therapy and prognosis.

Quantifying cancer biomarkers for acquiring the information on cancer progress *in vivo* and *in situ* is another challenge. NIR fluorescence imaging in the range of 700–1700 nm with suppressed photo-scattering and diminished auto-fluorescence facilitates the *in vivo* imaging with higher resolution and deeper tissue penetration as compared to conventional visible light imaging [295–297]. NIR QDs with the advantages of both commonly-used fluorescent QDs and NIR fluorescence are emerging as a new class of biolabels. So far, the fluorescence wavelength of NIR fluorescent QDs has been expanded from 700–900 nm (NIR-I window) to 900–1700 nm (NIR-II window), and the longer wavelength is able to cause a deeper penetration depth, followed by more precise imaging [298]. The compositions of NIR QDs are also changed from CdTe/CdSe [299,300], $CdTe_xSe_{1-x}/CdS$ [301], $CdTe_xSe_{1-x}$ [302], CdHgTe [303], and PbX (X=S, Se) [304,305], containing toxic heavy metals, to relatively environmentally-friendly Ag_2X (X=S, Se, Te) [306–313], InAs/ZnSe [314], InAs/InP [315,316], InP/ZnS [317,318], and Si [319]. Compared to NIR-I (700–900 nm) and NIR-IIa (900–1400 nm) imaging, the NIR-IIb (1500–1700 nm) imaging can preferably obtain minimized photon

scattering, and avoid high absorption by water in tissue [298]. However, there are still demands for NIR-IIb fluorescent labels with sufficient brightness, low toxicity and aqueous stability. To date, among these NIR QDs, only the emission of PbX (X=S, Se) QDs can be located in the NIR-IIb window. Recently, the PbS/CdS core-shell QDs were used for *in vivo* non-invasive imaging and 3D confocal imaging of the tumors in mice (Figure 20) [320]. The quantum yield of PEG-PbS/CdS dispersed in water could reach as high as 22%. Benefiting from the brightness and NIR-IIb window, the high-resolution confocal images of tumor vessels were obtained at a depth of up to ~1.3 mm [320]. Moreover, the signal ratio of tumor to normal tissue (T/N) was found to reach up to 32.0 [320], showing a highest ratio among all fluorescence-based tumor imaging with fluorophores. This NIR-IIb probe provides a precise imaging tool for cancer theranostics.

Besides the NIR fluorescence wavelength, the excretion and biodistribution of QDs are also crucial to the tumor imaging *in vivo* [321]. The heavy metal-free Ag_2X QDs have caught researchers' attention [321,322]. As Pang *et al.* [323] reported before, the water-dispersed Ag_2Se QDs could be cleared out at 168 h even at a high injection dosage, thus being only one kind of NIR QDs that can be totally excreted. This kind of Ag_2Se QDs has been prepared using a quasi-biosynthesis with peptides, enzyme, co-enzyme, and metal ions [305,324]. Under the relatively mild reactions, the Ag_2Se QDs were synthesized with ultra-small size of less than 3 nm and biocompatible surface, which might benefit
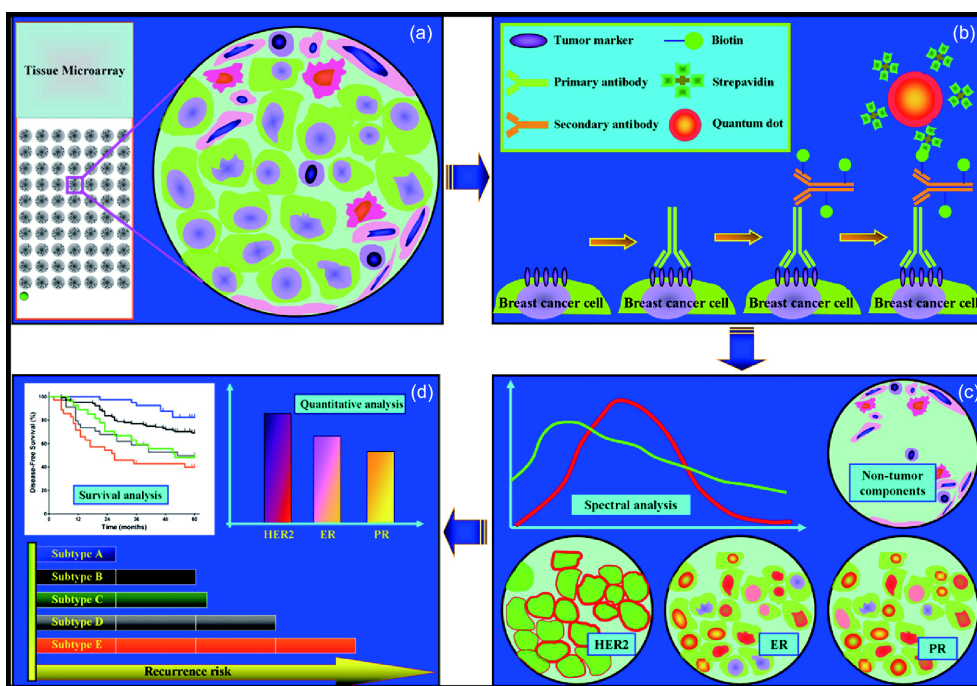
Figure 19   Molecular subtyping of breast cancers with different 5-year prognosis using QDs [290]. (a) Tissue microarrays of breast cancer specimens; (b) imaging of 3 key molecules of BC based on QD-IHC; (c) multi-spectral image analysis to acquire spectral information for each molecule of breast cancer specimens; (d) quantitative information of 3 key molecules for each breast cancer case related to 5-year disease free survival (color online).
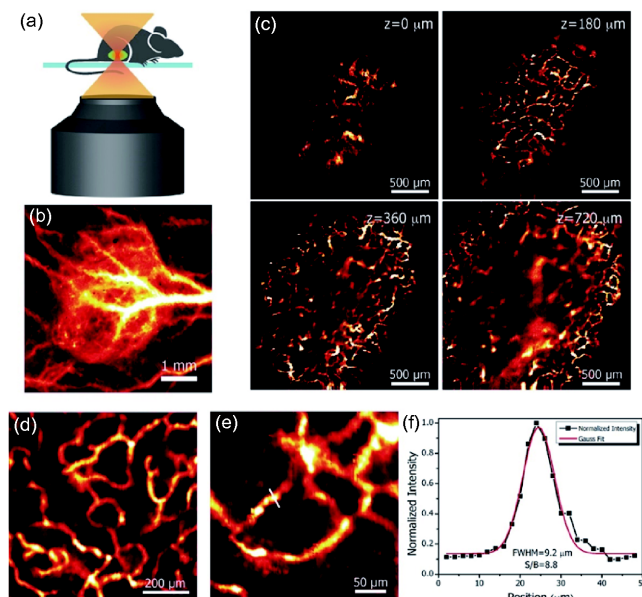
Figure 20   *In vivo* noninvasive fluorescence imaging of the tumor in the NIR-IIb window [320]. (a) Schematic drawing illustrating *in-vivo* confocal imaging of a mouse through the skin. (b) High-magnification (10× objective), wide-field fluorescence imaging (~1600 nm emission, 808 nm excitation) of a xenograft MC38 tumor on a mouse after tail vein i.v. injection of PEG-CSQDs (Scale bar: 1 mm). (c) *In vivo* layer-by-layer fluorescence confocal imaging of tumor vessels over an area (2500 μm×2500 μm) after an i.v. injection of PEG-CSQDs; *z*=0 is defined as the position when NIR-IIb signal started to show up in the tumor (Scale bar: 500 μm). (d, e) High-resolution fluorescence confocal imaging of tumor vessels at a depth of 180 μm. (d) 800 μm×800 μm (Scale bar: 200 μm); (e) 300 μm×300 μm (Scale bar: 50 μm). (f) Cross-sectional fluorescence intensity profile of the tumor vessel marked in J with the FWHM of ~9.2 and S/B ratio of 8.8 (color online).

Figure 21   Preparation and application of $Ag_2Se@Mn$ QDs [325]. (a) Fabrication of $Ag_2Se@Mn$ QDs by controlling the reaction of Mn^{2+} with the Ag_2Se nanocrystals having been pretreated in 80 °C NaOH solution (0.1 M) for 10 min. (b) $Ag_2Se@Mn$ QD labeling of cell-derived microvesicles (MVs) with the assistance of electroporation, and its applications in whole-body high-resolution dual-mode real-time tracking and *in situ* quantitative analysis of the dynamic bio-distribution of MVs *in vivo* (color online).

the excretion *in vivo* [324]. The ultrasmall size of Ag_2Se QDs ensured a high ratio of surface area-to-volume, thereby facilitating further surface engineering such as Mn-engineered Ag_2Se ($Ag_2Se@Mn$) QDs for the *in vivo* fluorescence and magnetic resonance imaging (Figure 21) [325]. Such a quasi-biosystem strategy opens a new window to explore more biocompatible NIR QDs.

Currently, many new methods are urgently needed for the fast and sensitive diagnosis and therapies of cancers. QDs-based nanomedicine is expected to renovate the diagnosis of cancers and also promote the understanding of cancer pathogenesis.

4   Nanoparticles for intelligent cancer therapy

To date, a variety of nanopaticles have been extensively explored as the emerging platform for cancer therapy, which are often demanded to overcome the sophisticated transport barriers, and effectively deliver payloads to target site for efficient anticancer therapy. In particular, the rational designs of smart nanoparticles that can respond to exogenous or in-
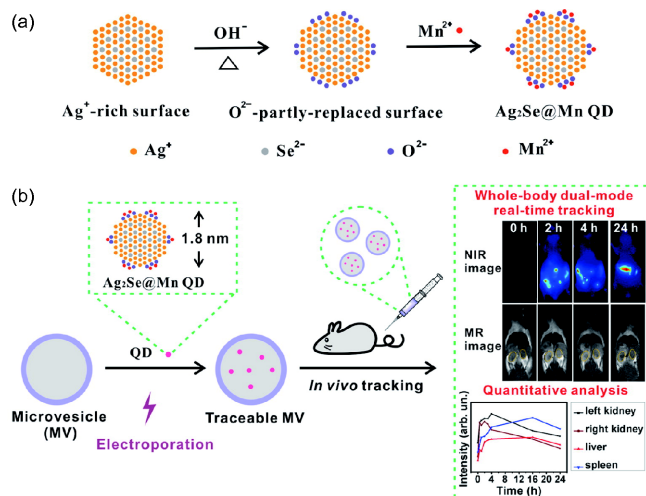
trinsic stimuli have been extensively explored to improve therapeutic efficiency with reduced adverse side effects. Here, we summarize several types of nanoparticles for gene therapy, chemotherapy, immunotherapy, phototherapy and interventional therapy, which have been established to achieve considerable *in vivo* therapeutic performances.

4.1   Highly efficient polycationic nanocarriers for gene therapy of cancer

Gene therapy has been proposed to be a promising strategy for treating various genetic human diseases by intentionally altering the gene expression in pathological cells, including cancer, hypercholesterolemia, hemophilia, and neurodegenerative diseases [326]. The aim of gene therapy is to transfer genes into target pathological cells to modify the expression of endogenous genes for treating or preventing progression of diseases. It is the most direct and effective strategy for the treatment of hereditary disorders, instead of conventional methods that often fail to cure many diseases caused by side effects and genetic anomalies [327,328]. However, the naked genes cannot be efficiently internalized by pathological cells, due to their rapid renal clearance, nuclease susceptibility, phagocyte uptake, and accidental immunotoxicity. Therefore, the further clinical application of naked genes is severely restricted. A successful gene therapy depends on the development of effective gene delivery systems [329]. Viral vectors have been proved to be efficient in transfection, but their practical application is criticized by safety concerns, such as virus replication, immunogenicity, and inflammatory

reaction [330]. Recently, with the rapid development of nanomedicine, the nanoparticles have been emerged to be the most promising vehicles for gene therapy because of their controlled structure, size, function, and biological behavior. A variety of the nanoparticles have been widely developed to achieve gene delivery for cancer therapy [331]. However, the development of safe, efficient, and controllable nanocarriers for gene therapy is still the most critical issue to satisfy the successful clinical applications for cancer therapy [332].

There are many factors that may affect the transfection efficiency of gene delivery systems in cancer cells. As we know that the electrostatic interactions between nanoparticles and DNA or cell membranes can influence their transfection efficiency by modulating DNA loading, DNA condensation, and endocytosis. Usually, increasing molecular weight of cationic carriers can improve their transfection efficiency. This is mainly because that the increase of molecular weight can improve the charge density of molecules, which is conducive to the DNA loading and cell endocytosis of gene carriers. However, the obvious cytotoxicity is increased with the enhanced charge density of cationic carriers. Thus, the cytotoxicity is the main obstacle for cationic carrier-mediated gene therapy, owing to the electrostatic interaction between cationic components of nanoparticles and anionic proteoglycans on cell surface, which can cause cytomembrane destabilization and meronecrobiosis [333]. To address this issue, the efficient transfection and low cytotoxicity can be achieved by introducing different types of interactions or segments. For instance, the hydrogen bond and hydrophobic effect are beneficial to the interaction between polymeric gene carrier and DNA, as well as the interaction between the nanoparticles and cell membrane [334,335]. Therefore, when regulating the charge density encounters the bottleneck, the regulation of cationic polymer on its charge density, hydrogen bonding and hydrophobic action is considered as the effective strategy to improve the transfection performance of cationic polymer nanoparticles with reduced long-term safety concern.

Recently, a comprehensive strategy has been explored to construct a highly efficient nanoparticle as a gene delivery system by introducing a "molecular string", arginine protected by tosyl group (RT), onto polylysine (PLL-RT) (Figure 22) [336]. Firstly, the transfection performance was significantly improved by the multiple interactions including the electrostatic interaction, hydrogen bond interaction, and hydrophobic interaction between PLL-RT and DNA. Secondly, PLL-RT showed the enhanced serum resistance, while the amount of its amino groups was not reduced as compared to PLL. Thirdly, introducing "RT string" onto cationic polymers act as a universal transfection enhancing strategy for the most kinds of polycationic gene carriers. In this study, shVEGF (plasmid DNA expressing shVEGF) was used as a
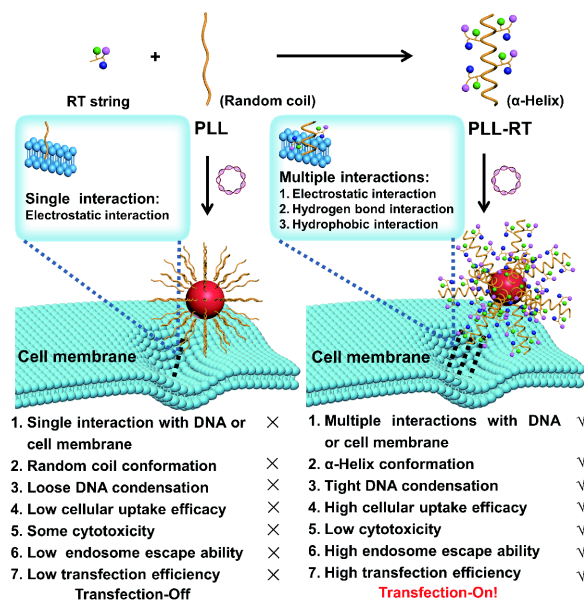
Figure 22 Construction of biodegradable and highly efficient nanoparticles for gene delivery by introducing multiple interactions into polylysine [336] (color online).

therapeutic gene. Vascular endothelial growth factor (VEGF) can promote the formation of tumor vessels and accelerate the growth of tumor. The complex of PLL-RT/plasmid DNA expressing shVEGF exhibited a significant antitumor effect and negligible pathological abnormalities after intratumoral injection. Thus, the multiple interactions or characteristics of the nanoparticles are expected to greatly improve their transfection efficiency.

Although several gene nanocarriers exhibit tremendous potentials for treating cancers, there are still many biological barriers to limit their clinical applications, including degradation by endonucleases, phagocytosis by macrophages or non-target cells, ineffective aggregation at the desired tissues or cells, low endocytosis by target cells, as well as inefficient gene delivery into cytoplasm or nucleus [337]. This PEGylation or shielding ability of the nanoparticles can achieve long circulation and reduced nonspecific phagocytosis [338,339]. In order to further improve the endocytosis of tumor cells, the sensitive groups in response to tumor microenvironment have been introduced into the nanoparticles, including pH-, hypoxia-, and reactive oxygen species-sensitive segments [340,341]. These nanoparticles with decreased zeta potential are able to realize the reduced cellular uptake in blood circulation. Upon arriving at the tumors, the outer layer of nanoparticles was detached, resulting in the increased zeta potentials, thus promoting cellular uptake for improved antitumor efficiency. The pH-sensitive PEG-tightened nanoparticles with charge/size dual-rebound properties were constructed using *in situ* Schiff base reaction (Figure 23) [342]. The long circulation, high tumor

Figure 23 Illustration of ultrasensitive pH-triggered charge/size-rebound nanoparticles as gene delivery system [342] (color online).

accumulation, and dramatic antitumor therapy were achieved using these nanoparticles. This strategy as a widely used regi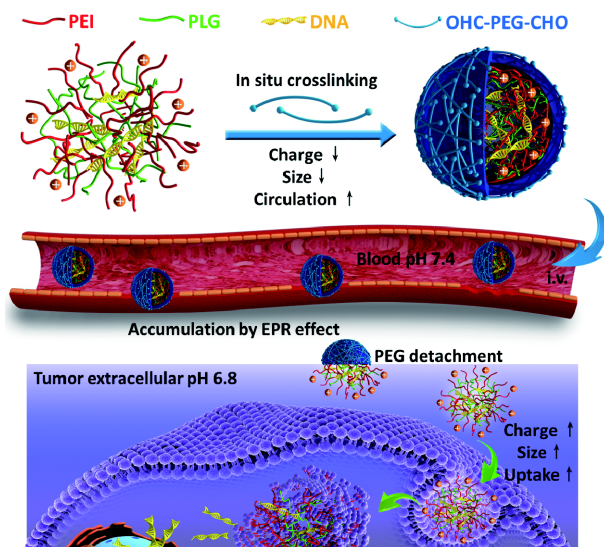me possesses several advantages for gene therapy including fast and efficient *in situ* reaction based on Schiff base; good stability in blood circulation and rapid de-shielding in acidic tumor extracellular pH for subsequently improving cellular uptake; dual charge/size-rebound properties for uptake efficiency and antitumor efficiency.

Gene therapy has its great potential for preventing or treating genetic diseases, and its clinical application is still restricted by the safety and effectiveness of gene delivery systems [343]. With the rapid development of nanomedicine, a comprehensive understanding of the obstacles in gene therapy will be beneficial to rationally design intelligent nanoparticles. Moreover, the sophisticated tumor microenvironment should be also considered for gene therapy, including low pH, hypoxia, immunological tolerance, and abnormal cell populations. In addition, the combination strategies such as the nanoparticle-based gene therapy with chemotherapy, cell therapy, immunotherapy, radiotherapy, or phototherapy provide new approaches for potential clinical translations in future.

4.2 Polymeric nanoparticles for cancer-targeted drug delivery

Various nanoparticles have been explored for cancer therapies and diagnosis, including nanocapsules [344] and polymersomes [345,346], black phosphorus [347], silica nanoparticles-assisted ruthenium(II) complexes [348], mesoporous silica nanoparticles [349], silica-coated manganese oxide nanoparticles [350], Pt nanocrystals/nanoclusters [351], 2D nanomaterials such as Pd-based nanomaterials

[352] and GO nanocomposites [353], and nanofibrous membranes [354]. But much focus is on more clinical relevant nanoparticles made from biocompatible organics [60], lipids [355], natural proteins (e.g. lipoprotein [356], H-ferritin [357]) and peptides [5,358]), as well as prodrugs [359–361] and polymeric nanostructures from layer-by-layer self-assembly of oppositely charged polymers [362] and nanogels from transition-metal complexation [363]. In addition to the dendrimers with well-defined unimolecular polymer nanoparticles [364–366], the micelles are considered as the effective polymeric nanoparticles that can be self-assembled from amphiphilic polymers [367–369], rationally designed polymers [77,370,371], or high-throughput screened polymers [372,373]. Recently, polymeric nanoparticles such as poly(*D,L*-lactide-*co*-glycolide) (PLGA) coated with erythrocyte membranes from red-blood cells [224,374–377], cancer cells [378,379], or macrophages [380,381], have attracted great attention because such systems usually combine the complex biological functions of natural cell membranes and physicochemical properties of synthetic nanomaterials for effective drug delivery. DNA, known for its precision assembly into various three-dimensional nanostructures, is also proposed for cancer-targetd drug delivery [382–384]. For instance, telomerase-responsive DNA icosahedron was designed to precisely release caged platinum nanodrug [385], and self-assembled floxuridine-containing DNA polyhedra was fibricated as a Trojan horse [386].

The ultimate goal of cancer-targeted drug delivery is to ship drugs into cancer cells for exerting their pharmaceutical effects [387]. Generally, the intravenously administered nanoparticles must go through a cascade of five steps [388], including circulation in blood compartments, accumulation in tumor via enhanced permeation and retention (EPR) effect, penetration into avascular tumor tissue to reach distal tumor cells, subsequent internalization into cytosol, and final drug release for actions (*CAPIR* cascade) (Figure 24). Thus, the overall delivery efficiency (Q) of nanoparticles is a product of efficiencies of these five steps (Q_C, Q_A, Q_P, Q_I and Q_R). Certainly, these processes can be simplified for local or intratumoral delivery as compared to intravenous administration.

The *CAPIR* cascade consists of a series of biological barriers to nanomedicine. After injection in the bloodstream, plasma proteins deposit onto the nanoparticles, thus causing opsonization and elimination by mononuclear phagocytic system (MPS) [389]. The RES in liver and spleen efficiently sequesters the nanoparticles [390]. Hence, solid tumors have many physiological barriers that limit their intratumoral accumulation and distribution [391,392]. The tumor blood vessels are poorly structured and heterogeneously distributed, and meanwhile the dense extracellular matrix [393,394], with tightly packed tumor cells [395] and high interstitial fluid pressure [396,397], makes nanoparticles al-
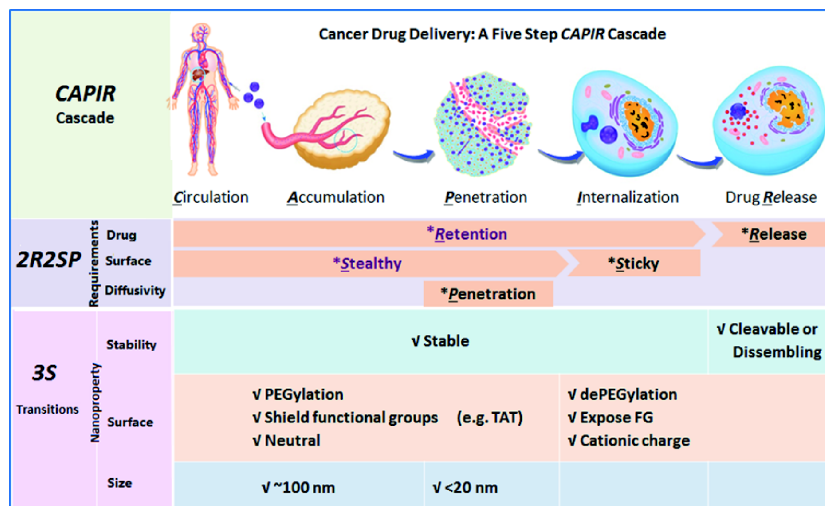
Figure 24   Summary of *2R2SP* requirements and the *3S* nanoproperty transitions in the *CAPIR* cascade for cancer nanomedicine [388,405] (color online).

most motionless in tumor, thus causing spatially heterogeneous distribution in tumor [398]. The cellular membrane also presents as a barrier for nanoparticles to access cytosol due to their difficult diffusion. P-glycoproteins as drug efflux pump can mediate multidrug resistance [399,400], and the cytosol can also accommodate genetic drug-resistance [401,402] such as drug metabolism [403].

The needed properties for nanoparticles to overcome biological barriers in each step are shown in Figure 24. These properties can be classified into three categories: (1) the stability, that is, the drugs are firmly loaded in the nanoparticles through either conjugation or encapsulation in the *CAPI* steps, but in *R* step, the drugs are quickly released by linker cleavage or carrier disassembly; (2) the surface properties: the nanoparticles have a stealth surface during the *CAP* steps by pegylation, being neutral and hiding the binding groups (e.g. targeting groups and TAT), but become depegylated, positively charged, followed by the exposure of binding groups to cell membrane for subsequent cell internalization; (3) particle size: the nanoparticles have a relatively large size to favor blood circulation and tumor accumulation during *CA* steps [404], but must become small, less than 30 nm to gain good tumor penetration ability. Thus, as shown in Figure 24, the three categories of nanoproperties for nanomedicine to gain the optimal efficiency are contradictory during the *CAPIR* cascade. The three dilemmas can be solved by making the nanoproperties adaptable to the cascade (i.e. from being stable in the *CAPI* steps to being unstable or disassembled in the *R* step; from being neutral/pegylated/shielding functional groups in the *CAP* steps to being cationic/depegylated/exposing functional groups in the *I* step; and from being large in the *CA* steps to being small in the *P* step); or simplifying three nanoproperty (*3S*) transitions in stability, surface and size [405]. Therefore, it can be concluded that the nanoparticles capable of the *3S* nano-

property transitions will be able to efficiently accomplish the *CAPIR* cascade to give rise to high therapeutic efficacy. The aim of the nanoparticle design is to engineer nanoparticles' *3S* nanoproperties that are utilized to overcome the barriers for improved therapeutic efficacies. The rational design of *3S* nanoproperty transitions for nanoparticles are summarized below [405].

4.2.1   Stability transition
An effective nanomedicine must be stable to retain drugs in the *CAPI* steps. Micellar polymer nanoparticles generally have premature burst release problem because of drug adsorption on the micelle core/shell interface [406], and quick dissociation of soft-core micelles induced by shear in narrow microvasculature and interaction [407]. Improving the micellar stability by lowering the critical micelle concentration [408,409], loading drugs inside the core [406,410], crosslinking the micelle cores [177,411,412] and conjugating drugs to the core [413], can reduce or even eliminate premature drug release. Increasing drug-binding affinity of nanoparticles by introducing an optimal drug-binding molecule can improve the stability of nanoparticles, thus leading to a sustained drug release, prolonged circulation, increased tolerance dose, reduced toxicity, effective tumor targeting and superior anticancer effect [414]. Physiologically stable polyprodrug-gated crosslinked vesicles via the self-assembly of camptothecin (CPT) polyprodrug amphiphiles had a high CPT loading (>30 wt%), together with minimized leakage of encapsulated DOX and extended blood circulation ($t_{1/2}$) of more than 13 h. Upon inside the cells, the cytosolic reduction environment triggered CPT unplugging from vesicle bilayers, thereby generating hydrophilic channels to release DOX [245]. Reversibly closing/opening the pores in mesoporous nanoparticles is another way to control drug release. For instance, the polymer decorated on the surface of mag-

netic mesoporous nanoparticles is cross-linked with disulfide bonds, leading to the mesopores being "closed" in blood circulation, but being "open" via removing the coating in cytoplasm [415]. Other examples of the reversible cross-linked polycation nanoparticles for gene delivery [416], have also been demonstrated to improve the polyplex stability including fluorination of polymers to increase polyplex hydrophobicity [417], and crosslinked nucleic acid nanogels [177].

4.2.2 Size transition and tumor penetration

The size of nanoparticles is one of the most important nanoproperties that affect its blood circulation time and tumor accumulation [418–422]. About 100 nm size seems favorable for blood circulation and tumor accumulation via the EPR effect [404,422,423], but this size is too big for nanoparticles to diffuse and accumulate at the blood-vessel extravasation site [404,424–427], making them inaccessible to the distal cells from blood vessels [428]. Hence, the nanoparticles often suffer from low tumor targeting ability. For instance, very low injected dose of intravenously administrated nanoparticles was delivered to targeted cancer cells. The majority of the intratumoral nanoparticles were either trapped in the extracellular matrix or taken up by perivascular tumor associated macrophages [429]. Thus, an emerging trend is to design the nanoparticles that can become smaller upon arriving tumors for enhancing their penetration ability [388,430,431].

For instance, the size-changeable polymeric micelles with the dual shells, which showed the increase in size under acidic pH, and became smaller due to intracellular GSH, were successfully developed. It is capable of directly delivering anticancer drugs into the nuclei of multidrug resistance (MDR) breast tumor cells [432]. A shell-stacked nanoparticles were also designed to undergo remarkable size reduction from about 145 to 40 nm, and surface charge reversal from −7.4 to 8.2 mV at acidic tumor tissue, thus showing about 4-fold increase in their penetration depth as compared to that of non-transformable nanoparticles, followed by preferable therapeutic efficacy [433]. Reversible swelling/shrinking or transformable nanoparticles in response to pH were also reported to achieve the similar ability to improve penetration depth in the tumors [434,435].

Morphologic and functional restoration of dysfunctional tumor vasculature (normalization) is another approach to increase tumor penetration by re-establishing the pressure gradient between intravascular and interstitial space, which is essential to transport the nanoparticles into solid tumors. This remodeling, however, is also able to reduce tumor vessel permeability that might limit the nanoparticle extravasation. The intermediate-size in the range of 20–40 nm is a reasonable window that might enhance the transvascular delivery of the nanoparticles. The smaller nanoparticles possess a significantly reduced diffusional hindrance, thus resulting in a more homogeneous distribution within the tumor interstitium. These findings suggest that the anti-angiogenic therapy and size control of nanoparticles can be combined to achieve optimal delivery into solid tumors [436].

4.2.3 Surface property transition

The surface of nanoparticles should undergo a transition from being stealthy in blood to being sticky to cell membrane once in tumor for enhanced cellular uptake [431,437]. The most widely used surface transition can be achieved by the control of pegylation/depegylation in response to acidity. For instance, an ultrasensitive gene delivery system with pH-triggered charge/size rebound was explored by the complexation of polyethylenimine (PEI), poly-*L*-glutamate (PLG), and aldehyde-modified polyethylene glycol (PEG) [342]. The cross-linked PEG shielded the surface positive charges and tightened the complex particles, thus leading to decreased cytotoxicity, improved stability, and prolonged circulation, while the PEG shielding could be rapidly cleaved by acidic pH in tumors, and then expose their positive potentials. In addition, the micelles incoporating DOX at normal pH were able to gradually swell at acidic environment, thus reducing premature drug release for decreased side effect [438].

Surface properties of the nanoparticles determine their intracellular fate [439]. The targeting ligands are capable of achieving "smart" stimuli-responsive surface transition [440]. For instance, cell-penetrating peptides (CPPs) promote the rapid penetration and fast endocytosis [441], but cannot be used *in vivo* due to their non-specific interactions. An engineered charge-reversal strategy was used to improve the tumor-specific activation of CPPs [441,442]. The lysine residuals of CPPs were amidized to de-activate CPPs. The amidized CPPs (aCPPs) had no influence on their stealthness for tumor accumulation, while aCPPs were regenerated to recover their CPP functions in the mildly acidic tumor environment, thus facilitating tumor penetration and endocytosis [441,442]. Another design was to bury CPPs in highly selective tumor-homing aptamers for enhanced penetration in aggressive pancreatic ductal adenocarcinoma. In tumor environment, the detaching of aptamer was able to expose the shielded CPPs to facilitate the penetration and endocytosis of the nanoparticles [434].

4.2.4 Modulating tumor microenvironment

Tumor microenvironment might account for tumor growth and metastasis [443]. The nanoparticles have been explored to modulate tumor microenvironment. Hypoxia is responsible for inducing drug resistance and metastasis of tumor cells. Oxygenation of the tumor by exogenous oxygen delivery [444] or *in-situ* oxygen generation [445,446], is

considered as effective strategy to relieve tumor hypoxia. For instance, the albumin-coated MnO_2 nanoparticles were capable of decomposing H_2O_2 into oxygen, thus modulating the tumor microenvironment by relieving the hypoxia [445]. On the other hand, the tumor de-oxygenation is also proposed to generate cancer starvation therapy. In the acidic tumor microenvironment, the magnesium silicide nanoparticles released the silane, which efficiently reacted with both tissue-dissolved and haemoglobin-bound oxygen for generating the silicon oxide aggregates and then preventing tumors from receiving oxygen and nutrient by blocking the tumor blood capillaries [447]. Shi *et al*. [448] introduced a sequential catalytic nanoparticle that converted glucose into arsenal. The natural glucose oxidase (GOD, enzyme catalyst) and ultrasmall Fe_3O_4 nanoparticles (inorganic nanozyme, Fenton reaction catalyst) were integrated into the biodegradable dendritic silica nanoparticles. GOD depleted glucose in tumor cells and also produced H_2O_2, thus producing highly toxic hydroxyl radicals via Fe_3O_4-mediated Fenton-like reaction. Reversal of the pancreatic desmoplasia by re-educating stellate cells [449] or delivery of HAase to degrade hyaluronic acid (HA), was able to increase the perfusion of nanoparticles in the tumor stroma [450]. The platelets protect tumor blood vessel integrity and thus impede the diffusion of the nanoparticles into solid tumours [451]. Polymer-lipid-peptide nanoparticles incoporating antiplatelet antibody R300 and doxorubicin were found to deplete tumour-associated platelets, and then enhanced vascular permeability and accumulation of the nanoparticles in tumors, thereby leading to the tumour regression and metastasis inhibition [452].

4.2.5   Multistage nanoparticle design

The nanoparticles are demanded to realize all *3S* nanoproperty transitions to efficiently traverse the *CAPIR* cascade for effective cancer-targeted drug delivery. Manipulating nanoproperties to achieve the separate transition has been well demonstrated [405]. Recently, much attention has been paid to design multifunctional nanoparticles for undergoing multistage transitions, such as size reduction and charge reversal [453,454] through the activation in tumor microenvironment [455], or dual-targeting [456] for enhanced therapy. For instance, the dendrimer-lipid nanoassembly with 45 nm diameter mimicking "cluster-bomb" was designed to illustrate the integration of all the necessary nanoproperties into one system to simultaneously achieve the *3S* transitions [388,430] (Figure 25). The poly(aminoester) dendrimer with 5 nm diameter was chosen as the "bomblet" [457], which were further coated by the stealthy lipid layer. In the tumors, the fusion of this nanoassembly between lipid and cell-membrane fusion was designed as a stimulus to remove the lipid layer to extracellularly and intracellularly release the DOX-loaded dendrimers for deeper tumor penetration. Meanwhile, these pH-sensitive dendrimers gradually displayed the positive charges at the tumor, thus facilitating the endocytosis and subsequent drug release for circumventing the multidrug resistance. The features of the nanoassembly successfully possess the *3S* transitions during the *CAPIR* cascade for enhanced therapeutic efficacy.

The *3S* properties of nanoparticles can be utilized to optimize the anticancer efficiencies. The limited tumor penetration and accumulation of the nanoparticles within the
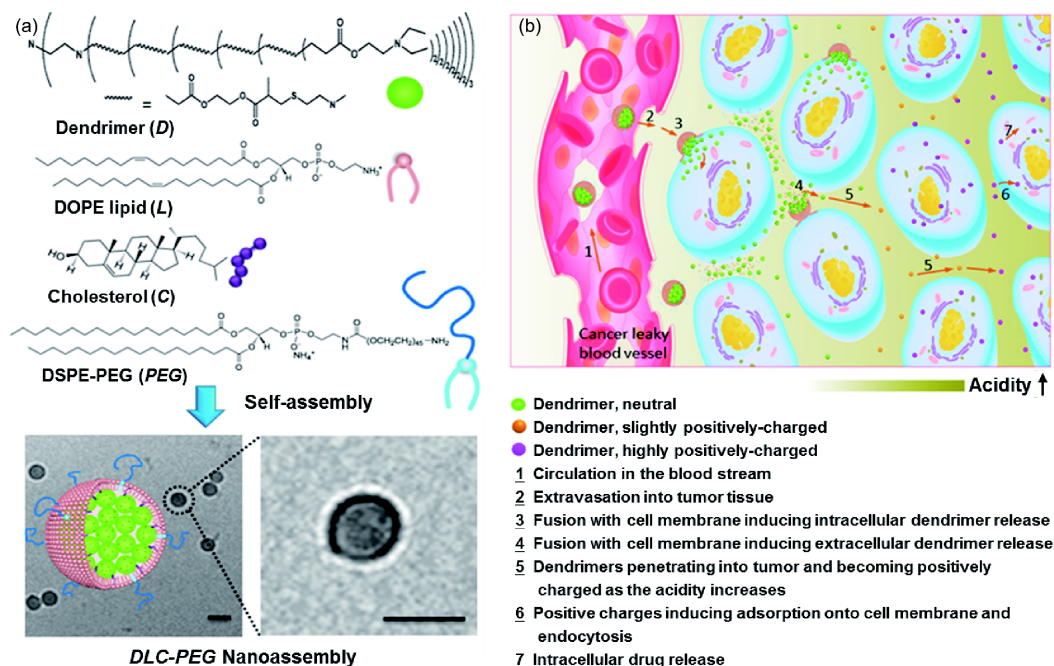

Figure 25   Scheme of the "cluster bomb"-like nanoassembly (a) and its *3S* nanoproperty transition and traversing the *CAPIR* cascade (b) [388] (color online).

tumors are still considered as the inherent bottleneck in cancer therapy due to the pathological characteristics of tumors [458], thus allowing a very small percentage of the injected dose to be deeply distributed into the tumors [459], together with uneven distribution in tumors [460]. The transient opening and closing at the tumor vasculature also restrict the extravasation of nanoparticles [461,462]. Meanwhile, the poor lymphatic drainage further worsens the interstitial fluid pressure, leading to the invalid drug diffusion against the flux gradient [440,463]. Moreover, the high concentrations of drugs stuck on blood vessel wall may deteriorate the vascular hyperpermeability, and then hamper additional drug extravasation. In addition, the limited tumor penetration of nanoparticles is also ascribed to their inherently large size compared to small molecules [391,392], as well as dense interstitial matrix with tight junctions [394,464,465]. Therefore, exploring more effective nanoparticles that can penetrate through tumor vasculature, and further quickly diffuse away, is one of the most important tasks.

4.3   Photoactive nanoparticles for cancer phototherapy

Phototherapy often relies on the use of external light such as visible and NIR light for therapeutic purposes including photodynamic therapy (PDT) and photothermal therapy (PTT). The photosensitizers are used to produce either ROS such as $^1O_2$, O_2^-, $HO^{\bullet}$, H_2O_2 [466], or hyperthermia [132,467], to cause tumor cell death upon light irradiation (Figure 26). The phototherapy continues to attract numerous research attention engaged in cancer therapy, since many cancers such as superficial bladder cancer, esophagus cancer, skin cancer, and lung cancer have been found to be highly susceptive to the phototherapy.

Nowadays, the application of the nanoparticles represents a major stride for resolving some significant challenges in cancer phototherapy, which is expected to promote the development of nanomedicine with high therapeutic efficacy, specificity, and personalization. The nanoparticles display several advantages for their application in phototherapy. For example, the nanoparticles can carry photosensitizing agents in a controlled manner that can prevent the premature leakage and achieve the on-demand drug release; The nanoparticles are able to preferably accumulate at tumor site through the EPR effect, and can further be modified with functional groups for altering their biological properties such as blood circulation, biodistribution, tumor targeting, and cellular uptake, thereby delivering the loaded agents across biological barriers to target the tumor cells; The nanoparticles are able to be engineered as the multifunctional nanoplatforms that involve multiple components (e.g., chemotherapeutic drugs, genes, imaging agents), thus allowing theranostics or combination/multimodal treatments.
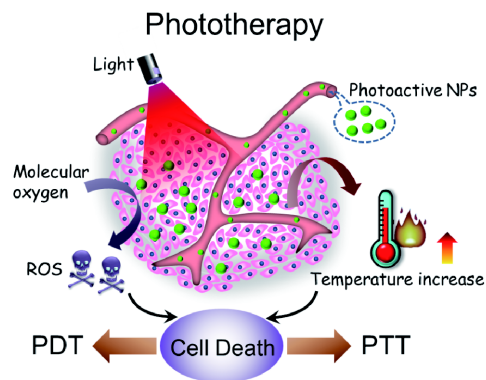

Figure 26   Photoactive nanoparticles (NPs)-based phototherapy for cancer treatment. In both forms of photodynamic therapy (PDT) and photothermal therapy (PTT), photoactive NPs accumulated at tumors are used to produce reactive oxygen species (ROS) or induce temperature elevation under light exposure at a specific wavelength for triggering cancer cell death (color online).

For PDT, the therapeutic efficacy relies on the photo-activation of photosensitizers in the presence of molecular oxygen to produce ROS, which can induce tumor inhibition through vascular destruction, apoptosis-mediated cell injury, and activation of immune response [468–470]. Importantly, exploring the photosensitizers with high quantum yield and good photostability plays a key role in ensuring high PDT efficiency. So far, many kinds of photosensitizers have been identified as excellent generators for efficent ROS production, including organic dyes (e.g., eosin and methylene blue), aromatic hydrocarbons (e.g., anthracenes, napthalenes and biphenyls), quinones, phthalocyanines, porphyrins, tetrapyrroles, and some transition metal complexes [471,472]. For cancer nanomedicine, many efforts have been made to engineer smart nanoparticles that can deliver photosensitizers to target site for greatly enhancing PDT efficacy. For example, the photosensitizers have been incorporated into a variety of nanoparticles such as polymeric nanostructures [473–475], protein constructs [445,476,477], and inorganic nanoparticles [478–480] via chemical conjugation or physical encapsulation. With the modification of targeting ligands that can sepcifically bind to the surface of tumor cells, the favorable selectivity of the nanoparticles toward the tumors can be achieved. Moreover, the use of the nanoparticles can also lead to the increased hydrophilicity and photochemical stability of photosensitizers, which is helpful to enhance the *in vivo* transportation efficiency and subsequent PDT efficacy. Some nanoparticles such as gold nanoparticles, quantum dots, upconversion nanoparticles (UCNPs) that are conjugated with photosensitizers serve as not just the drug carrier, but also the primary light absorber that can transfer energy to the attached photosensitizers through energy transfer, thereby resulting in the indirect activation of photosensitizers [481–484]. Hence, this strategy provides an alternative approach to activate photo-

sensitizer molecules by the light at the wavelength that can not be absorbed by themselves. In addition, some nanomaterials as the photoactive agents also have the ability to produce ROS including TiO_2, fullerene, and ZnO nanoparticles, due to their unique optical absorption properties [485–488]. Although these kinds of nanoparticles have many advantages such as good photostability and low photobleaching, they are usually activated by relatively short light that has very limited tissue penetration depth, and thus hampering their biological applications. This shortcoming can be overcome by incorporating another light absorber such as UCNPs that might convert NIR light into UV-Vis light, and then achieve their photoactivation via energy transfer, together with increased tissue penetration depth, reasonably providing a new avenue for effective treatment against deep-seated tumors.

Unlike PDT, PTT is able to destruct the tumor cells by light-induced temperature elevation and subsequent hyperthermia at tumor site. The photothermal absorbing agents can convert the light energy in NIR region (700–950 nm) into the potent hyperthermia for injuring the tumor [489–491]. The potent hyperthermia is expected to be well-localized at tumor site without affecting adjacent normal tissues, thereby greatly improving the therapeutic efficacy with reduced adverse side effects. In this regard, the nanomedicine is currently considered as the most promising strategy for remote and localized hyperthermia, since the properties of the photothermal nanoparticles can be finely tuned to satisfy the demands for effective PTT. To date, a broad range of photothermal nanoparticles have been explored, including organic photothermal conversional nanoagents and plasmonic inorganic nanomaterials. Generally, organic photothermal nanoagents can be engineered by incorporating NIR dyes such as IR825 and indocyanine green into various nanoparticles including liposomes, micelles, and proteins [492,493]. Certainly, the polymeric nanoparticles such as polydopamine, polyaniline and polypyrrole have the strong NIR absorption due to their extended π-electrons, thus allowing them to behave as efficient photothermal agents [439,494,495]. The others like porphysomes and melanin also have high extinction coefficients in NIR region, enabling their effective generation of photothermal conversion [496–498]. In addition, the inorganic plasmonic nanomaterials have been applied to generate photothermal conversion for killing tumor cells, including carbon nanomaterials (e.g., carbon dots, carbon nanotubes, and graphenes) [124,426,499], gold (Au) nanoarchitectures (e.g., Au nanocages and Au nanorods) [500,501], palladium nanomaterials (e.g., palladium nanosheets) [502,503], metal selenide (e.g., CuSe and Bi_2Se_3) [504,505], metal sulfide (e.g., CuS and WS_2) [506–509], metal oxide (e.g., $W_{18}O_{49}$) [510,511], Prussian blue [512,513], as well as black phosphorous [514]. These nanomaterials with high photothermal conversion ef-

ficiency have shown great capacity to destruct tumor cells through cell necrosis. However, the expression of heat shock proteins (HSP) in hyperthermia-treated cells is usually up-regulated during PTT, which might increase the thermal tolerance of tumor cells to heat stress for enhancing the cell viability, thus compromising PTT efficacy [515–518]. Therefore, it is necessary to explore more effective strategies to down-regulate HSP expression for inhibiting tumor thermoresistance, resulting in preferable photothermal efficacy with minimized adverse side effects.

Among these photoactive nanoparticles for phototherapy, a few types of nanoparticles possess both photodynamic and photothermal effects [519,520], and can also undergo a nanostructure-driven conversion between PTT and PDT [482,521,522], thereby showing the combination of PDT and PTT for synchronous photo-induced cell damage. More interestingly, it has been shown that the mild PTT effect is able to increase the intracellular PS concentration and alleviate the tumor hypoxia. Therefore, the PDT effect could be greatly enhanced with the combination of PTT, and then produce PTT-synergized PDT treatment [523–526]. Moreover, most of these nanoparticles can be used as the fluorescence imaging agents, thus enabling their potentials in image-guided therapy and therapeutic monitoring. For instance, the chlorin e6-loaded gold vesicles with strong absorbance in the NIR region were constructed (Figure 27(A)) [527], and were found to possess the trimodal fluorescence/thermal/photoacoustic imaging capacities (Figure 27(B)), reasonably allowing imaging-guided synergistic PDT/PTT efficacy (Figure 27(C)). With the integration of multiple imaging modalities with high spatial resolution and sensitivity, the complementary imaging charateristics were achieved, thereby overcoming the limitations of single imaging modality [262,528–530]. Moreover, the functionalization of these photoactive nanoparticles is also able to provide a possibility to generate multimodal synergistic therapies [531,532]. The multifunctional photoactive nanoparticles show a great promise in optimizing the anticancer efficacy with minimized adverse side effects for cancer phototherapy.

In addition to the administration of photoactive nanoparticles for cancer phototherapy under light exposure, the light sources such as lasers, light-emitting diodes, and filtered lamps can be employed as a fundamental tool for irradiating the diseased regions [533,534]. This externally applied light irradiation makes the phototherapy highly site-specific, and controllable. Thus, much more efforts should be devoted to improve the property of light instruments, which is greatly helpful to achieve convenient and effective improvements in cancer phototherapy.

Nevertheless, it is difficult to totally ablate the tumor using phototherapy, due to the non-homogeneous penetration of light as well as the uneven distribution of photoactive
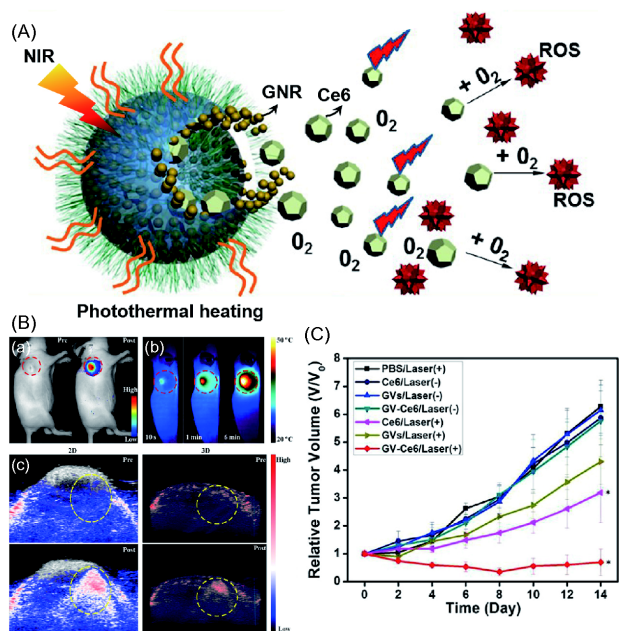
Figure 27 (A) Schematic illustration of Ce6-loaded gold vesicles for imaging-guided synergistic PTT/PDT; (B) *In vivo* NIR fluorescence imaging (a), thermal imaging (b), and photoacoustic imaging (c) of the tumor-bearing mice treated with the vesicles; (C) tumor growth profiles of tumor-bearing mice after different treatments [527] (color online).

nanoparticles within the tumors. The challenge of phototherapy still remains in their potential clinical translation, due to the tumor metastasis and residual tumor cells. Meanwhile, most of the current phototherapeutic studies such as anticancer efficacy, systemic toxicity, and clearance often relied on small rodents (e.g., mice), and were also carried out in a relatively short period of frequently less than 3 months, which are disadvantageous to their clinical translations. Therefore, the long-term toxicity, long-term stability, and biological fate of the nanoparticles should deserve an immediate attention. The properties of the nanoparticles (e. g., material type, shape, size, surface charge and coating) are also considered as the critical factors that determine their biodegradability and biocompatibility. Moreover, some new strategies like photo-controlled bacterial metabolite therapy [535], photo-activated immune-related therapy [536], and photocatalytic reaction-based therapy [537], have been also explored to induce efficient tumor ablation, thereby overcoming the critical obstacles in cancer phototherapy.

4.4 Upconversion nanoparticles for cancer therapy

Upconversion nanoparticles (UCNPs) with the ability to convert lower energy photons to higher energy photons have been widely exoplored in pre-clinical cancer theranostic applications. In general, UCNPs contain lanthanide, transitional metals or actinide dopant ions embedded in the lattice of inorganic crystalline host [538]. Due to their high pho-

tostability, NIR excitation wavelength, high signal-to-noise radio and low photo-damage to biological tissues, UCNPs have been mostly used as efficient luminescent nanomaterials in bioimaging or light-triggered therapy [539–552]. However, their main limitations are associated with inferior pharmacokinetics, unwanted or off-targeted accumulation in healthy tissue, as well as poor tumor penetration capacity. Recently, smart UCNPs that might utilize the components/ characteristics of tumor microenvironment (TME) or intracellular signals to accurately target or respond to tumors, have received much attention. Generally, the biophysico-chemical features of tumor microenvironment mainly include acidic pH, redox reactants, ATP and hypoxia [553], which have been utilized to trigger smartness of UCNPs. In addition, specific proteins or peptides, as well as intracellular mitochondrial and nucleus are also widely used in UCNPs-mediated cancer-targeted therapies. Compared to conventional light-induced cancer therapy, these on-site tumor responsiveness or active tumor-targeting of UCNPs can enhance the therapeutic efficacies and simultaneously reduce adverse side effects.

Due to the excessive tumor metabolism and limited oxygen/nutrition supply, the tumor-specific characteristics are generally applied as the responsiveness of UCNPs in cancer therapy. For instance, the acidic pH at tumor site is broadly used in locally triggered drug release [554–568]. Besides, based on the highly oxidative stresses resulting from over-expressed reactive oxygen species (ROS) in tumors, the redox components such as GSH [569–571] or H_2O_2 [572,573] are also applied for precise tumor destruction. As shown in a related work by Lin *et al*. [574], the Mn-doped UCNPs-DOX nanocomposites were able to simultaneously respond to mild reductive and acidic microenvironment for multiple imaging and chemotherapeutic applications. In this process, Mn–O could be disintegrated by GSH or low pH, thus causing the degradation of the nanocomposites for deeper tumor penetration as well as efficient DOX release. Additionally, Zhang *et al*. [485] reported the H_2O_2-responsive UCNPs@TiO$_2$@MnO$_2$ nanocomposites for overcoming the insufficient O_2 supply, inefficient ROS generation and low light penetration depth. In this typical design, MnO_2 was used to catalyze H_2O_2 to generate O_2 for improving oxygen level in cancer cells. Then, UCNPs were able to convert NIR light to UV light for activating TiO_2, subsequently leading to efficient ROS generation via water-splitting for deep cancer treatment. Besides, UCNPs and decomposed Mn^{2+} could be also applied for upconversion luminescence and magnetic resonance imaging. Moreover, other tumor-specific features such as hypoxia [575–577], high level of ATP [578], riboflavin [579], and excessive Zn^{2+} [580], are also able to be applied to achieve targeted/responsive tumor treatments using UCNPs. Lai *et al*. [578] reported the polypeptide-wrapped UCNPs as ATP-responsive nanoparticles. Zinc-di-

picolylamine analogue (TDPA-Zn^{2+}) was also functionalized on its surface, thus offering a higher affinity to ATP, followed by a competitive displacement of polypeptide-bound surface. This ATP response led to the release of entrapped chemotherapeutic drug for efficient chemotherapy. In addition, the use of UCNPs could not only provide a non-invasive method for long-term tracking of drug delivery using NIR excitation/emission, but also offer an alternative approach to monitor intracellular drug-release kinetics in a real-time manner via a luminescence resonance energy transfer (LRET) process (Figure 28). The UCNPs with multiple-emission peaks might enable such real-time monitoring method to be used for a variety of drugs with different UV-Vis absorption properties. This approach offers a unique strategy to establish the stimuli-responsive nanoparticles and monitor biochemical changes in cancer cells.

In addition to the biophysicochemical features of tumor microenvironment, some specific proteins that are generally overexpressed at tumors or stromal cell membranes have been also exploited to achieve UCNPs-mediated cancer therapy in this scenario, including folate receptor [372,581–598], hyaluronic acid receptor [599–601], transferrin receptor [602], somatostatin receptor [603], epithelial growth factor receptor (EGFR) [604], human epidermal growth

factor receptor 2 (HER-2) [605], angiopep-2 [606], arginine-glycine-aspartic acid (RGD) [607–611] and phospholipase A2 [612]. Among them, folate receptor is the most extensively studied receptor protein. For instance, Wu *et al.* [585] reported a dumbbell-like MnFe$_2$O$_4$-NaYF$_4$ UCNPs for efficient photothermal therapy, in which the high cellular uptake was realized by conjugating folic acid onto UCNPs. Very recently, Yu *et al.* [613] also introduced a pre-protective strategy for precise tumor targeting and PDT, in which UCNPs were modified with polyacrylic acid, folic acid, chlorin e6 functionalized DNA sequence. At first, the longer DNA could protect folic acid on shorter DNA from binding to folate receptors on normal cells. Once reaching the acidic environment in tumor, C-base-rich longer DNA could form a C-quadruplex, leading to the exposure of folic acid to folate receptors on cancer cells for realizing precise targeting. Meanwhile, chlorin e6 as a photosensitizer was also triggered by NIR light from UCNPs to generate singlet oxygen for destructing the tumors (Figure 29). In addition, intracellular components such as mitochondria [614–621] and nucleus [488,622] can also serve as the tumor-specific targets. As a representative example, Liu *et al.* [623] constructed a PDT system consisting of graphene oxide quantum dot-upconversion nanocrystal hybrid nanoparticles with two
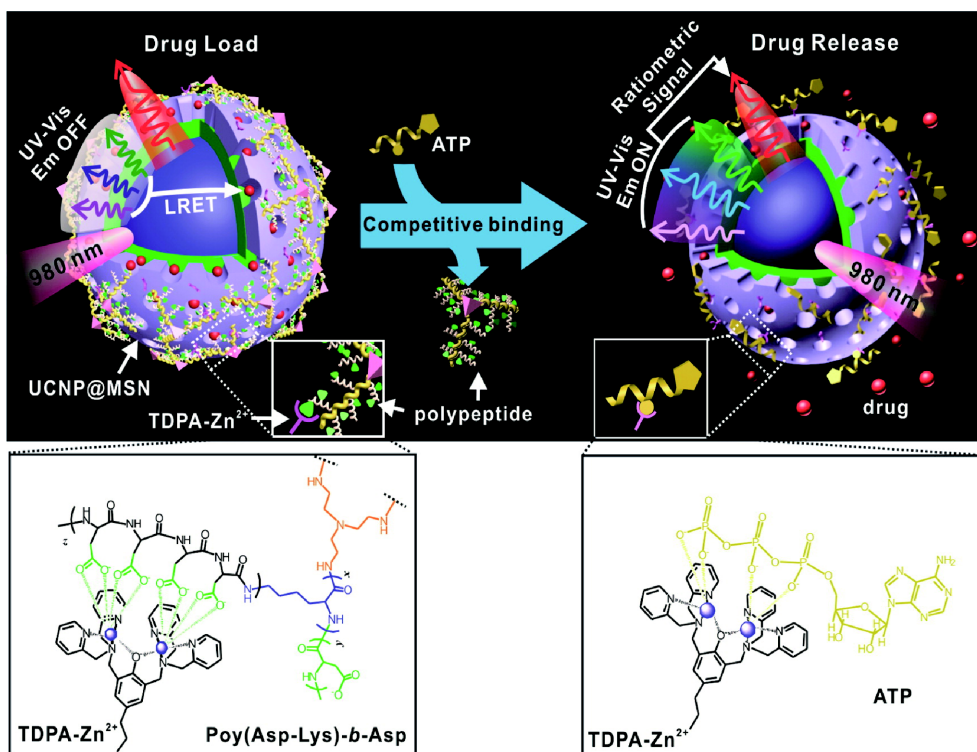
Figure 28   Schematic representation of the real-time monitoring of ATP-responsive drug release from polypeptide wrapped TDPA-Zn^{2+}-UCNP@MSNs. Small molecule drugs were entrapped within the mesopores of the silica shell on the hybrid nanoparticles by capping the pores through multivalent interaction between oligo-aspartate side chain in polypeptide and TDPA-Zn^{2+} complex on nanoparticles surface using polypeptide. The UV-Vis emission from the multicolor UCNP under 980 nm excitation was quenched because of LRET between the loaded drugs and UCNPs. The addition of ATP led to a competitive binding of ATP to the TDPA-Zn^{2+} complex, which then displaced the surface bound compact polypeptide due to the high binding affinity of ATP to the metallic complex. The drug release was accompanied with an enhancement in the UV-Vis emission of UCNPs, thus providing real-time monitoring of drug release [578] (color online).
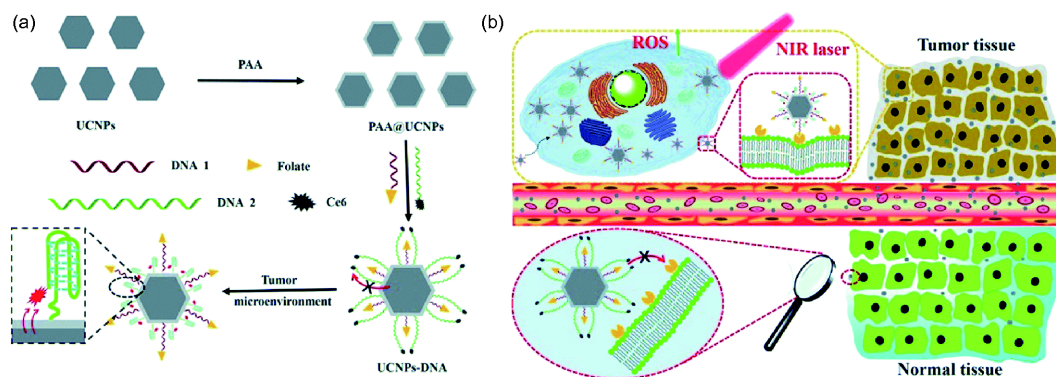
Figure 29   (a) Synthetic process of UCNPs@PAA-DNA; (b) details of precise tumor targeting and specific photodynamic therapy for cancer [613] (color online).

targeting ligands including folic acid and carboxybutyl triphenylphosphonium (a mitochondrion-targeting moiety). Such dual targeting modification not only resulted in a preferable *in vivo* targeting capacity, but also caused enhanced cell death through mitochondrial damage, reasonably improving their PDT efficacy. Distinctly, the smart UCNPs could realize a precise tumor target as well as enhanced theranostic outcomes.

4.5   Nanoparticles for immunotherapy of cancer

Recent studies have shown great clinical potentials of educating and awakening patients' immune systems to treat cancer, as evidenced by the fact that more than half of the current cancer clinical trials include formats of immunotherapy [624]. However, a major challenge still remains in current cancer immunotherapeutics. For example, the percentage of patients who can respond to cancer immunotherapy is relatively low. The adverse side effects such as autoimmune disorders and "cytokine storm", can severely pose threat to patients' health [625,626]. In recent years, the nanoparticles have attracted a great deal of interests for improving the response rate and therapeutic efficacy in cancer immunotherapy, together with reduced adverse side effect [627,628]. A diverse range of synthetic and biological nanoparticles with different physicochemical characteristics have been developed to stimulate the immune system to fight against cancer. The nanoparticles have also been exploited to achieve cancer-targeted delivery and controlled release of immunotherapeutic or immunomodulation agents [629,630]. Moreover, the nanoplatforms also enable the effective combination of immunotherapy with other therapeutic modalities for synergistic therapeutic performances [629,630].

With the assistance of nanomedicine, the combination of nanoparticles and immunotherapy could achieve synergetic anticancer effects. For example, the phototherapy of the nanoparticles including PTT and PDT has been to induce a strong antitumor immune response by releasing tumor antigens and immunostimulatory molecules to promote the subsequent activation of dendritic cells. With the further help of the immune checkpoint blockade therapy, the combination approach could significantly inhibit cancer relapse and metastasis, thus improving the potential response rate and therapy effect of immune checkpoint blockade [289,631–634]. Encouraged by this discovery, some other nanoparticles have been developed for treating cancer metastasis by the combination of PTT/PDT and immunotherapy. For instance, the combination of PTT and chemotherapeutic agent was found to synergistically elicit systemic antitumor immunity [635]. Similar to phototherapy, radiation therapy could also induce the antigen release and activation of dendritic cells. The nanoparticles were used as the tumor-associated antigen capturer after radiotherapy to prime the dendritic cells and T cell responses [636]. Recently, a stimulus-responsive hydrogel consisting of catalase labeled with ^{131}I radioisotope, CpG oligonucleotide, and sodium alginate has been explored [637]. This strategy was found to completely damage the solid tumors at a low radiogenic dose in mouse and patient-derived mouse xenografts, followed by an antitumor immune response. Upon combining with an immunological checkpoint inhibitor, the systemic therapeutic responses were boosted to effectively cooperate with local therapy, inducing the inhibition of tumor metastasis and protection against tumor recurrence (Figure 30).

A variety of nanoparticles with unique physicochemical properties have been also utilized to enhance the accumulation of drugs within tumors, showing a great promise in immuno-oncology applications. For example, the nanoparticles have been engineered as the nanovaccines for antigens or adjuvant delivery to antigen-presenting cells for priming T cell responses [638–641]. The lipid nanoparticles were reported to deliver RNA sequences that encoded the viral or mutant neoantigens to dendritic cells in spleen, thereby inducing the strong antitumor effector and memory T-cell responses in three melanoma patients [642]. In another
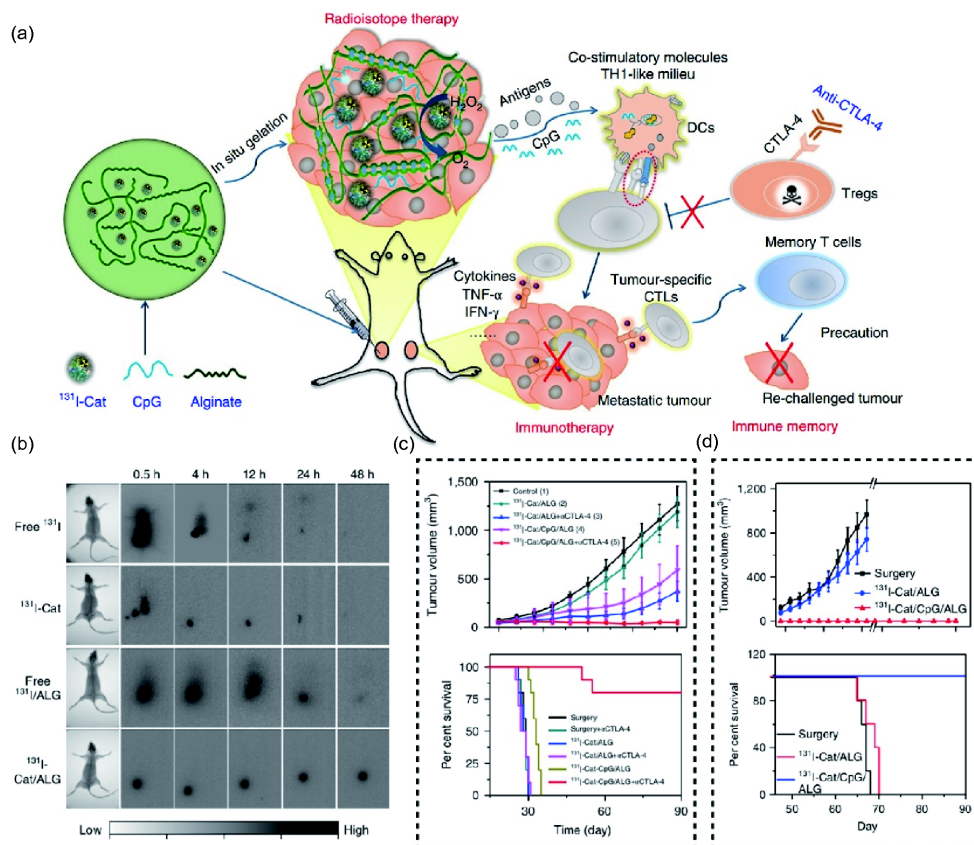
Figure 30 Local immunostimulatory radiation therapy based on the biomaterials together with systemic immune checkpoint blockade can induce a strong antitumor immune response to inhibit the tumor metastasis and prevent tumor recurrence. (a) Scheme of the combination of radioisotope therapy and immune therapy based on alginate hydrogel. (b) Gamma imaging of mice after i.t. injection of therapeutic agents. (c) Growth curves for tumors on mice after various treatments. Survival of mice with spontaneous metastases 4T1 tumors after various treatments to dispel their primary breast tumors. (d) Tumor growth curves of rechallenged tumors and survival curves of mice after various treatments [637] (color online).

example, the synthetic PLGA nanoparticles-stabilized Pickering emulsion adjuvant system (PPAS) was developed to enhance the antigen uptake and activation of antigen-presenting cells [638]. In addition, some biologically inspired nanoparticles can also be used as the nanocarriers for the antigen delivery. Yang *et al.* [643] reported the cancer cell membrane-capsuled immune-adjuvant nanoparticles, which possessed the efficient uptake by dendritic cells, and thus delayed the tumor deterioration.

Nanomedicine can also deliver other immune stimulants such as cytokines and antibodies to T cells for enhancing their activity [568,644–646]. The synthetic nanoparticles such as PLGA nanoparticles were reported to deliver leukemia-targeting chimeric antigen receptor (CAR) genes [647], or CTLA-4–small interfering RNA (siRNA) (NPsiCTLA-4) [648], systemically into T cells *in vivo*, significantly activating the effector T cells to attack cancer cells. Protein-based nanoparticles such as interleukin-15 super-agonist complex were also reported to conjugate cell surface of T cell, significantly expanding T cells by 16 times in tumors as compared to free interleukin-15 [646]. The anti-PD-L1 antibodies could also be engineered on the plasma membranes of the platelets that could accumulate in the re-

section cavity after resection of tumor [649]. After the activation of platelets, the nanoparticles with anti-PD-L1 were released from platelets to bind the residual tumor tissue in surgical bed, thus leading to the inhibition of cancer recurrence after surgery (Figure 31) [649].

4.6 Locally selective nanoparticles for interventional therapy of cancer

Local tumor chemotherapy is of considerable interest for improving antitumor efficacy and minimizing the damage to surrounding healthy tissues by direct delivery and long-term retention of therapeutic agents into tumor lesions. In particular, the nanomedicine acts as an increasingly important role in local tumor chemotherapy owing to their unique properties, such as high drug loading and controlled release [650]. The PLGA-coated superparamagnetic nanoparticles were locally injected into the tumor site for producing the magnetocaloric effect by applying an external magnetic field. The strategy caused the coagulative necrosis of tumors and then achieved the enhanced antitumor efficacy [651]. The blood-vessel-embolic microspheres with the so-called "nano-in-micro" structure were prepared using microfluidic
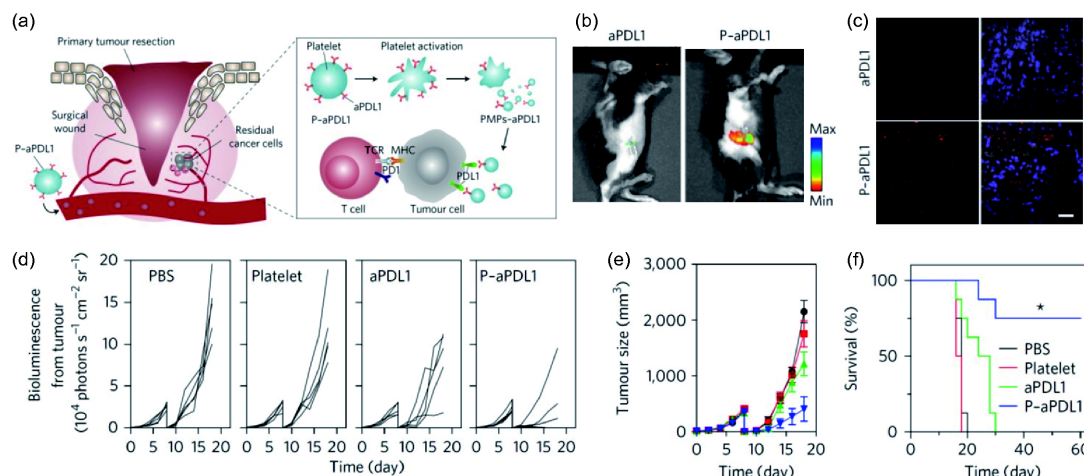
Figure 31 *In situ* activation of P-aPDL1 promoted the releases of anti-PDL1 (aPDL1) and cytokines. (a) Schematic illustration of the delivery of aPDL1 to the primary-tumor resection site by platelets; (b) fluorescence imaging of the mice 2 h after *i.v.* injection of P-aPDL1 or an equivalent dose of free aPDL1; (c) confocal images of the slices from residual tumors from the mice shown in (b); (d) quantified bioluminescence for the tumors from different treatment groups; (e, f) tumor growth (size) and survival curves [649] (color online).

technique, thereby displaying a good integration of CT/MRI with the antitumor effect of chemo-embolization against liver cancer [652].

As a minimally invasive approach, the interventional therapy usually introduces the specific devices or materials through natural human orifices or micro-incisions in the human body for the treatment of lesions under the guidance of medical imaging such as digital subtraction angiography, CT, ultrasound and MRI. The interventional therapy has been considered as one of extensively used therapeutic modalities in clinics due to its minimal invasion, accurate localization, high curative effect, less complication, quick effect and strong reproducibility. In particular, the interventional therapy plays a key role in the treatment of malignant tumors such as liver cancer. It enables the direct delivery of drugs and medical materials to the lesion site, effectively improving the therapeutic efficacy, decreasing adverse side effects on healthy tissues, and improving life quality. Generally, two kinds of interventional therapy including vascular intervention (e.g. arterial embolization and perfusion) and physical tumor ablation (e.g. radio-frequency, microwave, laser, ultrasound focusing and freezing), have been widely applied for treating liver cancer with different stages, according to Barcelona clinic liver cancer treatment standards [653] and Chinese liver cancer clinical treatment guidelines. For instance, radio-frequency ablation (RFA) is primarily used for early-stage liver cancer therapy, while transcather artery chemo-embolization (TACE) is used for the treatment of mid-stage liver cancer since it is able to selectively deliver embolic materials and chemotherapeutic agents to the peripheral blood vessels of the targeted tumor. It blocks the blood flow and gradually releases chemotherapeutic drugs to exert synergistic antitumor effect between physical embolization and chemotherapy. Given that the liver has a unique

portal vein and hepatic artery blood supply system, more than 75% of blood in the healthy liver is supplied by the portal vein, whereas blood for liver cancer tissue is mainly supplied by the hepatic artery. TACE can selectively block the hepatic artery blood supply, causing ischemic necrosis of liver cancer with less impact on the healthy counterparts [654,655]. In TACE surgery, the vascular embolization materials play a critical role in blocking blood supply and controlling drug release, therefore determining the anticancer efficacy against liver cancer.

The ideal embolic material needs to have the following characteristics: (1) good flowability and easy diffusion into tiny tumor arteries; (2) easy operation and control by a clinician; (3) complete and effective embolization on various levels of tumor arteries; (4) X-ray imaging ability within a long time for preoperative diagnosis and postoperative examination; (5) good biocompatibility; and (6) targeted delivery and sustained release of various therapeutics (growth factors, proteins, genes, drugs, etc.) along with vascular embolization. However, the clinically used embolic materials are still not able to satisfy these requirements. The solid embolic agents like PVA particles/microspheres and sodium alginate microspheres are difficult to push out from a catheter owing to their high friction coefficient. In contrast, liquid embolic agents are likely to adhere to the catheter and are difficult to control during operations. Liquid materials including lipiodol and anhydrous ethanol, fail to completely embolize the blood vessels of different size. A variety of embolic agents and their respective advantages and disadvantages are shown in Table 1.

Lipiodol and drug-eluting beads are frequently used blood-vessel-embolic agents for interventional therapy against solid tumors such as liver cancer. However, lipiodol is easily metabolized *in vivo*, and thus the embolization time and ef-

Table 1   Some classical embolic agents for clinical applications

Trade name	Material	Mechanism of embolization	Advantage	Disadvantage
Lipiodol®	Iodized poppy seed oil	Selective deposition in hepatocellular carcinoma, and frequently use with gelatin sponges	Excellent X-ray contrast and lipiodol deposition in tumor as gold standard for TACE	Pulmonary embolism caused by excessive dosage
Gelation sponge	Gelatin	Irregular shape, and mechanical embolization of blood vessels	Biodegradability	Usually use in combination with contrast agent, and not suitable for drug loading and long-term embolization
KMG microsphere	Sodium alginate	Mechanical embolization of microspheres into blood vessels	Biodegradability and standard microspheres	Usually use in combination with contrast agent and not suitable for drug loading
DC Bead®	Sulfonylated PVA	Mechanical embolization of blood vessels, and electrostatic interaction with chemotherapeutic drug	Extensive use as drug-eluting bead, high drug loading efficiency, and slow drug release	DC Bead is not superior to C-TACE in the treatment of liver cancer in clinic

fects can not be guaranteed. To satisfy the requirement on TACE time (at least 1–2 weeks [656]), drug-eluting beads (DEB) have been developed in recent years. Usually, some alkaloid drugs (e.g. doxorubicin and camptothecine) can be electrostatically adsorbed on sulphonated PVA microspheres, and efficiently delivered into tumor blood-vessels through a microcatheter, thus achieving simultaneous embolization and sustained drug release [657]. However, it is difficult for DEB microspheres to achieve peripheral vascular embolization owing to their limitation in microsphere size. Moreover, the tumor collateral circulation often occurs in TACE therapy of these embolic microspheres. In addition, the microspheres are likely to block the catheter during the injection, leading to the inconvenience in clinical operation. In some clinical studies, no significant difference of the survival time of patients in the TACE therapy against liver cancer was found between DEB microspheres and lipiodol based TACE therapy (conventional TACE) [658].

The temperature-sensitive polymeric nanogels with nanoscale three-dimensional networks have been recently explored as the emerging nanoparticles for interventional therapy, which is able to display some distinct changes on structure and property under a tiny stimuli of temperature. Upon reaching the critical gelation concentration, the nanogels were found to show the unique sol-gel phase transition at an unique temperature, which was tailored by controlling the monomer type and ratio, amount of the crosslinking agent, and nanogel concentration. The temperature-sensitive sol-gel phase transition was applied to address the dilemma between flowability and embolization that happens in clinically used embolic agents. As blood-vessel-embolic nanoparticles, the temperature-sensitive nanogels might totally occlude all the blood vessels, and then cause a preferable peripheral embolization as compared to Lipiodol (Figure 32) [311,659–661]. The thermosensitve nanogels also have the merits of high drug loading and long-term controlled drug release [662]. In addition, the nanocomposites consisting of gold nanoparticles and temperature-sensitive nanogels were also developed to accomplish the simultaneous diagnosis and treatment of liver cancer [663,664].

Currently, intratumoral injection is one of the common interventional therapy strategies. The intratumoral implants used in clinical practices include radioactive iodine-125 particles or oncolytic viruses [665,666]. The chemotherapeutic drugs can be incorporated on the temperature-sensitive nanogels through the electrostatic adsorption or coordination binding, which can gradually release the drugs within the tumor after intratumoral injection. For instance, a triblock temperature-sensitive polymer was employed to prepare the DOX-loaded nanoparticles at the loading of 41%, which showed a sustained drug release after intratumoral injection. The pH/temperature-sensitive polymeric nanogels were also coordinated with water-soluble platinum, and then resulted in the encouraging results after intratumoral injection [667,668]. There were also some studies about the na-
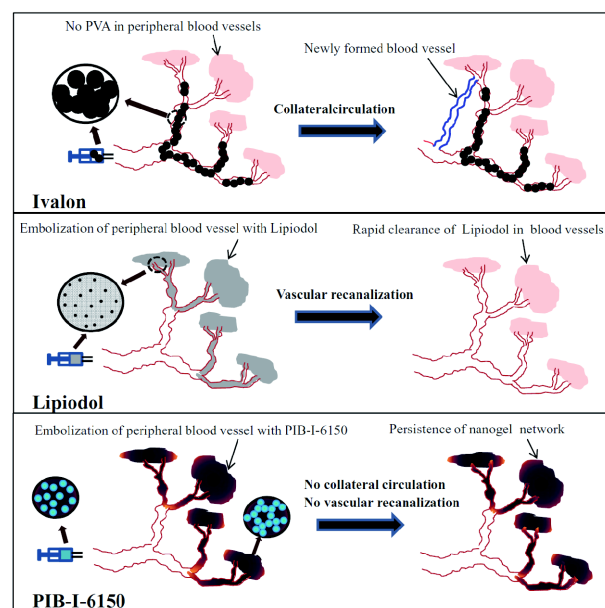
Figure 32   Embolization mechanisms for Ivalon (PVA microparticles), Lipiodol, and PIB-I-6150. Ivalon: collateral circulation occurs after embolization due to the large size of PVA microparticles; Lipiodol: embolization is rapidly eliminated due to blood scouring and tissue clearance in the peripheral blood vessels; PIB-I-6150: permanent and peripheral embolization is achieved by the formation of high-strength hierarchical 3D networks of nanogels through sol-gel transitions (color online).

nomedicine for radiosensitization and drug penetration through intratumoral injection [669].

The physical tumor ablation is one of the frequently used local treatment methods. Most ablation protocols include RFA [670], cryoablation [671] and HIFU ablation [672]. Recently, the RF-responsive nanoparticles such as gold nanoclusters, carbon nanotubes, graphenes and cobalt nanoparticles that depend on their preferable ability of RF electromagnetic waves to penetrate tumor tissue, have achieved the efficient thermal deposition in tumors at a deep and selective manner [673–675]. This provides an opportunity to overcome shortcomings of traditional RFA treatment including small ablation area, poor synergy with chemotherapy, and non-selective damage to the healthy tissues surrounding the tumor [676]. Although TACE showed an impressive therapeutic effect on the peritumoral tissues with a high blood supply, it was still ineffective in the central area of tumors that has a poor blood supply. Moreover, given that hypoxia-tolerant tumor cells/stem cells can proliferate in the central area of tumor, the hypoxic environment caused by TACE might further stimulate their growth, leading to the frequent recurrence and metastasis. Thus, the combined therapy of RFA and TACE is often used to treat liver cancer [677].

A variety of nanoparticles play the increasingly important role in the local treatment of tumors. In addition to TACE, intratumoral injection, and ablation therapy mentioned above, there are many nanoparticles that can be applied for orthopaedic restoration, wound adhesion prevention, and other local therapies. It is also necessary to carry out their detailed evaluations in the long-term safety issue for the implantation in living organisms.

5   Nanotoxicity in cancer nanomedicine

For the development of cancer nanomedicine, safety consideration is of prime importance. Interaction of the nanoparticles with biological system is highly dependent on their physicochemical properties like size, shape, surface charge, surface roughness and hydrophilicity/hydrophobicity [678]. Beside physicochemical properties, the biological fate of the nanoparticles is further determined by the nature of targeted cells and composition of biological fluids. Foreseeing the variables like physicochemical properties, environmental factors, and target cell properties, it is very complex to fully assess the toxicity of the nanoparticles [679]. Both *in vitro* and *in vivo* models have been applied to evaluate biological responses and behaviors of nanoparticles. It is important to obtain a better understanding of their pharmacokinetic processes, including absorption, distribution, metabolism, excretion, and toxicity (ADMET) in biological systems, so that their possible undesirable effects can be avoided.

5.1   Safety evaluation and risk assessment of cancer nanomedicine

Although our understanding of nano-bio interactions has been increased in the recent years, still there is a long way to explore the toxicity of nanoparticles in the perspective of cancer pathophysiology [680]. The pathways of their cellular uptake and trafficking (micro-pinocytosis, endocytosis, simple diffusion and phagocytosis) highly depend on the physicochemical properties, type of cells and bio-corona formation. Key development in high-resolution cellular *in vivo* imaging has enabled us to analyze single-cell pharmacokinetics and track cell-to-cell variability of cancer cells [681]. Furthermore, in the determination of theranostic potential and fate of the nanoparticles, the intracellular trafficking regulated by network of cellular endosomes, lysosomes, endoplasmic reticulum (ER), and Golgi apparatus is also very critical. In a recent study, the synchrotron radiation-based scanning transmission X-ray microscopy (STXM) was applied to demonstrate the uptake and sub-cellular dispersal of $Gd@C_{82}(OH)_{22}$ [682]. Moreover, $Gd@C_{82}(OH)_{22}$ produced the pro-inflammatory cytokines such as IL-1β via activation of primary mouse macrophages. The involvement of NLRP3 inflammasomes in the production of IL-1β was further confirmed through small interfering RNA (siRNA) knockdown. Thus, it is vital to explore the interactions between nanoparticles and cells in the context of tumor heterogeneity for minimized toxicity.

5.2   Potential mechanisms of nanotoxicity

There are numerous ways in which the cells sense and respond to nanoparticle-induced negative effects. The changes can be intracellular disruption of cellular membrane, damage to DNA, malfunctioning of mitochondria and endoplasmic reticulum, ROS production, activation of apoptosis pathways, genotoxicity, or extracellular release of inflammatory cytokines [683]. Though, the ROS generation is vital for normal cellular metabolism, and then the imbalanced production and elimination of intracellular ROS can lead to inflammation and genotoxicity. ROS can be generated from several sources including the surface of nanoparticles, mitochondrial dysfunction induced by the nanoparticles, activated macrophages and neutrophils caused by the nanoparticles, as well as oxygen metabolic products catalysed by transition metal [684]. Moreover, the nanoparticle-mediated immunotoxicity can result in the activation of inflammasomes, leading to a cascade of immune reactions [685]. In addition to the DNA damage caused by ROS generation, the nanoparticles with size less than 10 nm can cause genotoxic effects via point mutations, chromosomal fragmentation, and DNA strand breakages [686]. Furthermore, the lysosomal pathways are also vital for cellular

homeostasis as they are able to degrade the damaged organelles, unwanted proteins, intracellular pathogens, and nanoparticles. The nanoparticles having proton buffering potential can function as lysosomotropic agents, thus leading to the release of lysosomal hydrolases, damaging major organelles, and ultimately resulting in the apoptosis [687]. In the present context, the nanoparticle-induced mitochondrial dysfunction can also lead to apoptosis. The contact of the nanoparticles with ER can result in the activation of cell-rescue pathway (ER stress). Interestingly, ER stress has been utilized as biomarker of nanotoxicity for various nanoparticles. In parallel with the mitochondrial and lysosomal dysfunction, ER disruption also leads to the imbalance in cellular homeostasis [688].

5.3   Personalized protein coronas & therapeutic efficacy

The surface properties of the nanoparticles are altered when in contact with proteins present in the physiological media. The proteins can form a layer on the nanoparticles known as "protein corona" which influences their biological activity and therapeutic efficacy along with toxicological pathways [689]. Individual patients can react very differently to the therapeutic nanoparticles due to variation in physical states, which can result in variable protein corona and increase their opsonization via RES, resulting in fast blood clearance. For the development of personalized nanomedicine having minimal side effects and maximal therapeutic efficacy, it is vital to ponder over the factors that can affect the biological fate of the nanoparticles [690]. Furthermore, the disorders leading to disruption in blood homeostasis and protein structure variation can also considerably affect the protein corona of the nanoparticles. Specifically talking in the context of cancer pathophysiology, the variations in the secreted biomolecules in different type of cancers can differ in a patient-specific manner, which not only affects the protein corona composition but also the absorption, distribution, metabolism, and excretion (ADME) of the nanoparticles [679]. In a study by Hajipour *et al*. [691], effects of various medical conditions (e.g. breast cancer, rheumatoid arthritis, and hypercholesterolemia) on the composition of protein corona were demonstrated via incubating in the plasma of human subjects. Interestingly, the corona composition on the nanoparticle surface varied significantly in each medical condition and highly depended on the patient's personalized physiological condition.

The interaction of cells with nanoparticles largely depends on the protein corona instead of the bare nanoparticles. Cheng *et al*. [692] demonstrated the effect of protein corona on the cellular uptake of gold nanoparticles (AuNPs). In cell type and particle size dependent manner, the cellular internalization was significantly reduced due to protein corona

formation, thus giving useful information on the design of AuNPs for cancer theranostics. For acquiring information regarding nanotoxicity, it is vital to elucidate the binding structure and stability of protein corona on the nanoparticles. Wang *et al*. [693], analysed the structure of hard serum albumin protein corona (BSA) on CTAB-coated gold nanorods (AuNRs) via various techniques such as synchrotron radiation X-ray absorption spectroscopy, microbeam X-ray fluorescent spectroscopy, and circular dichroism in combination with molecular dynamics simulations (Figure 33). The cytotoxic potential of AuNPs was demonstrated to be reduced due to the formation of stable corona having 12 Au–S bonds responsible for protein adsorption. Understanding the key concepts of personalized protein corona formation and tracking the fate of the nanoparticles can result in the development of more effective cancer nanotherapeutics with minimal toxicity.

5.4   Emerging methods for cellular uptake and biotransformation evaluation of nanoparticles

As compared to the laboratory setting, the behaviour of the nanoparticles can be unprecedented in the pathophysiological environment of cancer. The growth rate, signalling pathways and dissimilar membrane properties of various types of cells can result in variable responses even to the same type of nanoparticles [694]. Their toxicity or therapeutic value can be determined upon elucidation of intracellular chemical transformations. Wang *et al*. [695]
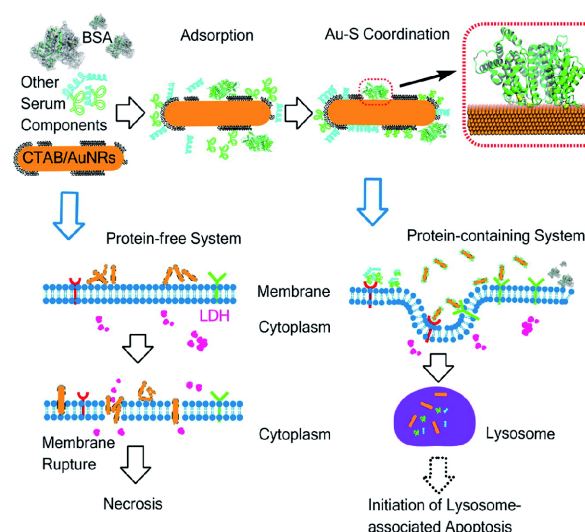
Figure 33 Role of serum proteins in the interaction of AuNRs with membranes. Partially exposed CTAB/AuNRs are incubated with BSA to form a hard BSA corona via Au−S coordination. The existence of the protein corona facilitates the protein receptor-mediated internalization and translocation of AuNRs to endo-/lysosomes, where the CTAB bilayer on AuNRs can probably induce lysosome-associated apoptosis. Without a protein coating, CTAB/AuNRs can directly destroy the cytoplasmic membrane, form defects, and cause the release of LDH, which eventually induces necrosis [693] (color online).

explored the chemical origin of silver nanoparticles (AgNPs) using synchrotron radiation-beam transmission X-ray microscopy (SR-TXM) and SR-X-ray absorption near edge structure (SR-XANES) spectroscopy. The 3D distribution and chemical transformation of AgNPs were explored in human monocytes (THP-1). The conversion from elemental silver $(Ag^0)_n$, to Ag^+ ions and Ag–O–, then Ag–S– species was the reason for the cytotoxicity of AgNPs. The studies in the chemical origins of cytotoxicity can be of high value in easing the clinical development of cancer nanomedicine. In another study by Chen *et al.* [696], the *in vivo* toxiological profile of T_1-weight MRI contrast agents such as gadopentetate dimeglumine injection (GDI), gadolinium (Gd)-based contrast agent (GBCAs), extremely small-sized iron oxide nanoparticles (ESIONs), and manganese oxide nanoparticles (MnONPs) were compared. Intrestingly, in comparison to GDI, GBCAs and MnONPs, ESIONs were proved as a least toxic agent, which could further be developed as potential MRI contrast agent.

Analytical methods have been recently used for elucidating the dynamics of ADME of the nanoparticles [697]. The absorption of the nanoparticles can be determined via photoacoustic imaging and Raman spectroscopy, while inductively coupled plasma mass spectrometry (ICP-MS), inductively coupled plasma optical emission spectrometry (ICP-OES), neutron activation analysis (NAA) and isotopic tracing (IT) can be used for quantifying tissue penetration. MRI, PET, and SPECT can be further utilized to analyse deep tissues propagation of the nanoparticles. Furthermore, laser ablation inductively coupled plasma mass spectrometry (LA-ICP-MS), secondary ion mass spectrometry (SIMS) and synchrotron radiation X-ray fluorescence spectroscopy (SRXRF) techniques are used for cellular distribution of the nanoparticles. Analysis of the metabolism in liver and elucidation of chemical and enzymatic processes can be performed using X-ray absorption spectroscopy (XAS) and high performance liquid chromatography (HPLC)-coupled ICP-MS (HPLC-ICP-MS). Mass spectrometry, optical methods and nuclear analytical techniques are also used for analyzing the excretion of nanoparticles (Figure 34) [698].

6 Conclusions and outlook

The nanoparticles have been extensively developed for precise cancer imaging and targeted cancer therapy, as evidenced by a few breakthroughs have been made in the explorations of preclinical and clinical nanomedicine. This review summarizes the explorations and recent trends of the nanoparticles in cancer nanomedicine. The synthesis, char-
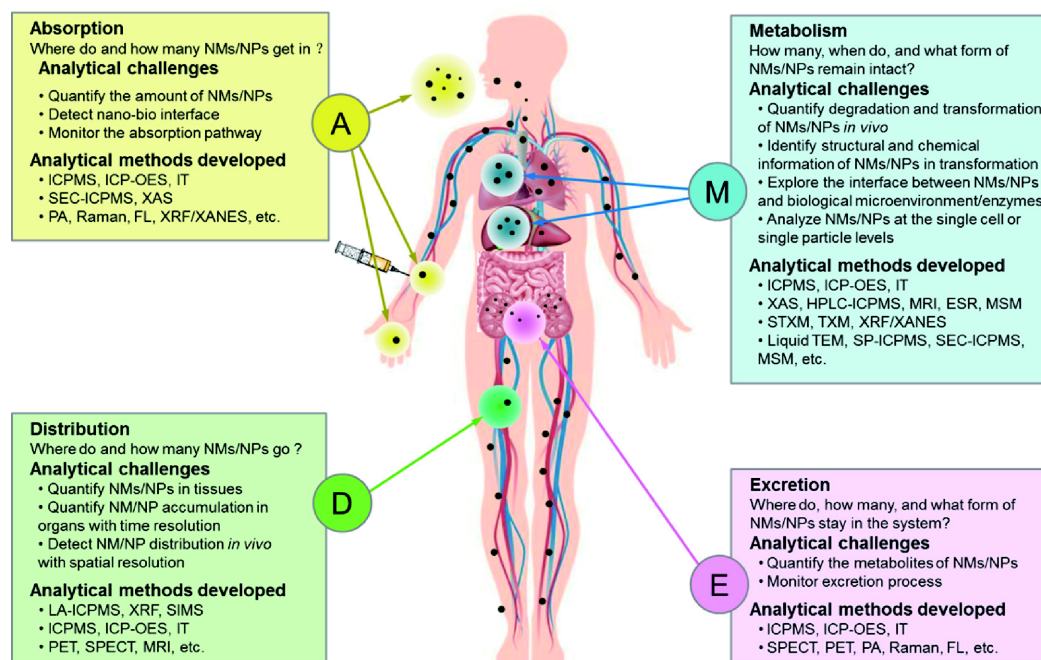
Figure 34 Diagram of the ADME processes of NMs/NPs *in vivo* and summary of the current challenges for their quantitative analysis. NMs/NPs are exposed to human beings mostly through four routes, i.e., oral intake, skin contact, inhalation, and intravenous injection. Upon entering the body, NMs/NPs are quickly distributed into specific organs and then metabolized primarily by the liver. The final excretion of NMs/NPs usually occurs in the liver and kidney in the form of urine and feces. In general, the most important issues regarding the ADME processes of NMs/NPs include: (1) Where do and how much NMs/NPs get in (via absorption)? (2) Where do and how much NMs/NPs go (via distribution)? (3) How much, when do, and what form of NMs/NPs remain intact (via metabolism)? (4) Where do, how much, and what form of NMs/NPs stay in the system (via excretion)? At various stages of the ADME processes, the challenges for *in vivo* analysis of NMs/NPs may become largely different. Important analytical methods to resolve the analytical challenges for each ADME process are summarized [698] (color online).

acterization, *in vitro* cell studies, as well as *in vivo* imaging or therapeutic performances have been comprehensively investigated for a variety of smart nanoparticles, showing an encouraging potential for cancer nanomedicine.

For intelligent therapy of cancer, a variety of physico-chemical characteristics of smart nanoparticles including size, morphology, charge, diffusion, stability, surface functionalization and nano-bio interaction, have to be reasonably optimized or balanced for sophisticated delivery cascade including blood circulation, vascular extravasation, tumor penetration, cellular uptake, intracellular translocation and subsequent release at subcellular target site. Especially, each step in the cascade certainly demands different properties, thus highly necessitating rational design of smart nanoparticles through tailoring their characteristics for satisfying each requirement. The systemic investigations of smart nanoparticles are thus needed to establish their rationality for potential clinical translations through the optimization of absorption, distribution, metabolism, excretion, and toxicity, thereby offering significant advantages of therapeutic efficacy or adverse side effect over clinically applied free drugs. However, to date, there are only a few injectable ingredients such as phospholipid, albumin, and PEG that can be directly utilized as clinically approved agents without additional safety concern. Then, applying new and safe ingredients in designing nanoparticles might play a crucial role in achieving successful development. Furthermore, despite of primary cancers, advanced tumor microenvironment such as hypoxia, tumor drug resistance, tumor metastasis, hypovascular tumor, residual or deeply located tumor cells surviving from treatment, and cancer stem cells might further complicate the design of nanoparticles, in which a few comprehensive designs might particularly be employed for combinational therapy or imaging-guided therapy. From the point of clinical translation, the complicated structure designs of nanoparticles that can satisfy the cascade might seriously suffer from the potential safety burdens such as immunogenicity, maximum tolerated dose, and long-term toxicity, although most of the frequently employed materials are considered as biocompatible and biodegradable ingredients. Hence, the frequently employed ingredient in nanoparticles has to be comprehensively evaluated for addressing these safety issues. Moreover, the *in vivo* performances of nanoparticles from animal studies might be still encountered with inconsistence with human clinical trials, and then a major challenge remains in establishing reasonable and highly relevant animal models such as patient-derived xenograft (PDX) for precisely predicting and indicating clinical translation potentials. Additionally, the quality control, reproducibility, and large-scale production are also demanded for engineering the nanoparticles. Although these aspects are often not viewed as crucial factors in the preclinial exploration, a rational consideration should be also made in the design of nanoparticles.

In any case, simplified and powerful designs of smart nanoparticles are highly desired for clinically potential cancer nanomedicine, as indicated by the emerging frontiers in this review that might bring new and promising concepts for cancer nanomedicine. The developments presented in this review, are expected to inspire more successful explorations and clinical translations of intelligent nanoparticles for the revolution of precise nanomedicine.

Conflict of interest   The authors declare that they have no conflict of interest.

1   Allemani C, Matsuda T, Di Carlo V, et al. *Lancet*, 2018, 391: 1023–1075

2   Wicki A, Witzigmann D, Balasubramanian V, Huwyler J. *J Control Release*, 2015, 200: 138–157

3   Laroui H, Rakhya P, Xiao B, Viennois E, Merlin D. *Dig Liver Dis*, 2013, 45: 995–1002

4   Du B, Yu M, Zheng J. *Nat Rev Mater*, 2018, 3: 358–374

5   Qi GB, Gao YJ, Wang L, Wang H. *Adv Mater*, 2018, 30: 1703444

6   Li S, Jiang Q, Liu S, Zhang Y, Tian Y, Song C, Wang J, Zou Y, Anderson GJ, Han JY, Chang Y, Liu Y, Zhang C, Chen L, Zhou G, Nie G, Yan H, Ding B, Zhao Y. *Nat Biotechnol*, 2018, 36: 258–264

7   Chen Y, Huang Z, Zhao H, Xu JF, Sun Z, Zhang X. *ACS Appl Mater Interfaces*, 2017, 9: 8602–8608

8   Meng H, Xing G, Blanco E, Song Y, Zhao L, Sun B, Li X, Wang PC, Korotcov A, Li W, Liang XJ, Chen C, Yuan H, Zhao F, Chen Z, Sun T, Chai Z, Ferrari M, Zhao Y. *Nanomed-Nanotechnol Biol Med*, 2012, 8: 136–146

9   Balogh LP. *Nanomed-Nanotechnol Biol Med*, 2015, 11: 867–869

10   Chen C, Xing G, Wang J, Zhao Y, Li B, Tang J, Jia G, Wang T, Sun J, Xing L, Yuan H, Gao Y, Meng H, Chen Z, Zhao F, Chai Z, Fang X. *Nano Lett*, 2005, 5: 2050–2057

11   Liu J, Kang SG, Wang P, Wang Y, Lv X, Liu Y, Wang F, Gu Z, Yang Z, Weber JK, Tao N, Qin Z, Miao Q, Chen C, Zhou R, Zhao Y. *Biomaterials*, 2018, 152: 24–36

12   Kang S, Zhou G, Yang P, Liu Y, Sun B, Huynh T, Meng H, Zhao L, Xing G, Chen C, Zhao Y, Zhou R. *Proc Natl Acad Sci USA*, 2012, 109: 15431–15436

13   Pan Y, Wang L, Kang S, Lu Y, Yang Z, Huynh T, Chen C, Zhou R, Guo M, Zhao Y. *ACS Nano*, 2015, 9: 6826–6836

14   Meng H, Xing G, Sun B, Zhao F, Lei H, Li W, Song Y, Chen Z, Yuan H, Wang X, Long J, Chen C, Liang X, Zhang N, Chai Z, Zhao Y. *ACS Nano*, 2010, 4: 2773–2783

15   Liang XJ, Meng H, Wang Y, He H, Meng J, Lu J, Wang PC, Zhao Y, Gao X, Sun B, Chen C, Xing G, Shen D, Gottesman MM, Wu Y, Yin JJ, Jia L. *Proc Natl Acad Sci USA*, 2010, 107: 7449–7454

16   Liu Y, Jiao F, Qiu Y, Li W, Lao F, Zhou G, Sun B, Xing G, Dong J, Zhao Y, Chai Z, Chen C. *Biomaterials*, 2009, 30: 3934–3945

17   Yin JJ, Lao F, Fu PP, Wamer WG, Zhao Y, Wang PC, Qiu Y, Sun B, Xing G, Dong J, Liang XJ, Chen C. *Biomaterials*, 2009, 30: 611–621

18   Tang J, Chen Z, Sun B, Dong J, Liu J, Zhou H, Wang L, Bai R, Miao Q, Zhao Y, Chen C, Liu Y. *Nanomed-Nanotechnol Biol Med*, 2016, 12: 945–954

19   Liu Y, Chen C, Qian P, Lu X, Sun B, Zhang X, Wang L, Gao X, Li H, Chen Z, Tang J, Zhang W, Dong J, Bai R, Lobie PE, Wu Q, Liu S, Zhang H, Zhao F, Wicha MS, Zhu T, Zhao Y. *Nat Commun*, 2015, 6: 5988

20   Gallud A, Líbalová H, Fadeel B. *Nanomedicine*, 2015, 10: 1859–1861

21 Ringsdorf H. *J Polym Sci C Polym Symp*, 1975, 51: 135–153
22 Chen H, Chen Y, Wu H, Xu JF, Sun Z, Zhang X. *Biomaterials*, 2018, 178: 697–705
23 Seeman NC, Sleiman HF. *Nat Rev Mater*, 2018, 3: 17068
24 Rothemund PWK. *Nature*, 2006, 440: 297–302
25 Jiang Q, Song C, Nangreave J, Liu X, Lin L, Qiu D, Wang ZG, Zou G, Liang X, Yan H, Ding B. *J Am Chem Soc*, 2012, 134: 13396–13403
26 Zhang Q, Jiang Q, Li N, Dai L, Liu Q, Song L, Wang J, Li Y, Tian J, Ding B, Du Y. *ACS Nano*, 2014, 8: 6633–6643
27 Jiang Q, Shi Y, Zhang Q, Li N, Zhan P, Song L, Dai L, Tian J, Du Y, Cheng Z, Ding B. *Small*, 2015, 11: 5134–5141
28 Du Y, Jiang Q, Beziere N, Song L, Zhang Q, Peng D, Chi C, Yang X, Guo H, Diot G, Ntziachristos V, Ding B, Tian J. *Adv Mater*, 2016, 28: 10000–10007
29 Liu J, Song L, Liu S, Jiang Q, Liu Q, Li N, Wang ZG, Ding B. *Nano Lett*, 2018, 18: 3328–3334
30 Ren D. *J Nanomed Res*, 2016, 4: 1–4
31 Fuchs S, Coester C. *J Drug Deliv Sci Tech*, 2010, 20: 331–342
32 Roudi NE, Saraygord-Afshari N, Hemmaty M. *F1000Research*, 2017, 6: 1541
33 Lohcharoenkal W, Wang L, Chen YC, Rojanasakul Y. *Biomed Res Int*, 2014, 2014(6679): 1–12
34 Tarhini M, Greige-Gerges H, Elaissari A. *Int J Pharm*, 2017, 522: 172–197
35 Kakkar A, Traverso G, Farokhzad OC, Weissleder R, Langer R. *Nat Rev Chem*, 2017, 1: 0063
36 Douglas SM, Bachelet I, Church GM. *Science*, 2012, 335: 831–834
37 Bhatia D, Surana S, Chakraborty S, Koushika SP, Krishnan Y. *Nat Commun*, 2011, 2: 339
38 Amir Y, Ben-Ishay E, Levner D, Ittah S, Abu-Horowitz A, Bachelet I. *Nat Nanotech*, 2014, 9: 353–357
39 Yuan Y, Du C, Sun C, Zhu J, Wu S, Zhang Y, Ji T, Lei J, Yang Y, Gao N, Nie G. *Nano Lett*, 2018, 18: 921–928
40 Senapati S, Mahanta AK, Kumar S, Maiti P. *Sig Transduct Target Ther*, 2018, 3: 7
41 Gradishar WJ, Tjulandin S, Davidson N, Shaw H, Desai N, Bhar P, Hawkins M, O'Shaughnessy J. *J Clin Oncol*, 2005, 23: 7794–7803
42 Thorn CF, Oshiro C, Marsh S, Hernandez-Boussard T, McLeod H, Klein TE, Altman RB. *Pharmacogenets Genomics*, 2011, 21: 440–446
43 D'Amico AV. *JAMA*, 1998, 280: 969
44 Baskar R, Lee KA, Yeo R, Yeoh KW. *Int J Med Sci*, 2012, 9: 193–199
45 DeVita Jr. VT, Chu E. *Cancer Res*, 2008, 68: 8643–8653
46 Macdonald JS, Smalley SR, Benedetti J, Hundahl SA, Estes NC, Stemmermann GN, Haller DG, Ajani JA, Gunderson LL, Jessup JM, Martenson JA. *N Engl J Med*, 2001, 345: 725–730
47 Zhang R, Song X, Liang C, Yi X, Song G, Chao Y, Yang Y, Yang K, Feng L, Liu Z. *Biomaterials*, 2017, 138: 13–21
48 Cao W, Wang L, Xu H. *Nano Today*, 2015, 10: 717–736
49 Song G, Cheng L, Chao Y, Yang K, Liu Z. *Adv Mater*, 2017, 29: 1700996
50 Barcellos-Hoff MH, Park C, Wright EG. *Nat Rev Cancer*, 2005, 5: 867–875
51 Xu H, Cao W, Zhang X. *Acc Chem Res*, 2013, 46: 1647–1658
52 Ma N, Li Y, Xu H, Wang Z, Zhang X. *J Am Chem Soc*, 2010, 132: 442–443
53 Cao W, Zhang X, Miao X, Yang Z, Xu H. *Angew Chem Int Ed*, 2013, 52: 6233–6237
54 Ma N, Xu H, An L, Li J, Sun Z, Zhang X. *Langmuir*, 2011, 27: 5874–5878
55 Cao W, Gu Y, Li T, Xu H. *Chem Commun*, 2015, 51: 7069–7071
56 Jiang J, Cao DP. *Sci China Chem*, 2013, 56: 249–255
57 Xu XH, Li CX, Li HP, Liu R, Jiang C, Wu Y, He B, Gu ZW. *Sci China Chem*, 2011, 54: 326–333
58 Li YY, Dong HQ, Wang K, Shi DL, Zhang XZ, Zhuo RX. *Sci China Chem*, 2010, 53: 447–457
59 Riehemann K, Schneider SW, Luger TA, Godin B, Ferrari M, Fuchs H. *Angew Chem Int Ed*, 2009, 48: 872–897
60 Hang Y, Cai X, Wang J, Jiang T, Hua J, Liu B. *Sci China Chem*, 2018, 61: 898–908
61 Sanhai WR, Sakamoto JH, Canady R, Ferrari M. *Nat Nanotech*, 2008, 3: 242–244
62 Kreyling WG, Abdelmonem AM, Ali Z, Alves F, Geiser M, Haberl N, Hartmann R, Hirn S, de Aberasturi DJ, Kantner K, Khadem-Saba G, Montenegro JM, Rejman J, Rojo T, de Larramendi IR, Ufartes R, Wenk A, Parak WJ. *Nat Nanotech*, 2015, 10: 619–623
63 Salvati A, Pitek AS, Monopoli MP, Prapainop K, Bombelli FB, Hristov DR, Kelly PM, Åberg C, Mahon E, Dawson KA. *Nat Nanotech*, 2013, 8: 137–143
64 Zhang H, Wu R. *Sci China Chem*, 2015, 58: 780–792
65 Wang B. *Sci China Ser B*, 2005, 48: 385–394
66 Hao X, Chen L, Sang W, Yan Q. *Adv Sci*, 2018, 5: 1700591
67 Xu AP, Yang PP, Yang C, Gao YJ, Zhao XX, Luo Q, Li XD, Li LZ, Wang L, Wang H. *Nanoscale*, 2016, 8: 14078–14083
68 Zhao Y, Xing G, Chai Z. *Nat Nanotech*, 2008, 3: 191–192
69 Klaine SJ, Alvarez PJJ, Batley GE, Fernandes TF, Handy RD, Lyon DY, Mahendra S, McLaughlin MJ, Lead JR. *Environ Toxicol Chem*, 2008, 27: 1825–1851
70 Tonigold M, Simon J, Estupiñán D, Kokkinopoulou M, Reinholz J, Kintzel U, Kaltbeitzel A, Renz P, Domogalla MP, Steinbrink K, Lieberwirth I, Crespy D, Landfester K, Mailänder V. *Nat Nanotech*, 2018, 13: 862–869
71 Li LL, Zeng Q, Liu WJ, Hu XF, Li Y, Pan J, Wan D, Wang H. *ACS Appl Mater Interfaces*, 2016, 8: 17936–17943
72 Hu XX, He PP, Qi GB, Gao YJ, Lin YX, Yang C, Yang PP, Hao H, Wang L, Wang H. *ACS Nano*, 2017, 11: 4086–4096
73 Li LL, Ma HL, Qi GB, Zhang D, Yu F, Hu Z, Wang H. *Adv Mater*, 2016, 28: 254–262
74 Qi GB, Zhang D, Liu FH, Qiao ZY, Wang H. *Adv Mater*, 2017, 29: 1703461
75 Yang PP, Luo Q, Qi GB, Gao YJ, Li BN, Zhang JP, Wang L, Wang H. *Adv Mater*, 2017, 29: 1605869
76 Zhang D, Qi GB, Zhao YX, Qiao SL, Yang C, Wang H. *Adv Mater*, 2015, 27: 6125–6130
77 Chang H, Lv J, Gao X, Wang X, Wang H, Chen H, He X, Li L, Cheng Y. *Nano Lett*, 2017, 17: 1678–1684
78 Li LL, Qiao SL, Liu WJ, Ma Y, Wan D, Pan J, Wang H. *Nat Commun*, 2017, 8: 1276
79 An HW, Qiao SL, Li LL, Yang C, Lin YX, Wang Y, Qiao ZY, Wang L, Wang H. *ACS Appl Mater Interfaces*, 2016, 8: 19202–19207
80 Callmann CE, Barback CV, Thompson MP, Hall DJ, Mattrey RF, Gianneschi NC. *Adv Mater*, 2015, 27: 4611–4615
81 Lehn JM. *Angew Chem Int Ed Engl*, 1988, 27: 89–112
82 Qiao ZY, Zhao WJ, Cong Y, Zhang D, Hu Z, Duan ZY, Wang H. *Biomacromolecules*, 2016, 17: 1643–1652
83 Yang PP, Zhai YG, Qi GB, Lin YX, Luo Q, Yang Y, Xu AP, Yang C, Li YS, Wang L, Wang H. *Small*, 2016, 12: 5423–5430
84 Liu Y, Zhang D, Qiao ZY, Qi GB, Liang XJ, Chen XG, Wang H. *Adv Mater*, 2015, 27: 5034–5042
85 Li HJ, Du JZ, Du XJ, Xu CF, Sun CY, Wang HX, Cao ZT, Yang XZ, Zhu YH, Nie S, Wang J. *Proc Natl Acad Sci USA*, 2016, 113: 4164–4169
86 Perrault SD, Chan WCW. *Proc Natl Acad Sci USA*, 2010, 107: 11194–11199
87 Wang P, Fan Y, Lu L, Liu L, Fan L, Zhao M, Xie Y, Xu C, Zhang F. *Nat Commun*, 2018, 9: 2898
88 Zhou L, Lv F, Liu L, Shen G, Yan X, Bazan GC, Wang S. *Adv Mater*, 2018, 30: 1704888
89 Yang Z, Xu K, Guo Z, Guo Z, Xu B. *Adv Mater*, 2007, 19: 3152–3156
90 Kuang Y, Shi J, Li J, Yuan D, Alberti KA, Xu Q, Xu B. *Angew Chem Int Ed*, 2014, 53: 8104–8107

91 Zhou J, Du X, Yamagata N, Xu B. *J Am Chem Soc*, 2016, 138: 3813–3823

92 Miao Q, Bai X, Shen Y, Mei B, Gao J, Li L, Liang G. *Chem Commun*, 2012, 48: 9738–9740

93 Tanaka A, Fukuoka Y, Morimoto Y, Honjo T, Koda D, Goto M, Maruyama T. *J Am Chem Soc*, 2015, 137: 770–775

94 Bal W, Sokołowska M, Kurowska E, Faller P. *Biochim Biophys Acta*, 2013, 1830: 5444–5455

95 Tanford C, Buzzell JG, Rands DG, Swanson SA. *J Am Chem Soc*, 1955, 77: 6421–6428

96 Hagolle N, Relkin P, Dalgleish DG, Launay B. *Food Hydrocolloids*, 1997, 11: 311–317

97 Hu HY, Du HN. *J Protein Chem*, 2000, 19: 177–183

98 Xie J, Zheng Y, Ying JY. *J Am Chem Soc*, 2009, 131: 888–889

99 Zhang B, Jin H, Li Y, Chen B, Liu S, Shi D. *J Mater Chem*, 2012, 22: 14494–14501

100 Sun C, Yuan Y, Xu Z, Ji T, Tian Y, Wu S, Lei J, Li J, Gao N, Nie G. *Bioconjug Chem*, 2015, 26: 193–196

101 Sun C, Yang H, Yuan Y, Tian X, Wang L, Guo Y, Xu L, Lei J, Gao N, Anderson GJ, Liang XJ, Chen C, Zhao Y, Nie G. *J Am Chem Soc*, 2011, 133: 8617–8624

102 Chen D, Tang Q, Xue W, Xiang J, Zhang L, Wang X. *J Biomed Res*, 2010, 24: 26–32

103 Desai N. *Nanomed Nanotechnol Biol Med*, 2007, 4: 339

104 Trynda-Lemiesz L. *Bioorg Med Chem*, 2004, 12: 3269–3275

105 Zhang L, Hou S, Zhang J, Hu W, Wang C. *Arch Pharm Res*, 2010, 33: 1193–1198

106 Zu Y, Yuan S, Zhao X, Zhang Y, Zhang X, Jiang R. *Acta Pharm Sin*, 2009, 44: 525–531

107 Guo CC, Tang YH, Hu HH, Yu LS, Jiang HD, Zeng S. *J Pharm Anal*, 2011, 1: 184–190

108 Ghuman J, Zunszain PA, Petitpas I, Bhattacharya AA, Otagiri M, Curry S. *J Mol Biol*, 2005, 353: 38–52

109 Setoguchi N, Takamura N, Fujita K, Ogata K, Tokunaga J, Nishio T, Chosa E, Arimori K, Kawai K, Yamamoto R. *Biopharm Drug Dispos*, 2013, 34: 125–136

110 Ozer I, Tacal O I. *Anal Biochem*, 2001, 294: 1–6

111 Takamura N, Maruyama T, Chosa E, Kawai K, Tsutsumi Y, Uryu Y, Yamasaki K, Deguchi T, Otagiri M. *Drug Metab Disposition*, 2005, 33: 596–602

112 Irache J, Merodio M, Arnedo A, Camapanero M, Mirshahi M, Espuelas S. *Mini Rev Med Chem*, 2005, 5: 293–305

113 Hu Q, Sun W, Lu Y, Bomba HN, Ye Y, Jiang T, Isaacson AJ, Gu Z. *Nano Lett*, 2016, 16: 1118–1126

114 Kundranda MN, Niu J. *Drug Des Devel Ther*, 2015, 9: 3767

115 Kratz F. *J Control Release*, 2008, 132: 171–183

116 Elsadek B, Kratz F. *J Control Release*, 2012, 157: 4–28

117 Tkachenko AG, Xie H, Coleman D, Glomm W, Ryan J, Anderson MF, Franzen S, Feldheim DL. *J Am Chem Soc*, 2003, 125: 4700–4701

118 Gao F, Cai P, Yang W, Xue J, Gao L, Liu R, Wang Y, Zhao Y, He X, Zhao L, Huang G, Wu F, Zhao Y, Chai Z, Gao X. *ACS Nano*, 2015, 9: 4976–4986

119 Andreozzi E, Wang P, Valenzuela A, Tu C, Gorin F, Dhenain M, Louie A. *Bioconjug Chem*, 2013, 24: 1455–1467

120 Fang J, Chandrasekharan P, Liu XL, Yang Y, Lv YB, Yang CT, Ding J. *Biomaterials*, 2014, 35: 1636–1642

121 Anishur Rahman ATM, Majewski P, Vasilev K. *Contrast Media Mol Imag*, 2013, 8: 92–95

122 Bridot JL, Faure AC, Laurent S, Rivière C, Billotey C, Hiba B, Janier M, Josserand V, Coll JL, Vander Elst L, Muller R, Roux S, Perriat P, Tillement O. *J Am Chem Soc*, 2007, 129: 5076–5084

123 Abdukayum A, Yang CX, Zhao Q, Chen JT, Dong LX, Yan XP. *Anal Chem*, 2014, 86: 4096–4101

124 Ge J, Jia Q, Liu W, Guo L, Liu Q, Lan M, Zhang H, Meng X, Wang P. *Adv Mater*, 2015, 27: 4169–4177

125 Yang T, Wang Y, Ke H, Wang Q, Lv X, Wu H, Tang Y, Yang X, Chen C, Zhao Y, Chen H. *Adv Mater*, 2016, 28: 5923–5930

126 Yang T, Tang Y', Liu L, Lv X, Wang Q, Ke H, Deng Y, Yang H, Yang X, Liu G, Zhao Y, Chen H. *ACS Nano*, 2017, 11: 1848–1857

127 Zhang J, Hao G, Yao C, Yu J, Wang J, Yang W, Hu C, Zhang B. *ACS Appl Mater Interfaces*, 2016, 8: 16612–16621

128 Wang Y, Wu Y, Liu Y, Shen J, Lv L, Li L, Yang L, Zeng J, Wang Y, Zhang LW, Li Z, Gao M, Chai Z. *Adv Funct Mater*, 2016, 26: 5335–5344

129 Mao F, Wen L, Sun C, Zhang S, Wang G, Zeng J, Wang Y, Ma J, Gao M, Li Z. *ACS Nano*, 2016, 10: 11145–11155

130 Zhou L, Yang T, Wang J, Wang Q, Lv X, Ke H, Guo Z, Shen J, Wang Y, Xing C, Chen H. *Theranostics*, 2017, 7: 764–774

131 Yang T, Ke H, Wang Q, Tang Y, Deng Y, Yang H, Yang X, Yang P, Ling D, Chen C, Zhao Y, Wu H, Chen H. *ACS Nano*, 2017, 11: 10012–10024

132 Chen WH, Luo GF, Lei Q, Hong S, Qiu WX, Liu LH, Cheng SX, Zhang XZ. *ACS Nano*, 2017, 11: 1419–1431

133 Sun SK, Dong LX, Cao Y, Sun HR, Yan XP. *Anal Chem*, 2013, 85: 8436–8441

134 Meldrum FC, Wade VJ, Nimmo DL, Heywood BR, Mann S. *Nature*, 1991, 349: 684–687

135 Mann S. *Nat Mater*, 2009, 8: 781–792

136 Meldrum FC, Heywood BR, Mann S. *Science*, 1992, 257: 522–523

137 Sun S, Murray CB, Weller D, Folks L, Moser A. *Science*, 2000, 287: 1989–1992

138 Ueno T, Suzuki M, Goto T, Matsumoto T, Nagayama K, Watanabe Y. *Angew Chem Int Ed*, 2004, 43: 2527–2530

139 Kudr J, Nejdl L, Skalickova S, Zurek M, Milosavljevic V, Kensova R, Ruttkay-Nedecky B, Kopel P, Hynek D, Novotna M, Adam V, Kizek R. *J Mater Chem B*, 2015, 3: 2109–2118

140 Meldrum FC, Douglas T, Levi S, Arosio P, Mann S. *J InOrg Biochem*, 1995, 58: 59–68

141 Geninatti Crich S, Cutrin JC, Lanzardo S, Conti L, Kálmán FK, Szabó I, Lago NR, Iolascon A, Aime S. *Contrast Media Mol Imag*, 2012, 7: 281–288

142 Wong KKW, Mann S. *Adv Mater*, 1996, 8: 928–932

143 Warne B, Kasyutich OI, Mayes EL, Wiggins JAL, Wong KKW. *IEEE Trans Magn*, 2000, 36: 3009–3011

144 Chasteen ND, Harrison PM. *J Struct Biol*, 1999, 126: 182–194

145 Hennequin B, Turyanska L, Ben T, Beltrán AM, Molina SI, Li M, Mann S, Patanè A, Thomas NR. *Adv Mater*, 2008, 20: 3592–3596

146 Fan J, Yin JJ, Ning B, Wu X, Hu Y, Ferrari M, Anderson GJ, Wei J, Zhao Y, Nie G. *Biomaterials*, 2011, 32: 1611–1618

147 Fan K, Cao C, Pan Y, Lu D, Yang D, Feng J, Song L, Liang M, Yan X. *Nat Nanotech*, 2012, 7: 459–464

148 Gao L, Zhuang J, Nie L, Zhang J, Zhang Y, Gu N, Wang T, Feng J, Yang D, Perrett S, Yan X. *Nat Nanotech*, 2007, 2: 577–583

149 Wang Z, Huang P, Jacobson O, Wang Z, Liu Y, Lin L, Lin J, Lu N, Zhang H, Tian R, Niu G, Liu G, Chen X. *ACS Nano*, 2016, 10: 3453–3460

150 Fantechi E, Innocenti C, Zanardelli M, Fittipaldi M, Falvo E, Carbo M, Shullani V, Di Cesare Mannelli L, Ghelardini C, Ferretti AM, Ponti A, Sangregorio C, Ceci P. *ACS Nano*, 2014, 8: 4705–4719

151 de la Escosura A, Nolte RJM, Cornelissen JJLM. *J Mater Chem*, 2009, 19: 2274–2278

152 Bode SA, Minten IJ, Nolte RJM, Cornelissen JJLM. *Nanoscale*, 2011, 3: 2376–2389

153 Uchida M, Klem M , Allen M, Suci P, Flenniken M, Gillitzer E, Varpness Z, Liepold L , Young M, Douglas T. *Adv Mater*, 2007, 19: 1025–1042

154 Douglas T, Young M. *Nature*, 1998, 393: 152–155

155 Douglas T, Strable E, Willits D, Aitouchen A, Libera M, Young M. *Adv Mater*, 2002, 14: 415–418

156 Klem MT, Young M, Douglas T. *J Mater Chem*, 2008, 18: 3821–3823

157 de la Escosura A, Verwegen M, Sikkema FD, Comellas-Aragonès M, Kirilyuk A, Rasing T, Nolte RJM, Cornelissen JJLM. *Chem Com-*

mun, 2008, 378: 1542

158   Liu C, Chung SH, Jin Q, Sutton A, Yan F, Hoffmann A, Kay BK, Bader SD, Makowski L, Chen L. *J Magn Magn Mater*, 2006, 302: 47–51

159   Hooker JM, Datta A, Botta M, Raymond KN, Francis MB. *Nano Lett*, 2007, 7: 2207–2210

160   Knez M, Bittner AM, Boes F, Wege C, Jeske H, Maiβ E, Kern K. *Nano Lett*, 2003, 3: 1079–1082

161   Knez M, Sumser M, Bittner A , Wege C, Jeske H, Martin T , Kern K. *Adv Funct Mater*, 2004, 14: 116–124

162   Tsukamoto R, Muraoka M, Seki M, Tabata H, Yamashita I. *Chem Mater*, 2007, 19: 2389–2391

163   Dujardin E, Peet C, Stubbs G, Culver JN, Mann S. *Nano Lett*, 2003, 3: 413–417

164   American Cancer Society. cancer facts & figures. 2015. http://www.cancer.org/research/cancerfactsstatistics/cancerfactsfigures2015/

165   Subramanian AP, John AA, Vellayappan MV, Balaji A, Jaganathan SK, Supriyanto E, Yusof M. *RSC Adv*, 2015, 5: 35608–35621

166   Hanahan D, Weinberg RA. *Cell*, 2000, 100: 57–70

167   Hanahan D, Weinberg RA. *Cell*, 2011, 144: 646–674

168   Cansiz S, Zhang L, Wu C, Wu Y, Teng IT, Hou W, Wang Y, Wan S, Cai R, Jin C, Liu Q, Tan W. *Chem Asian J*, 2015, 10: 2084–2094

169   He L, Lu DQ, Liang H, Xie S, Luo C, Hu M, Xu L, Zhang X, Tan W. *ACS Nano*, 2017, 11: 4060–4066

170   He L, Lu D, Liang H, Xie S, Zhang X, Liu Q, Yuan Q, Tan W. *J Am Chem Soc*, 2018, 140: 258–263

171   Peng R, Zheng X, Lyu Y, Xu L, Zhang X, Ke G, Liu Q, You C, Huan S, Tan W. *J Am Chem Soc*, 2018, 140: 9793–9796

172   Zhu G, Hu R, Zhao Z, Chen Z, Zhang X, Tan W. *J Am Chem Soc*, 2013, 135: 16438–16445

173   Hu R, Zhang X, Zhao Z, Zhu G, Chen T, Fu T, Tan W. *Angew Chem*, 2014, 126: 5931–5936

174   Han S, Lee JS, Lee JB. *Nanoscale*, 2017, 9: 14094–14102

175   Bi S, Dong Y, Jia X, Chen M, Zhong H, Ji B. *Nanoscale*, 2015, 7: 7361–7367

176   Li J, Zheng C, Cansiz S, Wu C, Xu J, Cui C, Liu Y, Hou W, Wang Y, Zhang L, Teng I, Yang HH, Tan W. *J Am Chem Soc*, 2015, 137: 1412–1415

177   Ding F, Mou Q, Ma Y, Pan G, Guo Y, Tong G, Choi CHJ, Zhu X, Zhang C. *Angew Chem Int Ed*, 2018, 57: 3064–3068

178   Chen WH, Yu X, Cecconello A, Sohn YS, Nechushtai R, Willner I. *Chem Sci*, 2017, 8: 5769–5780

179   Chen WH, Liao WC, Sohn YS, Fadeev M, Cecconello A, Nechushtai R, Willner I. *Adv Funct Mater*, 2017, 28: 1870053

180   Mirkin CA, Letsinger RL, Mucic RC, Storhoff JJ. *Nature*, 1996, 382: 607–609

181   Cutler JI, Auyeung E, Mirkin CA. *J Am Chem Soc*, 2012, 134: 1376–1391

182   Li H, Zhang B, Lu X, Tan X, Jia F, Xiao Y, Cheng Z, Li Y, Silva DO, Schrekker HS, Zhang K, Mirkin CA. *Proc Natl Acad Sci USA*, 2018, 115: 4340–4344

183   Mirkin CA, Petrosko SH. *Clin Chem*, 2018, 64: 971–972

184   Liu Z, Zhao J, Zhang R, Han G, Zhang C, Liu B, Zhang Z, Han MY, Gao X. *ACS Nano*, 2018, 12: 3629–3637

185   Jeong JH, Park TG. *Bioconjug Chem*, 2001, 12: 917–923

186   Ding K, Alemdaroglu FE, Börsch M, Berger R, Herrmann A. *Angew Chem Int Ed*, 2007, 46: 1172–1175

187   Huang F, You M, Chen T, Zhu G, Liang H, Tan W. *Chem Commun*, 2014, 50: 3103–3105

188   Zhang R, Gao S, Wang Z, Han D, Liu L, Ma Q, Tan W, Tian J, Chen X. *Adv Funct Mater*, 2017, 27: 1701027

189   Jin C, Zhang H, Zou J, Liu Y, Zhang L, Li F, Wang R, Xuan W, Ye M, Tan W. *Angew Chem Int Ed*, 2018, 57: 8994–8997

190   Hussain T, Nguyen QT. *Adv Drug Deliver Rev*, 2014, 66: 90–100

191   Weissleder R. *Science*, 2006, 312: 1168–1171

192   Pysz MA, Gambhir SS, Willmann JK. *Clin Radiol*, 2010, 65: 500–516

193   Margolis DJA, Hoffman JM, Herfkens RJ, Jeffrey RB, Quon A, Gambhir SS. *Radiology*, 2007, 245: 333–356

194   Hickson J. *Urol Oncol Semin Orig Investig*, 2009, 27: 295–297

195   Liu JB, Yang XH, He XX, Wang KM, Wang Q, Guo QP, Shi H, Huang J, Huo XQ. *Sci China Chem*, 2011, 54: 1157–1176

196   Li K, Ding D, Zhao QL, Sun JZ, Tang BZ, Liu B. *Sci China Chem*, 2013, 56: 1228–1233

197   Zhang H, Fan J, Wang J, Zhang S, Dou B, Peng X. *J Am Chem Soc*, 2013, 135: 11663–11669

198   Zhang H, Fan J, Wang J, Dou B, Zhou F, Cao J, Qu J, Cao Z, Zhao W, Peng X. *J Am Chem Soc*, 2013, 135: 17469–17475

199   Fan J, Guo S, Wang S, Kang Y, Yao Q, Wang J, Gao X, Wang H, Du J, Peng X. *Chem Commun*, 2017, 53: 4857–4860

200   Gu K, Xu Y, Li H, Guo Z, Zhu S, Zhu S, Shi P, James TD, Tian H, Zhu WH. *J Am Chem Soc*, 2016, 138: 5334–5340

201   Wang F, Zhu Y, Zhou L, Pan L, Cui Z, Fei Q, Luo S, Pan D, Huang Q, Wang R, Zhao C, Tian H, Fan C. *Angew Chem Int Ed*, 2015, 54: 7349–7353

202   Hong Y, Lam JWY, Tang BZ. *Chem Soc Rev*, 2011, 40: 5361–5388

203   Gao M, Su H, Lin G, Li S, Yu X, Qin A, Zhao Z, Zhang Z, Tang BZ. *Nanoscale*, 2016, 8: 15027–15032

204   Shi H, Tang Z, Kim Y, Nie H, Huang YF, He X, Deng K, Wang K, Tan W. *Chem Asian J*, 2010, 5: 2209–2213

205   Shangguan D, Meng L, Cao ZC, Xiao Z, Fang X, Li Y, Cardona D, Witek RP, Liu C, Tan W. *Anal Chem*, 2008, 80: 721–728

206   Chen X, Estevez MC, Zhu Z, Huang YF, Chen Y, Wang L, Tan W. *Anal Chem*, 2009, 81: 7009–7014

207   Shi H, He X, Wang K, Wu X, Ye X, Guo Q, Tan W, Qing Z, Yang X, Zhou B. *Proc Natl Acad Sci USA*, 2011, 108: 3900–3905

208   Wang Y, Zhou K, Huang G, Hensley C, Huang X, Ma X, Zhao T, Sumer BD, DeBerardinis RJ, Gao J. *Nat Mater*, 2014, 13: 204–212

209   Zheng X, Wang S, Mao H, Wu W, Liu B, Jiang X. *Nat Commun*, 2015, 6: 5834

210   Zheng X, Tang H, Xie C, Zhang J, Wu W, Jiang X. *Angew Chem Int Ed*, 2015, 54: 8094–8099

211   Zheng X, Mao H, Huo D, Wu W, Liu B, Jiang X. *Nat Biomed Eng*, 2017, 1: 0057

212   Hori SS, Tummers WS, Gambhir SS. *Nat Biomed Eng*, 2017, 1: 0062

213   Wan H, Yue J, Zhu S, Uno T, Zhang X, Yang Q, Yu K, Hong G, Wang J, Li L, Ma Z, Gao H, Zhong Y, Su J, Antaris AL, Xia Y, Luo J, Liang Y, Dai H. *Nat Commun*, 2018, 9: 1171

214   Antaris AL, Chen H, Cheng K, Sun Y, Hong G, Qu C, Diao S, Deng Z, Hu X, Zhang B, Zhang X, Yaghi OK, Alamparambil ZR, Hong X, Cheng Z, Dai H. *Nat Mater*, 2016, 15: 235–242

215   Yao J, Wang LV. *IEEE Photonics J*, 2014, 6: 1–6

216   Wang LV, Gao L. *Annu Rev Biomed Eng*, 2014, 16: 155–185

217   Chen H, Zhang W, Zhu G, Xie J, Chen X. *Nat Rev Mater*, 2017, 2: 17024

218   Park SM, Aalipour A, Vermesh O, Yu JH, Gambhir SS. *Nat Rev Mater*, 2017, 2: 17014

219   Wang Z, Wang J, Liu G. Chapter 19: Theranostic magnetic nanoparticles as molecular imaging agents for sirna delivery. In: Conde J, Ed. *Handbook of Nanomaterials for Cancer Theranostics*. Elsevier, 2018. 551–576

220   Wang J, Mi P, Lin G, Wáng YXJ, Liu G, Chen X. *Adv Drug Deliver Rev*, 2016, 104: 44–60

221   Goel S, England CG, Chen F, Cai W. *Adv Drug Deliver Rev*, 2017, 113: 157–176

222   Xing Y, Zhao J, Conti PS, Chen K. *Theranostics*, 2014, 4: 290–306

223   Kim BYS, Rutka JT, Chan WCW. *N Engl J Med*, 2010, 363: 2434–2443

224   Niu G, Chen X. *Nat Nanotech*, 2018, 13: 359–360

225   Mirshojaei SF, Ahmadi A, Morales-Avila E, Ortiz-Reynoso M, Reyes-Perez H. *J Drug Target*, 2016, 24: 91–101

226   Thorek D, Robertson R, Bacchus WA, Hahn J, Rothberg J, Beattie BJ, Grimm J. *Am J Nucl Med Mol Imaging*, 2012, 2: 163–173

227   Ciarrocchi E, Belcari N. *EJNMMI Phys*, 2017, 4: 14

228 Hu Z, Liang J, Yang W, Fan W, Li C, Ma X, Chen X, Ma X, Li X, Qu X, Wang J, Cao F, Tian J. *Opt Express*, 2010, 18: 24441–24450

229 Zhong J, Qin C, Yang X, Zhu S, Zhang X, Tian J. *Int J Biomed Imag*, 2011, 2011(7): 1–6

230 Hu Z, Ma X, Qu X, Yang W, Liang J, Wang J, Tian J. *PLoS ONE*, 2012, 7: e37623

231 Zhong J, Tian J, Yang X, Qin C. *Ann Biomed Eng*, 2011, 39: 1728–1735

232 Hu Z, Yang W, Ma X, Ma W, Qu X, Liang J, Wang J, Tian J. *Mol Imag*, 2013, 12: 173–181

233 Yang W, Qin W, Hu Z, Suo Y, Zhao R, Ma X, Ma W, Wang T, Liang J, Tian J, Wang J. *Nucl Med Biol*, 2012, 39: 948–953

234 Hu Z, Zhang Z, Guo H, Liu M, Shi X, Tian J. *J Nucl Med*, 2017, 58: 527

235 Hu Z, Zhang Z, Guo H, Tian J. *J Nucl Med*, 2018, 59: 246

236 Spinelli AE, Boschi F. *Phys Med*, 2015, 31: 120–129

237 Chi C, Du Y, Ye J, Kou D, Qiu J, Wang J, Tian J, Chen X. *Theranostics*, 2014, 4: 1072–1084

238 Grootendorst MR, Cariati M, Kothari A, Tuch DS, Purushotham A. *Clin Transl Imag*, 2016, 4: 353–366

239 Spinelli AE, Schiariti MP, Grana CM, Ferrari M, Cremonesi M, Boschi F. *J Biomed Opt*, 2016, 21: 050502

240 Currie G, Wheat J, Davidson R, Kiat H. *Radiographer*, 2011, 58: 46–52

241 Bailey DL, Willowson KP. *J Nucl Med*, 2013, 54: 83–89

242 Iwata K, Coco B, Zhang J, Wagenaar D. *J Nucl Med*, 2010, 51: 527–527

243 Mauri M, Elli T, Caviglia G, Uboldi G, Azzi M. Rawgraphs: a visualisation platform to create open outputs. In: *Proceedings of the 12th Biannual Conference on Italian SIGCHI Chapter*. New York: ACM, 2017

244 Chu C, Lin H, Liu H, Wang X, Wang J, Zhang P, Gao H, Huang C, Zeng Y, Tan Y, Liu G, Chen X. *Adv Mater*, 2017, 29: 1605928

245 Hu X, Zhai S, Liu G, Xing D, Liang H, Liu S. *Adv Mater*, 2018, 30: 1706307

246 Lei Z, Wang J, Lv P, Liu G. *Sci Bull*, 2018, 63: 663–665

247 Ren E, Lei Z, Wang J, Zhang Y, Liu G. *Adv Ther*, 1: 1800080

248 Li L, Pang X, Liu G. *ACS Biomater Sci Eng*, 2018, 4: 1928–1941

249 Miao T, Wang J, Zeng Y, Liu G, Chen X. *Adv Sci*, 2018, 5: 1700513

250 Lamb J, Holland JP. *J Nucl Med*, 2018, 59: 382–389

251 Stockhofe K, Postema JM, Schieferstein H, Ross TL. *Pharmaceuticals*, 2014, 7: 392–418

252 Guerrero S, Herance JR, Rojas S, Mena JF, Gispert JD, Acosta GA, Albericio F, Kogan MJ. *Bioconjug Chem*, 2012, 23: 399–408

253 Rojas S, Gispert JD, Abad S, Buaki-Sogo M, Victor VM, Garcia H, Herance JR. *Mol Pharm*, 2012, 9: 3543–3550

254 Torres Martin de Rosales R, Tavaré R, Paul RL, Jauregui-Osoro M, Protti A, Glaria A, Varma G, Szanda I, Blower PJ. *Angew Chem Int Ed*, 2011, 50: 5509–5513

255 Devaraj NK, Keliher EJ, Thurber GM, Nahrendorf M, Weissleder R. *Bioconjug Chem*, 2009, 20: 397–401

256 Thorek DLJ, Ulmert D, Diop NFM, Lupu ME, Doran MG, Huang R, Abou DS, Larson SM, Grimm J. *Nat Commun*, 2014, 5: 3097

257 Goel S, Chen F, Ehlerding EB, Cai W. *Small*, 2014, 10: 3825–3830

258 Black KCL, Wang Y, Luehmann HP, Cai X, Xing W, Pang B, Zhao Y, Cutler CS, Wang LV, Liu Y, Xia Y. *ACS Nano*, 2014, 8: 4385–4394

259 Boros E, Bowen AM, Josephson L, Vasdev N, Holland JP. *Chem Sci*, 2015, 6: 225–236

260 Chen F, Ellison PA, Lewis CM, Hong H, Zhang Y, Shi S, Hernandez R, Meyerand ME, Barnhart TE, Cai W. *Angew Chem Int Ed*, 2013, 52: 13319–13323

261 Chakravarty R, Valdovinos HF, Chen F, Lewis CM, Ellison PA, Luo H, Meyerand ME, Nickles RJ, Cai W. *Adv Mater*, 2014, 26: 5119–5123

262 Liu T, Shi S, Liang C, Shen S, Cheng L, Wang C, Song X, Goel S, Barnhart TE, Cai W, Liu Z. *ACS Nano*, 2015, 9: 950–960

263 Goel S, Chen F, Luan S, Valdovinos HF, Shi S, Graves SA, Ai F, Barnhart TE, Theuer CP, Cai W. *Adv Sci*, 2016, 3: 1600122

264 Shi S, Xu C, Yang K, Goel S, Valdovinos HF, Luo H, Ehlerding EB, England CG, Cheng L, Chen F, Nickles RJ, Liu Z, Cai W. *Angew Chem Int Ed*, 2017, 56: 2889–2892

265 Shaffer TM, Wall MA, Harmsen S, Longo VA, Drain CM, Kircher MF, Grimm J. *Nano Lett*, 2015, 15: 864–868

266 Wall MA, Shaffer TM, Harmsen S, Tschaharganeh DF, Huang CH, Lowe SW, Drain CM, Kircher MF. *Theranostics*, 2017, 7: 3068–3077

267 Son DH, Hughes SM, Yin Y, Paul Alivisatos A. *Science*, 2004, 306: 1009–1012

268 Sun X, Huang X, Guo J, Zhu W, Ding Y, Niu G, Wang A, Kiesewetter DO, Wang ZL, Sun S, Chen X. *J Am Chem Soc*, 2014, 136: 1706–1709

269 Sun Y, Zhu X, Peng J, Li F. *ACS Nano*, 2013, 7: 11290–11300

270 Di Pasqua AJ, Yuan H, Chung Y, Kim JK, Huckle JE, Li C, Sadgrove M, Tran TH, Jay M, Lu X. *J Nucl Med*, 2013, 54: 111–116

271 Munaweera I, Shi Y, Koneru B, Saez R, Aliev A, Di Pasqua AJ, Balkus Jr. KJ. *Mol Pharm*, 2015, 12: 3588–3596

272 Pérez-Campaña C, Gómez-Vallejo V, Puigivila M, Martín A, Calvo-Fernández T, Moya SE, Ziolo RF, Reese T, Llop J. *ACS Nano*, 2013, 7: 3498–3505

273 Pérez-Campaña C, Gómez-Vallejo V, Martin A, San Sebastián E, Moya SE, Reese T, Ziolo RF, Llop J. *Analyst*, 2012, 137: 4902–4906

274 Tang L, Sun X, Liu N, Zhou Z, Yu F, Zhang X, Sun X, Chen X. *ACS Appl Nano Mater*, 2018, 1: 1741–1749

275 Liu Y, Miao Q, Zou P, Liu L, Wang X, An L, Zhang X, Qian X, Luo S, Liang G. *Theranostics*, 2015, 5: 1058–1067

276 Wang J, Tao W, Chen X, Farokhzad OC, Liu G. *Theranostics*, 2017, 7: 3915–3919

277 Wang J, Liu G, Leung K, Loffroy R, Lu PX, J. Wáng Y. *Curr Pharm Des*, 2015, 21: 5401–5416

278 Wang J, Liu G. *Angew Chem Int Ed*, 2018, 57: 3008–3010

279 Li Y, Zhang W, Wu H, Liu G. *Biomed Res Int*, 2014, 2014(4): 1–13

280 Ferrari M. *Nat Rev Cancer*, 2005, 5: 161–171

281 Nie S, Xing Y, Kim GJ, Simons JW. *Annu Rev Biomed Eng*, 2007, 9: 257–288

282 Chan WCW, Nie S. *Science*, 1998, 281: 2016–2018

283 Alivisatos AP. *Science*, 1996, 271: 933–937

284 Bruchez Jr. M, Moronne M, Gin P, Weiss S, Paul Alivisatos A. *Science*, 1998, 281: 2013–2016

285 Peng CW, Liu XL, Chen C, Liu X, Yang XQ, Pang DW, Zhu XB, Li Y. *Biomaterials*, 2011, 32: 2907–2917

286 Chen C, Peng J, Xia HS, Yang GF, Wu QS, Chen LD, Zeng LB, Zhang ZL, Pang DW, Li Y. *Biomaterials*, 2009, 30: 2912–2918

287 Wen CY, Wu LL, Zhang ZL, Liu YL, Wei SZ, Hu J, Tang M, Sun EZ, Gong YP, Yu J, Pang DW. *ACS Nano*, 2014, 8: 941–949

288 Wen CY, Xie HY, Zhang ZL, Wu LL, Hu J, Tang M, Wu M, Pang DW. *Nanoscale*, 2016, 8: 12406–12429

289 Yang G, Xu L, Chao Y, Xu J, Sun X, Wu Y, Peng R, Liu Z. *Nat Commun*, 2017, 8: 902

290 Chen C, Sun SR, Gong YP, Qi CB, Peng CW, Yang XQ, Liu SP, Peng J, Zhu S, Hu MB, Pang DW, Li Y. *Biomaterials*, 2011, 32: 7592–7599

291 Medintz IL, Uyeda HT, Goldman ER, Mattoussi H. *Nat Mater*, 2005, 4: 435–446

292 Gao X, Cui Y, Levenson RM, Chung LWK, Nie S. *Nat Biotechnol*, 2004, 22: 969–976

293 Wang HZ, Wang HY, Liang RQ, Ruan KC. *Acta Biochim Biophysica Sin*, 2004, 36: 681–686

294 Yezhelyev M, Al-Hajj A, Morris C, Marcus A, Liu T, Lewis M, Cohen C, Zrazhevskiy P, Simons J, Rogatko A, Nie S, Gao X, O'Regan R. *Adv Mater*, 2007, 19: 3146–3151

295 Zhong Y, Ma Z, Zhu S, Yue J, Zhang M, Antaris AL, Yuan J, Cui R, Wan H, Zhou Y, Wang W, Huang NF, Luo J, Hu Z, Dai H. *Nat Commun*, 2017, 8: 737

296   Hong G, Diao S, Antaris AL, Dai H. *Chem Rev*, 2015, 115: 10816–10906

297   Hong G, Antaris AL, Dai H. *Nat Biomed Eng*, 2017, 1: 0010

298   Diao S, Blackburn JL, Hong G, Antaris AL, Chang J, Wu JZ, Zhang B, Cheng K, Kuo CJ, Dai H. *Angew Chem Int Ed*, 2015, 54: 14758–14762

299   Kim S, Fisher B, Eisler HJ, Bawendi M. *J Am Chem Soc*, 2003, 125: 11466–11467

300   Seo H, Kim SW. *Chem Mater*, 2007, 19: 2715–2717

301   Jiang W, Singhal A, Zheng J, Wang C, Chan WCW. *Chem Mater*, 2006, 18: 4845–4854

302   Bailey RE, Nie S. *J Am Chem Soc*, 2003, 125: 7100–7106

303   Qian H, Dong C, Peng J, Qiu X, Xu Y, Ren J. *J Phys Chem C*, 2007, 111: 16852–16857

304   Cademartiri L, Bertolotti J, Sapienza R, Wiersma DS, von Freymann G, Ozin GA. *J Phys Chem B*, 2006, 110: 671–673

305   Cui R, Gu YP, Zhang ZL, Xie ZX, Tian ZQ, Pang DW. *J Mater Chem*, 2012, 22: 3713–3716

306   Du Y, Xu B, Fu T, Cai M, Li F, Zhang Y, Wang Q. *J Am Chem Soc*, 2010, 132: 1470–1471

307   Shen S, Zhang Y, Peng L, Du Y, Wang Q. *Angew Chem Int Ed*, 2011, 50: 7115–7118

308   Hong G, Robinson JT, Zhang Y, Diao S, Antaris AL, Wang Q, Dai H. *Angew Chem Int Ed*, 2012, 51: 9818–9821

309   Zhang Y, Hong G, Zhang Y, Chen G, Li F, Dai H, Wang Q. *ACS Nano*, 2012, 6: 3695–3702

310   Jiang P, Zhu CN, Zhang ZL, Tian ZQ, Pang DW. *Biomaterials*, 2012, 33: 5130–5135

311   Zhao Y, Zheng C, Wang Q, Fang J, Zhou G, Zhao H, Yang Y, Xu H, Feng G, Yang X. *Adv Funct Mater*, 2012, 21: 2035–2042

312   Zhu CN, Chen G, Tian ZQ, Wang W, Zhong WQ, Li Z, Zhang ZL, Pang DW. *Small*, 2017, 13: 1602309

313   Zhu CN, Jiang P, Zhang ZL, Zhu DL, Tian ZQ, Pang DW. *ACS Appl Mater Interfaces*, 2013, 5: 1186–1189

314   Zimmer JP, Kim SW, Ohnishi S, Tanaka E, Frangioni JV, Bawendi MG. *J Am Chem Soc*, 2006, 128: 2526–2527

315   Cao YW, Banin U. *J Am Chem Soc*, 2000, 122: 9692–9702

316   Cao YW, Banin U. *Angew Chem Int Ed*, 1999, 38: 3692–3694

317   Haubold S, Haase M, Kornowski A, Weller H. *ChemPhysChem*, 2001, 2: 331–334

318   Xie R, Battaglia D, Peng X. *J Am Chem Soc*, 2007, 129: 15432–15433

319   Erogbogbo F, Yong KT, Roy I, Hu R, Law WC, Zhao W, Ding H, Wu F, Kumar R, Swihart MT, Prasad PN. *ACS Nano*, 2010, 5: 413–423

320   Zhang M, Yue J, Cui R, Ma Z, Wan H, Wang F, Zhu S, Zhou Y, Kuang Y, Zhong Y, Pang DW, Dai H. *Proc Natl Acad Sci USA*, 2018, 115: 6590–6595

321   Zhang Y, Zhang Y, Hong G, He W, Zhou K, Yang K, Li F, Chen G, Liu Z, Dai H, Wang Q. *Biomaterials*, 2013, 34: 3639–3646

322   Tang H, Yang ST, Yang YF, Ke DM, Liu JH, Chen X, Wang H, Liu Y. *ACS Appl Mater Interfaces*, 2016, 8: 17859–17869

323   Ge XL, Zhang ZL, Xie ZX, Cui R, Pang DW. *New J Chem*, 2017, 41: 12721–12725

324   Gu YP, Cui R, Zhang ZL, Xie ZX, Pang DW. *J Am Chem Soc*, 2012, 134: 79–82

325   Zhao JY, Chen G, Gu YP, Cui R, Zhang ZL, Yu ZL, Tang B, Zhao YF, Pang DW. *J Am Chem Soc*, 2016, 138: 1893–1903

326   Niidome T, Huang L. *Gene Ther*, 2002, 9: 1647–1652

327   Chen J, Guo Z, Tian H, Chen X. *Mol Ther-Meth Clin Dev*, 2016, 3: 16023

328   Yu X, Gong L, Zhang J, Zhao Z, Zhang X, Tan W. *Sci China Chem*, 2017, 60: 1318–1323

329   Xu C, Tian H, Chen X. *Sci China Chem*, 2017, 60: 319–328

330   Lehrman S. *Nature*, 1999, 401: 517–518

331   Tian H, Chen J, Chen X. *Small*, 2013, 9: 2034–2044

332   Zhou Z, Liu X, Zhu D, Wang Y, Zhang Z, Zhou X, Qiu N, Chen X, Shen Y. *Adv Drug Deliver Rev*, 2017, 115: 115–154

333   Chen J, Dong X, Feng T, Lin L, Guo Z, Xia J, Tian H, Chen X. *Acta Biomater*, 2015, 26: 45–53

334   Wang H, Wang Y, Wang Y, Hu J, Li T, Liu H, Zhang Q, Cheng Y. *Angew Chem Int Ed*, 2015, 54: 11647–11651

335   Chen J, Tian H, Dong X, Guo Z, Jiao Z, Li F, Kano A, Maruyama A, Chen X. *Macromol Biosci*, 2013, 13: 1438–1446

336   Fang H, Guo Z, Lin L, Chen J, Sun P, Wu J, Xu C, Tian H, Chen X. *J Am Chem Soc*, 2018, 140: 11992–12000

337   Yin H, Kanasty RL, Eltoukhy AA, Vegas AJ, Dorkin JR, Anderson DG. *Nat Rev Genet*, 2014, 15: 541–555

338   Guo Z, Chen J, Lin L, Guan X, Sun P, Chen M, Tian H, Chen X. *ACS Appl Mater Interfaces*, 2017, 9: 15297–15306

339   He Y, Nie Y, Cheng G, Xie L, Shen Y, Gu Z. *Adv Mater*, 2014, 26: 1534–1540

340   Du JZ, Sun TM, Song WJ, Wu J, Wang J. *Angew Chem Int Ed*, 2010, 49: 3621–3626

341   Tian H, Guo Z, Lin L, Jiao Z, Chen J, Gao S, Zhu X, Chen X. *J Control Release*, 2014, 174: 117–125

342   Guan X, Guo Z, Lin L, Chen J, Tian H, Chen X. *Nano Lett*, 2016, 16: 6823–6831

343   Chen J, Guan X, Hu Y, Tian H, Chen X. *Top Curr Chem (Z)*, 2017, 375: 32

344   Xiao J, Hu Y, Du J. *Sci China Chem*, 2018, 61: 569–575

345   Wang F, Xiao J, Chen S, Sun H, Yang B, Jiang J, Zhou X, Du J. *Adv Mater*, 2018, 30: 1705674

346   Zou Y, Zheng M, Yang W, Meng F, Miyata K, Kim HJ, Kataoka K, Zhong Z. *Adv Mater*, 2017, 29: 1703285

347   Deng L, Xu Y, Sun C, Yun B, Sun Q, Zhao C, Li Z. *Sci Bull*, 2018, 63: 917–924

348   Wen J, Yan H, Xia P, Xu Y, Li H, Sun S. *Sci China Chem*, 2017, 60: 799–805

349   Huang G, Liu R, Hu Y, Li SH, Wu Y, Qiu Y, Li J, Yang HH. *Sci China Chem*, 2018, 61: 806–811

350   Wei J, Yu C, Wang L, Wang J, Zhou Z, Yang H, Yang S. *Sci China Chem*, 2015, 58: 1537–1543

351   Hu X, Li F, Noor N, Ling D. *Sci Bull*, 2017, 62: 589–596

352   Chen X, Shi S, Wei J, Chen M, Zheng N. *Sci Bull*, 2017, 62: 579–588

353   Tong C, Zhang X, Fan J, Li B, Liu B, Daniyal M, Wang W. *Sci Bull*, 2018, 63: 935–946

354   Guo M, Zhou G, Liu Z, Liu J, Tang J, Xiao Y, Xu W, Liu Y, Chen C. *Sci Bull*, 2018, 63: 92–100

355   Sun M, Li J, Zhang C, Xie Y, Qiao H, Su Z, Oupický D, Ping Q. *Adv Healthc Mater*, 2017, 6: 1600693

356   Huang JL, Jiang G, Song QX, Gu X, Hu M, Wang XL, Song HH, Chen LP, Lin YY, Jiang D, Chen J, Feng JF, Qiu YM, Jiang JY, Jiang XG, Chen HZ, Gao XL. *Nat Commun*, 2017, 8: 15144

357   Liang M, Fan K, Zhou M, Duan D, Zheng J, Yang D, Feng J, Yan X. *Proc Natl Acad Sci USA*, 2014, 111: 14900–14905

358   Cheng K, Ding Y, Zhao Y, Ye S, Zhao X, Zhang Y, Ji T, Wu H, Wang B, Anderson GJ, Ren L, Nie G. *Nano Lett*, 2018, 18: 3250–3258

359   Sun B, Luo C, Yu H, Zhang X, Chen Q, Yang W, Wang M, Kan Q, Zhang H, Wang Y, He Z, Sun J. *Nano Lett*, 2018, 18: 3643–3650

360   Jia H, Chen S, Zhuo R, Feng J, Zhang X. *Sci China Chem*, 2016, 59: 1397–1404

361   Luo C, Sun J, Liu D, Sun B, Miao L, Musetti S, Li J, Han X, Du Y, Li L, Huang L, He Z. *Nano Lett*, 2016, 16: 5401–5408

362   Wang P, Liu YG, Wang SB. *Chin Sci Bull*, 2017, 62: 1233–1240

363   Li Y, Yu H, Sun H, Liu J, Tang Z, Wang D, Yu L, Chen X. *Chin J Polym Sci*, 2015, 33: 763–771

364   Zhou YC, Zhou ZX, Shen YQ. *Acta Polym Sin*, 2017: 359–366

365   Zhou Z, Ma X, Murphy CJ, Jin E, Sun Q, Shen Y, Van Kirk EA, Murdoch WJ. *Angew Chem Int Ed*, 2014, 53: 10949–10955

366   Shao S, Zhou Q, Si J, Tang J, Liu X, Wang M, Gao J, Wang K, Xu R, Shen Y. *Nat Biomed Eng*, 2017, 1: 745–757

367   Zhang SY, Wu Y, He B, Luo K, Gu ZW. *Sci China Chem*, 2014, 57:

461–475

368 Zhang Y, Xiao CS, Li MQ, Ding JX, Yang CG, Zhuang XL, Chen XS. *Sci China Chem*, 2014, 57: 624–632

369 Lin B, Su H, Jin R, Li D, Wu C, Jiang X, Xia C, Gong Q, Song B, Ai H. *Sci Bull*, 2015, 60: 1272–1280

370 Li N, Zhao L, Qi L, Li Z, Luan Y. *Prog Polymer Sci*, 2016, 58: 1–26

371 Zheng CX, Zhao Y, Liu Y. *Chin J Polym Sci*, 2018, 36: 322–346

372 Zhang Y, Ren K, Zhang X, Chao Z, Yang Y, Ye D, Dai Z, Liu Y, Ju H. *Biomaterials*, 2018, 163: 55–66

373 Liu Y, Du J, Choi J, Chen KJ, Hou S, Yan M, Lin WY, Chen KS, Ro T, Lipshutz GS, Wu L, Shi L, Lu Y, Tseng HR, Wang H. *Angew Chem Int Ed*, 2016, 55: 169–173

374 Chen W, Zeng K, Liu H, Ouyang J, Wang L, Liu Y, Wang H, Deng L, Liu YN. *Adv Funct Mater*, 2017, 27: 1605795

375 Guo Y, Wang D, Song Q, Wu T, Zhuang X, Bao Y, Kong M, Qi Y, Tan S, Zhang Z. *ACS Nano*, 2015, 9: 6918–6933

376 Gao M, Liang C, Song X, Chen Q, Jin Q, Wang C, Liu Z. *Adv Mater*, 2017, 29: 1701429

377 Pei Q, Hu X, Zheng X, Liu S, Li Y, Jing X, Xie Z. *ACS Nano*, 2018, 12: 1630–1641

378 Wang X, Valiev RR, Ohulchanskyy TY, Ågren H, Yang C, Chen G. *Chem Soc Rev*, 2017, 46: 4150–4167

379 Rao L, Bu LL, Cai B, Xu JH, Li A, Zhang WF, Sun ZJ, Guo SS, Liu W, Wang TH, Zhao XZ. *Adv Mater*, 2016, 28: 3460–3466

380 Xuan M, Shao J, Dai L, He Q, Li J. *Adv Healthc Mater*, 2015, 4: 1645–1652

381 Zhang Y, Cai K, Li C, Guo Q, Chen Q, He X, Liu L, Zhang Y, Lu Y, Chen X, Sun T, Huang Y, Cheng J, Jiang C. *Nano Lett*, 2018, 18: 1908–1915

382 Wu X, Wu C, Zhang C. *Chin J Polym Sci*, 2017, 35: 1–24

383 Zhu X, Li J, Qiu X, Liu Y, Feng W, Li F. *Nat Commun*, 2018, 9: 2176

384 Zhang Y, Tu J, Wang D, Zhu H, Maity SK, Qu X, Bogaert B, Pei H, Zhang H. *Adv Mater*, 2018, 30: 1703658

385 Ma Y, Wang Z, Ma Y, Han Z, Zhang M, Chen H, Gu Y. *Angew Chem Int Ed*, 2018, 57: 5389–5393

386 Mou Q, Ma Y, Pan G, Xue B, Yan D, Zhang C, Zhu X. *Angew Chem Int Ed*, 2017, 56: 12528–12532

387 Brannon-Peppas L, Blanchette JO. *Adv Drug Deliver Rev*, 2004, 56: 1649–1659

388 Sun Q, Sun X, Ma X, Zhou Z, Jin E, Zhang B, Shen Y, Van Kirk EA, Murdoch WJ, Lott JR, Lodge TP, Radosz M, Zhao Y. *Adv Mater*, 2014, 26: 7615–7621

389 Mikhail AS, Allen C. *J Control Release*, 2009, 138: 214–223

390 Li SD, Huang L. *Mol Pharm*, 2008, 5: 496–504

391 Jang SH, Wientjes MG, Lu D, Au JLS. *Pharm Res*, 2003, 20: 1337–1350

392 Jain RK. *Science*, 2005, 307: 58–62

393 Choi J, Credit K, Henderson K, Deverkadra R, He Z, Wiig H, Vanpelt H, Flessner MF. *Clin Cancer Res*, 2006, 12: 1906–1912

394 Alexandrakis G, Brown EB, Tong RT, McKee TD, Campbell RB, Boucher Y, Jain RK. *Nat Med*, 2004, 10: 203–207

395 Flessner MF, Choi J, Credit K, Deverkadra R, Henderson K. *Clin Cancer Res*, 2005, 11: 3117–3125

396 Boucher Y, Baxter LT, Jain RK. *Cancer Res*, 1990, 50: 4478–4484

397 Heldin CH, Rubin K, Pietras K, Ostman A. *Nat Rev Cancer*, 2004, 4: 806–813

398 Jain RK. *Adv Drug Deliver Rev*, 2001, 46: 149–168

399 Gottesman MM. *Annu Rev Med*, 2002, 53: 615–627

400 Batrakova EV, Kabanov AV. *J Control Release*, 2008, 130: 98–106

401 Agarwal R, Kaye SB. *Nat Rev Cancer*, 2003, 3: 502–516

402 Wang G, Reed E, Li Q. *Oncol Rep*, 2004, 12: 955–965

403 Michael M, Doherty MM. *J Clin Oncol*, 2005, 23: 205–229

404 Cabral H, Matsumoto Y, Mizuno K, Chen Q, Murakami M, Kimura M, Terada Y, Kano MR, Miyazono K, Uesaka M, Nishiyama N, Kataoka K. *Nat Nanotech*, 2011, 6: 815–823

405 Sun Q, Zhou Z, Qiu N, Shen Y. *Adv Mater*, 2017, 29: 1606628

406 Shen Y, Zhan Y, Tang J, Xu P, Johnson PA, Radosz M, Van Kirk EA, Murdoch WJ. *AIChE J*, 2008, 54: 2979–2989

407 Sun X, Wang G, Zhang H, Hu S, Liu X, Tang J, Shen Y. *ACS Nano*, 2018, 12: 6179–6192

408 Green J, Tyrrell Z, Radosz M. *J Phys Chem C*, 2010, 114: 16082–16086

409 Tyrrell ZL, Shen Y, Radosz M. *J Phys Chem C*, 2011, 115: 11951–11956

410 Tyrrell ZL, Shen Y, Radosz M. *Macromolecules*, 2012, 45: 4809–4817

411 Yu S, Ding J, He C, Cao Y, Xu W, Chen X. *Adv Healthc Mater*, 2014, 3: 752–760

412 Li X, Figg CA, Wang R, Jiang Y, Lyu Y, Sun H, Liu Y, Wang Y, Teng IT, Hou W, Cai R, Cui C, Li L, Pan X, Sumerlin BS, Tan W. *Angew Chem Int Ed*, 2018, 57: 11589–11593

413 Hu Q, Rijcken CJ, Bansal R, Hennink WE, Storm G, Prakash J. *Biomaterials*, 2015, 53: 370–378

414 Shi C, Guo D, Xiao K, Wang X, Wang L, Luo J. *Nat Commun*, 2015, 6: 7449

415 Tang Z, Gao Y, Li D, Zhou S. *Adv Healthc Mater*, 2017, 6: 1600919

416 Chen G, Wang Y, Wu P, Zhou Y, Yu F, Zhu C, Li Z, Hang Y, Wang K, Li J, Sun M, Oupicky D. *ACS Nano*, 2018, 12: 6620–6636

417 Chen G, Wang K, Wang Y, Wu P, Sun M, Oupický D. *Adv Healthc Mater*, 2018, 7: 1700978

418 Chithrani BD, Ghazani AA, Chan WCW. *Nano Lett*, 2006, 6: 662–668

419 Jin H, Heller DA, Sharma R, Strano MS. *ACS Nano*, 2009, 3: 149–158

420 Zhang S, Li J, Lykotrafitis G, Bao G, Suresh S. *Adv Mater*, 2009, 21: 419–424

421 Popović Z, Liu W, Chauhan VP, Lee J, Wong C, Greytak AB, Insin N, Nocera DG, Fukumura D, Jain RK, Bawendi MG. *Angew Chem Int Ed*, 2010, 49: 8649–8652

422 Wang J, Mao W, Lock LL, Tang J, Sui M, Sun W, Cui H, Xu D, Shen Y. *ACS Nano*, 2015, 9: 7195–7206

423 Maeda H. *Adv Enzyme Regul*, 2001, 41: 189–207

424 Jain RK. *Cancer Res*, 1990, 50: S814–S819

425 Yuan F, Leunig M, Huang SK, Berk DA, Papahadjopoulos D, Jain RK. *Cancer Res*, 1994, 54: 3352–3356

426 Yang K, Zhang S, Zhang G, Sun X, Lee ST, Liu Z. *Nano Lett*, 2010, 10: 3318–3323

427 Holback H, Yeo Y. *Pharm Res*, 2011, 28: 1819–1830

428 Tomida A, Tsuruo T. *Anti-Cancer Drug Des*, 1999, 14: 169–177

429 Dai Q, Wilhelm S, Ding D, Syed AM, Sindhwani S, Zhang Y, Chen YY, MacMillan P, Chan WCW. *ACS Nano*, 2018, 12: 8423–8435

430 Wang C. *Sci Bull*, 2015: 1–2

431 Dai L, Li K, Li M, Zhao X, Luo Z, Lu L, Luo Y, Cai K. *Adv Funct Mater*, 2018, 28: 1707249

432 Guo X, Wei X, Jing Y, Zhou S. *Adv Mater*, 2015, 27: 6450–6456

433 Chen J, Ding J, Wang Y, Cheng J, Ji S, Zhuang X, Chen X. *Adv Mater*, 2017, 29: 1701170

434 Ju C, Mo R, Xue J, Zhang L, Zhao Z, Xue L, Ping Q, Zhang C. *Angew Chem Int Ed*, 2014, 53: 6253–6258

435 Xue X, Huang Y, Bo R, Jia B, Wu H, Yuan Y, Wang Z, Ma Z, Jing D, Xu X, Yu W, Lin TY, Li Y. *Nat Commun*, 2018, 9: 3653

436 Jiang W, Huang Y, An Y, Kim BYS. *ACS Nano*, 2015, 9: 8689–8696

437 Wang JL, Sun JS, Shi XH. *Chin Sci Bull (Chin Ver)*, 2015, 60: 1976–1986

438 Sun D, Ding J, Xiao C, Chen J, Zhuang X, Chen X. *Adv Healthc Mater*, 2015, 4: 844–855

439 Ding L, Zhu X, Wang Y, Shi B, Ling X, Chen H, Nan W, Barrett A, Guo Z, Tao W, Wu J, Shi X. *Nano Lett*, 2017, 17: 6790–6801

440 Minchinton AI, Tannock IF. *Nat Rev Cancer*, 2006, 6: 583–592

441 Jin E, Zhang B, Sun X, Zhou Z, Ma X, Sun Q, Tang J, Shen Y, Van Kirk E, Murdoch WJ, Radosz M. *J Am Chem Soc*, 2013, 135: 933–940

442 Jing Y, Xiong X, Ming Y, Zhao J, Guo X, Yang G, Zhou S. *Adv*

Healthc Mater, 2018, 7: 1700974

443 Quail DF, Joyce JA. *Nat Med*, 2013, 19: 1423–1437

444 Song X, Feng L, Liang C, Yang K, Liu Z. *Nano Lett*, 2016, 16: 6145–6153

445 Chen Q, Feng L, Liu J, Zhu W, Dong Z, Wu Y, Liu Z. *Adv Mater*, 2016, 28: 7129–7136

446 Jia Q, Ge J, Liu W, Zheng X, Chen S, Wen Y, Zhang H, Wang P. *Adv Mater*, 2018, 30: 1706090

447 Zhang C, Ni D, Liu Y, Yao H, Bu W, Shi J. *Nat Nanotech*, 2017, 12: 378–386

448 Huo M, Wang L, Chen Y, Shi J. *Nat Commun*, 2017, 8: 357

449 Han X, Li Y, Xu Y, Zhao X, Zhang Y, Yang X, Wang Y, Zhao R, Anderson GJ, Zhao Y, Nie G. *Nat Commun*, 2018, 9: 3390

450 Zhu Q, Chen X, Xu X, Zhang Y, Zhang C, Mo R. *Adv Funct Mater*, 2018, 28: 1707371

451 Gros A, Syvannarath V, Lamrani L, Ollivier V, Loyau S, Goerge T, Nieswandt B, Jandrot-Perrus M, Ho-Tin-Noé B. *Blood*, 2015, 126: 1017–1026

452 Li S, Zhang Y, Wang J, Zhao Y, Ji T, Zhao X, Ding Y, Zhao X, Zhao R, Li F, Yang X, Liu S, Liu Z, Lai J, Whittaker AK, Anderson GJ, Wei J, Nie G. *Nat Biomed Eng*, 2017, 1: 667–679

453 Li L, Sun W, Zhong J, Yang Q, Zhu X, Zhou Z, Zhang Z, Huang Y. *Adv Funct Mater*, 2015, 25: 4101–4113

454 Lu G, Li F, Zhang F, Huang LL, Zhang L, Lv Y, Wei W, Xie HY. *Adv Funct Mater*, 2018, 28: 1707596

455 He B, Tan T, Wang H, Hu H, Wang Z, Wang J, Li J, Sun K, Zhang Z, Li Y. *Adv Funct Mater*, 2018, 28: 1705622

456 Dahmani FZ, Xiao Y, Zhang J, Yu Y, Zhou J, Yao J. *Adv Healthc Mater*, 2016, 5: 1447–1461

457 Shen Y, Ma X, Zhang B, Zhou Z, Sun Q, Jin E, Sui M, Tang J, Wang J, Fan M. *Chem Eur J*, 2011, 17: 5319–5326

458 Chauhan VP, Stylianopoulos T, Boucher Y, Jain RK. *Annu Rev Chem Biomol Eng*, 2011, 2: 281–298

459 Wilhelm S, Tavares AJ, Dai Q, Ohta S, Audet J, Dvorak HF, Chan WCW. *Nat Rev Mater*, 2016, 1: 16014

460 Leu AJ, Berk DA, Lymboussaki A, Alitalo K, Jain RK. *Cancer Res*, 2000, 60: 4324–4327

461 Matsumoto Y, Nichols JW, Toh K, Nomoto T, Cabral H, Miura Y, Christie RJ, Yamada N, Ogura T, Kano MR, Matsumura Y, Nishiyama N, Yamasoba T, Bae YH, Kataoka K. *Nat Nanotech*, 2016, 11: 533–538

462 Stirland DL, Matsumoto Y, Toh K, Kataoka K, Bae YH. *J Control Release*, 2016, 227: 38–44

463 Primeau AJ, Rendon A, Hedley D, Lilge L, Tannock IF. *Clin Cancer Res*, 2005, 11: 8782–8788

464 Levental KR, Yu H, Kass L, Lakins JN, Egeblad M, Erler JT, Fong SFT, Csiszar K, Giaccia A, Weninger W, Yamauchi M, Gasser DL, Weaver VM. *Cell*, 2009, 139: 891–906

465 Jain RK, Stylianopoulos T. *Nat Rev Clin Oncol*, 2010, 7: 653–664

466 Zhou Z, Song J, Nie L, Chen X. *Chem Soc Rev*, 2016, 45: 6597–6626

467 Cherukuri P, Glazer ES, Curley SA. *Adv Drug Deliver Rev*, 2010, 62: 339–345

468 Luo GF, Chen WH, Hong S, Cheng Q, Qiu WX, Zhang XZ. *Adv Funct Mater*, 2017, 27: 1702122

469 Chen WH, Luo GF, Qiu WX, Lei Q, Liu LH, Wang SB, Zhang XZ. *Biomaterials*, 2017, 117: 54–65

470 Dolmans DEJGJ, Fukumura D, Jain RK. *Nat Rev Cancer*, 2003, 3: 380–387

471 Lucky SS, Soo KC, Zhang Y. *Chem Rev*, 2015, 115: 1990–2042

472 Li X, Lee S, Yoon J. *Chem Soc Rev*, 2018, 47: 1174–1188

473 Vannostrum C. *Adv Drug Deliver Rev*, 2004, 56: 9–16

474 Nishiyama N, Morimoto Y, Jang WD, Kataoka K. *Adv Drug Deliver Rev*, 2009, 61: 327–338

475 Chen JX, Wang HY, Li C, Han K, Zhang XZ, Zhuo RX. *Biomaterials*, 2011, 32: 1678–1684

476 Jeong H, Huh MS, Lee SJ, Koo H, Kwon IC, Jeong SY, Kim K. *Theranostics*, 2011, 1: 230–239

477 Abbas M, Zou Q, Li S, Yan X. *Adv Mater*, 2017, 29: 1605021

478 Idris NM, Gnanasammandhan MK, Zhang J, Ho PC, Mahendran R, Zhang Y. *Nat Med*, 2012, 18: 1580–1585

479 Zeng JY, Zou MZ, Zhang M, Wang XS, Zeng X, Cong H, Zhang XZ. *ACS Nano*, 2018, 12: 4630–4640

480 Pan L, Liu J, Shi J. *Adv Funct Mater*, 2014, 24: 7318–7327

481 Shi L, Hernandez B, Selke M. *J Am Chem Soc*, 2006, 128: 6278–6279

482 Jang B, Park JY, Tung CH, Kim IH, Choi Y. *ACS Nano*, 2011, 5: 1086–1094

483 Li F, Du Y, Liu J, Sun H, Wang J, Li R, Kim D, Hyeon T, Ling D. *Adv Mater*, 2018, 30: 1802808

484 Wang C, Tao H, Cheng L, Liu Z. *Biomaterials*, 2011, 32: 6145–6154

485 Zhang C, Chen WH, Liu LH, Qiu WX, Yu WY, Zhang XZ. *Adv Funct Mater*, 2017, 27: 1700626

486 Huang YY, Sharma SK, Yin R, Agrawal T, Chiang LY, Hamblin MR. *J Biomed Nanotechnol*, 2014, 10: 1918–1936

487 Zhang C, Zhao K, Bu W, Ni D, Liu Y, Feng J, Shi J. *Angew Chem Int Ed*, 2015, 54: 1770–1774

488 Yu Z, Pan W, Li N, Tang B. *Chem Sci*, 2016, 7: 4237–4244

489 Zhang Z, Wang J, Chen C. *Adv Mater*, 2013, 25: 3869–3880

490 Jaque D, Martínez Maestro L, del Rosal B, Haro-Gonzalez P, Benayas A, Plaza JL, Martín Rodríguez E, García Solé J. *Nanoscale*, 2014, 6: 9494–9530

491 Chen WH, Luo GF, Zhang XZ. *Adv Mater*, 2018, 113: 1802725

492 Zhao P, Zheng M, Yue C, Luo Z, Gong P, Gao G, Sheng Z, Zheng C, Cai L. *Biomaterials*, 2014, 35: 6037–6046

493 Song X, Chen Q, Liu Z. *Nano Res*, 2014, 8: 340–354

494 Zhou J, Lu Z, Zhu X, Wang X, Liao Y, Ma Z, Li F. *Biomaterials*, 2013, 34: 9584–9592

495 Zha Z, Yue X, Ren Q, Dai Z. *Adv Mater*, 2013, 25: 777–782

496 MacDonald TD, Liu TW, Zheng G. *Angew Chem Int Ed*, 2014, 53: 6956–6959

497 Lovell JF, Jin CS, Huynh E, Jin H, Kim C, Rubinstein JL, Chan WCW, Cao W, Wang LV, Zheng G. *Nat Mater*, 2011, 10: 324–332

498 Wang X, Zhang J, Wang Y, Wang C, Xiao J, Zhang Q, Cheng Y. *Biomaterials*, 2016, 81: 114–124

499 Moon HK, Lee SH, Choi HC. *ACS Nano*, 2009, 3: 3707–3713

500 Chen WH, Yang CX, Qiu WX, Luo GF, Jia HZ, Lei Q, Wang XY, Liu G, Zhuo RX, Zhang XZ. *Adv Healthc Mater*, 2015, 4: 2247–2259

501 Wang XQ, Gao F, Zhang XZ. *Angew Chem Int Ed*, 2017, 56: 9029–9033

502 Huang X, Tang S, Mu X, Dai Y, Chen G, Zhou Z, Ruan F, Yang Z, Zheng N. *Nat Nanotech*, 2010, 6: 28–32

503 Dumas A, Couvreur P. *Chem Sci*, 2015, 6: 2153–2157

504 Song G, Liang C, Gong H, Li M, Zheng X, Cheng L, Yang K, Jiang X, Liu Z. *Adv Mater*, 2015, 27: 6110–6117

505 Hessel CM, Pattani VP, Rasch M, Panthani MG, Koo B, Tunnell JW, Korgel BA. *Nano Lett*, 2011, 11: 2560–2566

506 Tian Q, Tang M, Sun Y, Zou R, Chen Z, Zhu M, Yang S, Wang J, Wang J, Hu J. *Adv Mater*, 2011, 23: 3542–3547

507 Zhou M, Zhang R, Huang M, Lu W, Song S, Melancon MP, Tian M, Liang D, Li C. *J Am Chem Soc*, 2010, 132: 15351–15358

508 Cheng L, Liu J, Gu X, Gong H, Shi X, Liu T, Wang C, Wang X, Liu G, Xing H, Bu W, Sun B, Liu Z. *Adv Mater*, 2014, 26: 1886–1893

509 Zhang C, Yong Y, Song L, Dong X, Zhang X, Liu X, Gu Z, Zhao Y, Hu Z. *Adv Healthc Mater*, 2016, 5: 2776–2787

510 Chen Z, Wang Q, Wang H, Zhang L, Song G, Song L, Hu J, Wang H, Liu J, Zhu M, Zhao D. *Adv Mater*, 2013, 25: 2095–2100

511 Deng K, Hou Z, Deng X, Yang P, Li C, Lin J. *Adv Funct Mater*, 2015, 25: 7280–7290

512 Fu G, Liu W, Feng S, Yue X. *Chem Commun*, 2012, 48: 11567

513 Cheng L, Gong H, Zhu W, Liu J, Wang X, Liu G, Liu Z. *Biomaterials*, 2014, 35: 9844–9852

514 Sun C, Wen L, Zeng J, Wang Y, Sun Q, Deng L, Zhao C, Li Z. *Biomaterials*, 2016, 91: 81–89

515 Wang S, Tian Y, Tian W, Sun J, Zhao S, Liu Y, Wang C, Tang Y, Ma X, Teng Z, Lu G. *ACS Nano*, 2016, 10: 8578–8590

516 Jego G, Hazoumé A, Seigneuric R, Garrido C. *Cancer Lett*, 2013, 332: 275–285

517 Miyagawa T, Saito H, Minamiya Y, Mitobe K, Takashima S, Takahashi N, Ito A, Imai K, Motoyama S, Ogawa J. *Int J Clin Oncol*, 2013, 19: 722–730

518 Wang BK, Yu XF, Wang JH, Li ZB, Li PH, Wang H, Song L, Chu PK, Li C. *Biomaterials*, 2016, 78: 27–39

519 Guo W, Guo C, Zheng N, Sun T, Liu S. *Adv Mater*, 2017, 29: 1604157

520 Zhang K, Meng X, Cao Y, Yang Z, Dong H, Zhang Y, Lu H, Shi Z, Zhang X. *Adv Funct Mater*, 2018, 28: 1804634

521 Wang J, Zhu G, You M, Song E, Shukoor MI, Zhang K, Altman MB, Chen Y, Zhu Z, Huang CZ, Tan W. *ACS Nano*, 2012, 6: 5070–5077

522 Jin CS, Lovell JF, Chen J, Zheng G. *ACS Nano*, 2013, 7: 2541–2550

523 Luo GF, Chen WH, Lei Q, Qiu WX, Liu YX, Cheng YJ, Zhang XZ. *Adv Funct Mater*, 2016, 26: 4339–4350

524 Vijayaraghavan P, Liu CH, Vankayala R, Chiang CS, Hwang KC. *Adv Mater*, 2014, 26: 6689–6695

525 Sahu A, Choi WI, Lee JH, Tae G. *Biomaterials*, 2013, 34: 6239–6248

526 Tian B, Wang C, Zhang S, Feng L, Liu Z. *ACS Nano*, 2011, 5: 7000–7009

527 Lin J, Wang S, Huang P, Wang Z, Chen S, Niu G, Li W, He J, Cui D, Lu G, Chen X, Nie Z. *ACS Nano*, 2013, 7: 5320–5329

528 Lim EK, Kim T, Paik S, Haam S, Huh YM, Lee K. *Chem Rev*, 2014, 115: 327–394

529 Kim J, Piao Y, Hyeon T. *Chem Soc Rev*, 2009, 38: 372–390

530 Lee DE, Koo H, Sun IC, Ryu JH, Kim K, Kwon IC. *Chem Soc Rev*, 2012, 41: 2656–2672

531 Ji C, Gao Q, Dong X, Yin W, Gu Z, Gan Z, Zhao Y, Yin M. *Angew Chem Int Ed*, 2018, 57: 11384–11388

532 Zheng M, Yue C, Ma Y, Gong P, Zhao P, Zheng C, Sheng Z, Zhang P, Wang Z, Cai L. *ACS Nano*, 2013, 7: 2056–2067

533 Pelaz B, Alexiou C, Alvarez-Puebla RA, Alves F, Andrews AM, Ashraf S, Balogh LP, Ballerini L, Bestetti A, Brendel C, Bosi S, Carril M, Chan WCW, Chen C, Chen X, Chen X, Cheng Z, Cui D, Du J, Dullin C, Escudero A, Feliu N, Gao M, George M, Gogotsi Y, Grünweller A, Gu Z, Halas NJ, Hampp N, Hartmann RK, Hersam MC, Hunziker P, Jian J, Jiang X, Jungebluth P, Kadhiresan P, Kataoka K, Khademhosseini A, Kopeček J, Kotov NA, Krug HF, Lee DS, Lehr CM, Leong KW, Liang XJ, Ling Lim M, Liz-Marzán LM, Ma X, Macchiarini P, Meng H, Möhwald H, Mulvaney P, Nel AE, Nie S, Nordlander P, Okano T, Oliveira J, Park TH, Penner RM, Prato M, Puntes V, Rotello VM, Samarakoon A, Schaak RE, Shen Y, Sjöqvist S, Skirtach AG, Soliman MG, Stevens MM, Sung HW, Tang BZ, Tietze R, Udugama BN, VanEpps JS, Weil T, Weiss PS, Willner I, Wu Y, Yang L, Yue Z, Zhang Q, Zhang Q, Zhang XE, Zhao Y, Zhou X, Parak WJ. *ACS Nano*, 2017, 11: 2313–2381

534 Wilson BC, Patterson MS. *Phys Med Biol*, 2008, 53: R61–R109

535 Zheng DW, Chen Y, Li ZH, Xu L, Li CX, Li B, Fan JX, Cheng SX, Zhang XZ. *Nat Commun*, 2018, 9: 1680

536 Lan G, Ni K, Lin W. *Coordin Chem Rev*, 2019, 379: 65–81

537 Zheng DW, Li B, Li CX, Xu L, Fan JX, Lei Q, Zhang XZ. *Adv Mater*, 2017, 29: 1703822

538 Lim WQ, Phua SZF, Xu HV, Sreejith S, Zhao Y. *Nanoscale*, 2016, 8: 12510–12519

539 Zhao L, Peng J, Huang Q, Li C, Chen M, Sun Y, Lin Q, Zhu L, Li F. *Adv Funct Mater*, 2014, 24: 363–371

540 Zhou L, Chen Z, Dong K, Yin M, Ren J, Qu X. *Adv Mater*, 2014, 26: 2424–2430

541 Min Y, Li J, Liu F, Yeow EKL, Xing B. *Angew Chem Int Ed*, 2014, 53: 1012–1016

542 Chen Q, Wang C, Cheng L, He W, Cheng Z, Liu Z. *Biomaterials*, 2014, 35: 2915–2923

543 Li X, Zhou L, Wei Y, El-Toni AM, Zhang F, Zhao D. *J Am Chem Soc*, 2014, 136: 15086–15092

544 Karimi M, Sahandi Zangabad P, Baghaee-Ravari S, Ghazadeh M, Mirshekari H, Hamblin MR. *J Am Chem Soc*, 2017, 139: 4584–4610

545 Zhang X, Tian G, Yin W, Wang L, Zheng X, Yan L, Li J, Su H, Chen C, Gu Z, Zhao Y. *Adv Funct Mater*, 2015, 25: 3049–3056

546 Zuo J, Tu L, Li Q, Feng Y, Que I, Zhang Y, Liu X, Xue B, Cruz LJ, Chang Y, Zhang H, Kong X. *ACS Nano*, 2018, 12: 3217–3225

547 Xu J, Gulzar A, Liu Y, Bi H, Gai S, Liu B, Yang D, He F, Yang P. *Small*, 2017, 13: 1701841

548 Yao C, Wang P, Li X, Hu X, Hou J, Wang L, Zhang F. *Adv Mater*, 2016, 28: 9341–9348

549 Zhao H, Hu W, Ma H, Jiang R, Tang Y, Ji Y, Lu X, Hou B, Deng W, Huang W, Fan Q. *Adv Funct Mater*, 2017, 27: 1702592

550 Zhang Y, Yu Z, Li J, Ao Y, Xue J, Zeng Z, Yang X, Tan TTY. *ACS Nano*, 2017, 11: 2846–2857

551 Zhang X, Guo Z, Liu J, Tian G, Chen K, Yu S, Gu Z. *Sci Bull*, 2017, 62: 985–996

552 Huang Y, Xiao Q, Hu H, Zhang K, Feng Y, Li F, Wang J, Ding X, Jiang J, Li Y, Shi L, Lin H. *Small*, 2016, 12: 4200–4210

553 Overchuk M, Zheng G. *Biomaterials*, 2018, 156: 217–237

554 Ai F, Wang N, Zhang X, Sun T, Zhu Q, Kong W, Wang F, Zhu G. *Nanoscale*, 2018, 10: 4432–4441

555 Li C, Zuo J, Zhang L, Chang Y, Zhang Y, Tu L, Liu X, Xue B, Li Q, Zhao H, Zhang H, Kong X. *Sci Rep*, 2016, 6: 38617

556 Liu B, Chen Y, Li C, He F, Hou Z, Huang S, Zhu H, Chen X, Lin J. *Adv Funct Mater*, 2015, 25: 4717–4729

557 Tan L, Huang R, Li X, Liu S, Shen YM. *Acta Biomater*, 2017, 57: 498–510

558 Wang Y, Song S, Liu J, Liu D, Zhang H. *Angew Chem Int Ed*, 2015, 54: 536–540

559 Wei R, Xi W, Wang H, Liu J, Mayr T, Shi L, Sun L. *Nanoscale*, 2017, 9: 12885–12896

560 Xu J, Kuang Y, Lv R, Yang P, Li C, Bi H, Liu B, Yang D, Dai Y, Gai S, He F, Xing B, Lin J. *Biomaterials*, 2017, 130: 42–55

561 Zhao J, Yang H, Li J, Wang Y, Wang X. *Sci Rep*, 2017, 7: 18014

562 Wang S, Yang W, Cui J, Li X, Dou Y, Su L, Chang J, Wang H, Li X, Zhang B. *Biomater Sci*, 2016, 4: 338–345

563 Liu X, Fan Z, Zhang L, Jin Z, Yan D, Zhang Y, Li X, Tu L, Xue B, Chang Y, Zhang H, Kong X. *Biomaterials*, 2017, 144: 73–83

564 Wang S, Zhang L, Dong C, Su L, Wang H, Chang J. *Chem Commun*, 2015, 51: 406–408

565 Lv R, Yang P, He F, Gai S, Yang G, Dai Y, Hou Z, Lin J. *Biomaterials*, 2015, 63: 115–127

566 Cai H, Shen T, Kirillov AM, Zhang Y, Shan C, Li X, Liu W, Tang Y. *Inorg Chem*, 2017, 56: 5295–5304

567 Li H, Wei R, Yan GH, Sun J, Li C, Wang H, Shi L, Capobianco JA, Sun L. *ACS Appl Mater Interfaces*, 2018, 10: 4910–4920

568 Han R, Yi H, Shi J, Liu Z, Wang H, Hou Y, Wang Y. *Phys Chem Chem Phys*, 2016, 18: 25497–25503

569 Bi H, Dai Y, Yang P, Xu J, Yang D, Gai S, He F, Liu B, Zhong C, An G, Lin J. *Small*, 2018, 14: 1703809

570 Zhu K, Liu G, Hu J, Liu S. *Biomacromolecules*, 2017, 18: 2571–2582

571 Xu J, Han W, Cheng Z, Yang P, Bi H, Yang D, Niu N, He F, Gai S, Lin J. *Chem Sci*, 2018, 9: 3233–3247

572 Fan W, Bu W, Shen B, He Q, Cui Z, Liu Y, Zheng X, Zhao K, Shi J. *Adv Mater*, 2015, 27: 4155–4161

573 Yao C, Wang W, Wang P, Zhao M, Li X, Zhang F. *Adv Mater*, 2018, 30: 1704833

574 Xu J, He F, Cheng Z, Lv R, Dai Y, Gulzar A, Liu B, Bi H, Yang D, Gai S, Yang P, Lin J. *Chem Mater*, 2017, 29: 7615–7628

575 Liu Y, Liu Y, Bu W, Cheng C, Zuo C, Xiao Q, Sun Y, Ni D, Zhang C, Liu J, Shi J. *Angew Chem Int Ed*, 2015, 54: 8105–8109

576 Liu Y, Liu Y, Bu W, Xiao Q, Sun Y, Zhao K, Fan W, Liu J, Shi J. *Biomaterials*, 2015, 49: 1–8

577 Wang P, Li X, Yao C, Wang W, Zhao M, El-Toni AM, Zhang F. *Biomaterials*, 2017, 125: 90–100

578 Lai J, Shah BP, Zhang Y, Yang L, Lee KB. *ACS Nano*, 2015, 9: 5234–5245

579 Khaydukov EV, Mironova KE, Semchishen VA, Generalova AN, Nechaev AV, Khochenkov DA, Stepanova EV, Lebedev OI, Zvyagin AV, Deyev SM, Panchenko VY. *Sci Rep*, 2016, 6: 35103

580 Hu P, Wang R, Zhou L, Chen L, Wu Q, Han MY, El-Toni AM, Zhao D, Zhang F. *Anal Chem*, 2017, 89: 3492–3500

581 Zhou J, Yao H, Meng L, Sun C, Ye W, Du Q. *ChemMedChem*, 2017, 12: 1191–1200

582 Zhang L, Zeng L, Pan Y, Luo S, Ren W, Gong A, Ma X, Liang H, Lu G, Wu A. *Biomaterials*, 2015, 44: 82–90

583 Zeng L, Luo L, Pan Y, Luo S, Lu G, Wu A. *Nanoscale*, 2015, 7: 8946–8954

584 Wu Q, Lin Y, Wo F, Yuan Y, Ouyang Q, Song J, Qu J, Yong KT. *Small*, 2017, 13: 1701129

585 Wang X, Meng G, Zhang S, Liu X. *Sci Rep*, 2016, 6: 29911

586 Tong R, Lin H, Chen Y, An N, Wang G, Pan X, Qu F. *Mater Sci Eng-C*, 2017, 78: 998–1005

587 Rao L, Meng QF, Bu LL, Cai B, Huang Q, Sun ZJ, Zhang WF, Li A, Guo SS, Liu W, Wang TH, Zhao XZ. *ACS Appl Mater Interfaces*, 2017, 9: 2159–2168

588 Liu C, Qi Y, Qiao R, Hou Y, Chan K, Li Z, Huang J, Jing L, Du J, Gao M. *Nanoscale*, 2016, 8: 12579–12587

589 Han J, Xia H, Wu Y, Kong SN, Deivasigamani A, Xu R, Hui KM, Kang Y. *Nanoscale*, 2016, 8: 7861–7865

590 Guan M, Dong H, Ge J, Chen D, Sun L, Li S, Wang C, Yan C, Wang P, Shu C. *NPG Asia Mater*, 2015, 7: e205

591 Gu B, Pliss A, Kuzmin AN, Baev A, Ohulchanskyy TY, Damasco JA, Yong KT, Wen S, Prasad PN. *Biomaterials*, 2016, 104: 78–86

592 Gnanasammandhan MK, Idris NM, Bansal A, Huang K, Zhang Y. *Nat Protoc*, 2016, 11: 688–713

593 Chowdhuri AR, Laha D, Chandra S, Karmakar P, Sahu SK. *Chem Eng J*, 2017, 319: 200–211

594 Chen CW, Chan YC, Hsiao M, Liu RS. *ACS Appl Mater Interfaces*, 2016, 8: 32108–32119

595 Wong PT, Chen D, Tang S, Yanik S, Payne M, Mukherjee J, Coulter A, Tang K, Tao K, Sun K, Baker Jr. JR, Choi SK. *Small*, 2015, 11: 6078–6090

596 Chowdhuri AR, Laha D, Pal S, Karmakar P, Sahu SK. *Dalton Trans*, 2016, 45: 18120–18132

597 Yang D, Yang G, Wang X, Lv R, Gai S, He F, Gulzar A, Yang P. *Nanoscale*, 2015, 7: 12180–12191

598 Luo CH, Huang CT, Su CH, Yeh CS. *Nano Lett*, 2016, 16: 3493–3499

599 Du B, Cao X, Zhao F, Su X, Wang Y, Yan X, Jia S, Zhou J, Yao H. *J Mater Chem B*, 2016, 4: 2038–2050

600 Zhou L, Chen E, Jin W, Wang Y, Zhou J, Wei S. *Dalton Trans*, 2016, 45: 15170–15179

601 Su X, Zhao F, Wang Y, Yan X, Jia S, Du B. *Nanomed-Nanotechnol Biol Med*, 2017, 13: 1761–1772

602 Wang D, Zhu L, Pu Y, Wang JX, Chen JF, Dai L. *Nanoscale*, 2017, 9: 11214–11221

603 Chen G, Jaskula-Sztul R, Esquibel CR, Lou I, Zheng Q, Dammalapati A, Harrison A, Eliceiri KW, Tang W, Chen H, Gong S. *Adv Funct Mater*, 2017, 27: 1604671

604 Lucky SS, Idris NM, Huang K, Kim J, Li Z, Thong PSP, Xu R, Soo KC, Zhang Y. *Theranostics*, 2016, 6: 1844–1865

605 Zeng L, Pan Y, Zou R, Zhang J, Tian Y, Teng Z, Wang S, Ren W, Xiao X, Zhang J, Zhang L, Li A, Lu G, Wu A. *Biomaterials*, 2016, 103: 116–127

606 Tsai YC, Vijayaraghavan P, Chiang WH, Chen HH, Liu TI, Shen MY, Omoto A, Kamimura M, Soga K, Chiu HC. *Theranostics*, 2018, 8: 1435–1448

607 Liu Y, Li L, Guo Q, Wang L, Liu D, Wei Z, Zhou J. *Theranostics*, 2016, 6: 1491–1505

608 Lv R, Yang D, Yang P, Xu J, He F, Gai S, Li C, Dai Y, Yang G, Lin J. *Chem Mater*, 2016, 28: 4724–4734

609 Zhou A, Wei Y, Chen Q, Xing D. *J Biomed Nanotechnol*, 2015, 11: 2003–2010

610 Gao W, Wang Z, Lv L, Yin D, Chen D, Han Z, Ma Y, Zhang M, Yang M, Gu Y. *Theranostics*, 2016, 6: 1131–1144

611 Liu Q, Wang W, Zhan C, Yang T, Kohane DS. *Nano Lett*, 2016, 16: 4516–4520

612 Sharipov M, Tawfik SM, Gerelkhuu Z, Huy BT, Lee YI. *Sci Rep*, 2017, 7: 16073

613 Yu Z, Ge Y, Sun Q, Pan W, Wan X, Li N, Tang B. *Chem Sci*, 2018, 9: 3563–3569

614 Liu Y, Zhang J, Zuo C, Zhang Z, Ni D, Zhang C, Wang J, Zhang H, Yao Z, Bu W. *Nano Res*, 2016, 9: 3257–3266

615 Chang Y, Li X, Zhang L, Xia L, Liu X, Li C, Zhang Y, Tu L, Xue B, Zhao H, Zhang H, Kong X. *Sci Rep*, 2017, 7: 45633

616 Hu P, Wu T, Fan W, Chen L, Liu Y, Ni D, Bu W, Shi J. *Biomaterials*, 2017, 141: 86–95

617 Zhang D, Wen L, Huang R, Wang H, Hu X, Xing D. *Biomaterials*, 2018, 153: 14–26

618 Guan Y, Lu H, Li W, Zheng Y, Jiang Z, Zou J, Gao H. *ACS Appl Mater Interfaces*, 2017, 9: 26731–26739

619 Yu Z, Sun Q, Pan W, Li N, Tang B. *ACS Nano*, 2015, 9: 11064–11074

620 Zhu X, Wang H, Zheng L, Zhong Z, Li X, Zhao J, Kou J, Jiang Y, Zheng X, Liu Z, Li H, Cao W, Tian Y, Wang Y, Yang L. *Int J Nanomed*, 2015, 10: 3719–3736

621 Chen D, Tao R, Tao K, Chen B, Choi SK, Tian Q, Xu Y, Zhou G, Sun K. *Small*, 2017, 13: 1602053

622 Fan W, Shen B, Bu W, Zheng X, He Q, Cui Z, Zhao K, Zhang S, Shi J. *Chem Sci*, 2015, 6: 1747–1753

623 Liu Y, Xu Y, Geng X, Huo Y, Chen D, Sun K, Zhou G, Chen B, Tao K. *Small*, 2018, 14: 1800293

624 Ribas A, Wolchok JD. *Science*, 2018, 359: 1350–1355

625 Giavridis T, van der Stegen SJC, Eyquem J, Hamieh M, Piersigilli A, Sadelain M. *Nat Med*, 2018, 24: 731–738

626 Postow MA, Sidlow R, Hellmann MD. *N Engl J Med*, 2018, 378: 158–168

627 Fan Q, Chen Z, Wang C, Liu Z. *Adv Funct Mater*, 2018, 28: 1802540

628 Wang C, Ye Y, Hu Q, Bellotti A, Gu Z. *Adv Mater*, 2017, 29: 1606036

629 Wang H, Mooney DJ. *Nat Mater*, 2018, 17: 761–772

630 Gosselin EA, Eppler HB, Bromberg JS, Jewell CM. *Nat Mater*, 2018, 17: 484–498

631 Xu J, Xu L, Wang C, Yang R, Zhuang Q, Han X, Dong Z, Zhu W, Peng R, Liu Z. *ACS Nano*, 2017, 11: 4463–4474

632 Yang G, Xu L, Xu J, Zhang R, Song G, Chao Y, Feng L, Han F, Dong Z, Li B, Liu Z. *Nano Lett*, 2018, 18: 2475–2484

633 Chen Q, Xu L, Liang C, Wang C, Peng R, Liu Z. *Nat Commun*, 2016, 7: 13193

634 Wang C, Xu L, Liang C, Xiang J, Peng R, Liu Z. *Adv Mater*, 2014, 26: 8154–8162

635 Nam J, Son S, Ochyl LJ, Kuai R, Schwendeman A, Moon JJ. *Nat Commun*, 2018, 9: 1074

636 Min Y, Roche KC, Tian S, Eblan MJ, McKinnon KP, Caster JM, Chai S, Herring LE, Zhang L, Zhang T, DeSimone JM, Tepper JE, Vincent BG, Serody JS, Wang AZ. *Nat Nanotech*, 2017, 12: 877–882

637 Chao Y, Xu L, Liang C, Feng L, Xu J, Dong Z, Tian L, Yi X, Yang K, Liu Z. *Nat Biomed Eng*, 2018, 2: 611–621

638 Xia Y, Wu J, Wei W, Du Y, Wan T, Ma X, An W, Guo A, Miao C, Yue H, Li S, Cao X, Su Z, Ma G. *Nat Mater*, 2018, 17: 187–194

639 Moon JJ, Suh H, Bershteyn A, Stephan MT, Liu H, Huang B, Sohail M, Luo S, Ho Um S, Khant H, Goodwin JT, Ramos J, Chiu W, Irvine DJ. *Nat Mater*, 2011, 10: 243–251

640 Kuai R, Ochyl LJ, Bahjat KS, Schwendeman A, Moon JJ. *Nat Mater*, 2017, 16: 489–496

641 Li AW, Sobral MC, Badrinath S, Choi Y, Graveline A, Stafford AG, Weaver JC, Dellacherie MO, Shih TY, Ali OA, Kim J, Wucherpfennig KW, Mooney DJ. *Nat Mater*, 2018, 17: 528–534

642 Kranz LM, Diken M, Haas H, Kreiter S, Loquai C, Reuter KC, Meng M, Fritz D, Vascotto F, Hefesha H, Grunwitz C, Vormehr M,

Hüsemann Y, Selmi A, Kuhn AN, Buck J, Derhovanessian E, Rae R, Attig S, Diekmann J, Jabulowsky RA, Heesch S, Hassel J, Langguth P, Grabbe S, Huber C, Türeci Ö, Sahin U. *Nature*, 2016, 534: 396–401

643 Yang R, Xu J, Xu L, Sun X, Chen Q, Zhao Y, Peng R, Liu Z. *ACS Nano*, 2018, 12: 5121–5129

644 Park J, Wrzesinski SH, Stern E, Look M, Criscione J, Ragheb R, Jay SM, Demento SL, Agawu A, Licona Limon P, Ferrandino AF, Gonzalez D, Habermann A, Flavell RA, Fahmy TM. *Nat Mater*, 2012, 11: 895–905

645 Stephan MT, Moon JJ, Um SH, Bershteyn A, Irvine DJ. *Nat Med*, 2010, 16: 1035–1041

646 Tang L, Zheng Y, Melo MB, Mabardi L, Castaño AP, Xie YQ, Li N, Kudchodkar SB, Wong HC, Jeng EK, Maus MV, Irvine DJ. *Nat Biotechnol*, 2018, 37: 707–716

647 Smith TT, Stephan SB, Moffett HF, McKnight LE, Ji W, Reiman D, Bonagofski E, Wohlfahrt ME, Pillai SPS, Stephan MT. *Nat Nanotech*, 2017, 12: 813–820

648 Li SY, Liu Y, Xu CF, Shen S, Sun R, Du XJ, Xia JX, Zhu YH, Wang J. *J Control Release*, 2016, 231: 17–28

649 Wang C, Sun W, Ye Y, Hu Q, Bomba HN, Gu Z. *Nat Biomed Eng*, 2017, 1: 0011

650 Wolinsky JB, Colson YL, Grinstaff MW. *J Control Release*, 2012, 159: 14–26

651 Chen Y, Jiang L, Wang R, Lu M, Zhang Q, Zhou Y, Wang Z, Lu G, Liang P, Ran H, Chen H, Zheng Y. *Adv Mater*, 2014, 26: 7468–7473

652 Wang Q, Xiao A, Liu S, Zheng C, Xu H, Yang X, Yang Y. *Nanomed Nanotechnol Biol Med*, 2018, 14: 1746–1747

653 European Association for the Study of the Liver, European Organisation for Research and Treatment of Cancer. *J Hepatol*, 2012, 56: 908–943

654 Golfieri R, Cappelli A, Cucchetti A, Piscaglia F, Carpenzano M, Peri E, Ravaioli M, D'Errico-Grigioni A, Pinna AD, Bolondi L. *Hepatology*, 2011, 53: 1580–1589

655 Llovet JM, Real MI, Montaña X, Planas R, Coll S, Aponte J, Ayuso C, Sala M, Muchart J, Solà R, Rodés J, Bruix J. *Lancet*, 2002, 359: 1734–1739

656 de Baere T, Arai Y, Lencioni R, Geschwind JF, Rilling W, Salem R, Matsui O, Soulen MC. *Cardiovasc Intervent Radiol*, 2016, 39: 334–343

657 Poursaid A, Jensen MM, Huo E, Ghandehari H. *J Control Release*, 2016, 240: 414–433

658 Angelico M. *Dig Liver Dis*, 2016, 48: 796–797

659 Wang Q, Zhao Y, Yang Y, Xu H, Yang X. *Colloid Polym Sci*, 2007, 285: 515–521

660 Wang Q, Zhao Y, Xu H, Yang X, Yang Y. *J Appl Polym Sci*, 2009, 113: 321–326

661 Zhao H, Zheng C, Feng G, Zhao Y, Liang H, Wu H, Zhou G, Liang B, Wang Y, Xia X. *Am J Neuroradiol*, 2012, 34: 169–176

662 Qian K, Ma Y, Wan J, Geng S, Li H, Fu Q, Peng X, Kan X, Zhou G, Liu W, Xiong B, Zhao Y, Zheng C, Yang X, Xu HB. *J Control Release*, 2015, 212: 41–49

663 Liu Y, Peng X, Qian K, Ma Y, Wan J, Li H, Zhang H, Zhou G, Xiong B, Zhao Y, Zheng C, Yang X. *J Mater Chem B*, 2017, 5: 907–916

664 Ma Y, Wan J, Qian K, Geng S, He N, Zhou G, Zhao Y, Yang X. *J Mater Chem B*, 2014, 2: 6044–6053

665 Li J, Yu M, Xiao Y, Yang L, Zhang J, Ray E, Yang X. *Mol Clin Oncol*, 2013, 1: 1019–1024

666 Antonio Chiocca E. *Nat Rev Cancer*, 2002, 2: 938–950

667 Wan J, Geng S, Zhao H, Peng X, Zhou Q, Li H, He M, Zhao Y, Yang X, Xu H. *J Control Release*, 2016, 235: 328–336

668 Zhao H, Xu J, Wan J, Geng S, Li H, Peng X, Fu Q, He M, Zhao Y,

Yang X. *Nanoscale*, 2017, 9: 5859–5871

669 Xie J, Gong L, Zhu S, Yong Y, Gu Z, Zhao Y. *Adv Mater*, 2018, 136: 1802244

670 Manthe RL, Foy SP, Krishnamurthy N, Sharma B, Labhasetwar V. *Mol Pharm*, 2010, 7: 1880–1898

671 Song KD. *Clin Mol Hepatol*, 2016, 22: 509–515

672 Lang BHH, Wu ALH. *J Ther Ultrasound*, 2017, 5: 11

673 Liu X, Chen H, Chen X, Alfadhl Y, Yu J, Wen D. *Appl Phys Rev*, 2015, 2: 011103

674 Raoof M, Curley SA. *Int J Hepatol*, 2011, 2011(3): 1–6

675 Corr SJ, Raoof M, Mackeyev Y, Phounsavath S, Cheney MA, Cisneros BT, Shur M, Gozin M, McNally PJ, Wilson LJ, Curley SA. *J Phys Chem C*, 2012, 116: 24380–24389

676 Rejinold NS, Jayakumar R, Kim YC. *J Control Release*, 2015, 204: 85–97

677 Chen L, Sun J, Yang X. *Cancer Lett*, 2016, 370: 78–84

678 Behzadi S, Serpooshan V, Tao W, Hamaly MA, Alkawareek MY, Dreaden EC, Brown D, Alkilany AM, Farokhzad OC, Mahmoudi M. *Chem Soc Rev*, 2017, 46: 4218–4244

679 Shi J, Kantoff PW, Wooster R, Farokhzad OC. *Nat Rev Cancer*, 2017, 17: 20–37

680 Azhdarzadeh M, Saei AA, Sharifi S, Hajipour MJ, Alkilany AM, Sharifzadeh M, Ramazani F, Laurent S, Mashaghi A, Mahmoudi M. *Nanomedicine*, 2015, 10: 2931–2952

681 Chittajallu DR, Florian S, Kohler RH, Iwamoto Y, Orth JD, Weissleder R, Danuser G, Mitchison TJ. *Nat Methods*, 2015, 12: 577–585

682 Chen Z, Liu Y, Sun B, Li H, Dong J, Zhang L, Wang L, Wang P, Zhao Y, Chen C. *Small*, 2014, 10: 2362–2372

683 Wang Y, Santos A, Evdokiou A, Losic D. *J Mater Chem B*, 2015, 3: 7153–7172

684 Fu PP, Xia Q, Hwang HM, Ray PC, Yu H. *J Food Drug Anal*, 2014, 22: 64–75

685 Smith MJ, Brown JM, Zamboni WC, Walker NJ. *Toxicol Sci*, 2014, 138: 249–255

686 Magdolenova Z, Collins A, Kumar A, Dhawan A, Stone V, Dusinska M. *Nanotoxicology*, 2014, 8: 233–278

687 Folick A, Oakley HD, Yu Y, Armstrong EH, Kumari M, Sanor L, Moore DD, Ortlund EA, Zechner R, Wang MC. *Science*, 2015, 347: 83–86

688 Tsai YY, Huang YH, Chao YL, Hu KY, Chin LT, Chou SH, Hour AL, Yao YD, Tu CS, Liang YJ, Tsai CY, Wu HY, Tan SW, Chen HM. *ACS Nano*, 2011, 5: 9354–9369

689 Monopoli MP, Aberg C, Salvati A, Dawson KA. *Nat Nanotech*, 2012, 7: 779–786

690 Vizirianakis IS. *Nanomed-Nanotechnol Biol Med*, 2011, 7: 11–17

691 Hajipour MJ, Laurent S, Aghaie A, Rezaee F, Mahmoudi M. *Biomater Sci*, 2014, 2: 1210–1221

692 Cheng X, Tian X, Wu A, Li J, Tian J, Chong Y, Chai Z, Zhao Y, Chen C, Ge C. *ACS Appl Mater Interfaces*, 2015, 7: 20568–20575

693 Wang L, Li J, Pan J, Jiang X, Ji Y, Li Y, Qu Y, Zhao Y, Wu X, Chen C. *J Am Chem Soc*, 2013, 135: 17359–17368

694 Chen R, Qiao J, Bai R, Zhao Y, Chen C. *Anal Bioanal Chem*, 2018: 1–16

695 Wang L, Zhang T, Li P, Huang W, Tang J, Wang P, Liu J, Yuan Q, Bai R, Li B, Zhang K, Zhao Y, Chen C. *ACS Nano*, 2015, 9: 6532–6547

696 Chen R, Ling D, Zhao L, Wang S, Liu Y, Bai R, Baik S, Zhao Y, Chen C, Hyeon T. *ACS Nano*, 2015, 9: 12425–12435

697 Li YF, Zhao J, Qu Y, Gao Y, Guo Z, Liu Z, Zhao Y, Chen C. *Nanomed-Nanotechnol Biol Med*, 2015, 11: 1531–1549

698 Wang L, Yan L, Liu J, Chen C, Zhao Y. *Anal Chem*, 2017, 90: 589–614